MECHANISMS OF ANDROGEN RECEPTOR STIMULATION OF

INSULIN SECRETION IN THE MALE

AN ABSTRACT

SUBMITTED ON THE TWENTIETH DAY OF SEPTEMBER 2018

TO THE GRADUATE PROGRAM IN BIOMEDICAL SCIENCES

IN PARTIAL FULFILLMENT OF THE REQUIREMENTS

OF THE SCHOOL OF MEDICNE

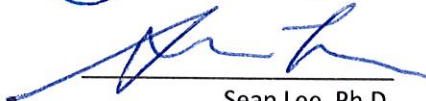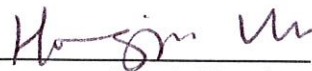OF TULANE UNIVERSITY

FOR THE DEGREE

OF

DOCTOR OF PHILOSOPHY

BY

_____
Weiwei Xu

APPROVED: _____
Franck Mauvais-Jarvis, Ph.D.
Director

_____
Sarah Lindsey, Ph.D.

_____
Sean Lee, Ph.D.

_____
Hongju Wu, Ph.D.

_____
Haitao Zhang, PhD

ABSTRACT

Although men with testosterone deficiency are at increased risk for type 2 diabetes (T2D), previous studies have ignored the role of testosterone and the androgen receptor (AR) in pancreatic β–cell. Our study shows that male pancreatic β–cell specific AR knockout (βARKO^{MIP}) mice develop glucose intolerance because AR potentiates glucose-stimulated insulin secretion (GSIS) through increasing cyclic AMP (cAMP) accumulation and amplifying the insulinotropic effect of glucagon-like peptide-1 (GLP-1). Using transcriptome analysis, we find that AR-deficient islets exhibit altered expression of genes involved in inflammation and insulin secretion demonstrating the importance of androgen action in β-cell health in the male. Our recent study shows that male βARKO^{MIP} mice exhibit impaired intraperitoneal (IP) glucose tolerance- because of impaired IP-GSIS- without alteration in oral glucose tolerance, suggesting that AR amplifies the islet-derived, but not the gut-derived GLP-1 to potentiate GSIS. Dihydrotestosterone (DHT) increases the insulinotropic effect of GLP-1, not gastric inhibitory polypeptide (GIP) and glucagon, in male insulin-secreting β-cell line 832/3 cells and wild-type male mouse islets. Accordingly, using 832/3 cells transduced with exchange factor directly activated by a cAMP (EPAC)-based fluorescence resonance energy transfer (FRET) sensor, we observe that the AR agonist dihydrotestosterone (DHT) specifically allows GLP-1, not GIP and glucagon, to increase cAMP production above level of the individual hormones. The insulinotropic effect of DHT is abolished using EPAC and PKA inhibitors as well as rapamycin indicating that DHT stimulates GSIS via a cAMP/PKA/EPAC pathway and activation of mTOR. This study identifies AR as a novel receptor that enhances β–cell function, a finding with implications for the prevention of type 2 diabetes (T2D) in aging men.

MECHANISMS OF ANDROGEN RECEPTOR STIMULATION OF

INSULIN SECRETION IN THE MALE

A DISSERTATION

SUBMITTED ON THE TWENTIETH DAY OF SEPTEMBER 2018

TO THE GRADUATE PROGRAM IN BIOMEDICAL SCIENCES

IN PARTIAL FULFILLMENT OF THE REQUIREMENTS

OF THE SCHOOL OF MEDICNE

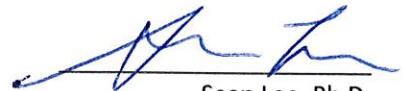OF TULANE UNIVERSITY

FOR THE DEGREE

OF

DOCTOR OF PHILOSOPHY
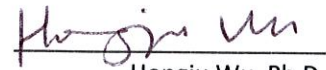
BY

_____
Weiwei Xu

APPROVED: _____
Franck Mauvais-Jarvis, Ph.D.
Director

_____
Sarah Lindsey, Ph.D.

_____
Sean Lee, Ph.D.

_____
Hongju Wu, Ph.D.

_____
Haitao Zhang, Ph.D.

ACKNOWLEDGEMENTS

I would like to gratefully thank my mentor, Dr. Franck Mauvais-Jarvis, for inviting me into his lab for my first rotation and later recruiting me as his student. His open-door policy enabled me to discuss my experiments, projects, and even career-related issues with him throughout my time here as a student. I do appreciate that he always supported my data and discoveries, even though under some circumstances they were against our previous hypothesis and expectation. His guidance has prepared me to think analytically and work innovatively, and his trust in my potentials has encouraged me to pursue a lifetime career in science, which I owe my sincere gratitude to.

To my mother, Sulan Xu, she is both a mother and father, and I am very lucky to have her tremendous love and support throughout my life. I have seen in her the strength of a powerful woman. She had made a big move in her life and left her comfort zone so that I could have a better environment to grow and succeed. She unconditionally supported every decision I made, and I know that sometimes she had to defend my ground on my behalf against the mainstream criticisms. She raised me to be kind, caring, and responsible, which helped me arrive where I am today. I am very proud to be her daughter and I hope I will make her proud.

To my lab mates past and present, Beibei (Dr. Xu), Camille (Dr. Allard), Chandra, Jamie, Taylor (Dr. Fuselier), they have all been an essential part of my training and life, and supported me in my journey to become a good scientist and at the same time challenge me to achieve for better and think outside of the box. I specially thank Camille for taking the initiative to train me when I first joined the lab, and patiently teaching me most of the in vivo experiments that I now know and use daily. It has been a great pleasure working with each one of them.

To my committee members, Dr. Lindsey, Dr. Lee, Dr. Wu, and Dr. Zhang, they have all

ii

generously offered me their time and guidance. Dr. Lindsey met me in the very first days I arrived in the US, when I barely knew anyone. Ever since, she has always made herself available to me to discuss problems with my research and life. Dr. Lee has been very helpful and encouraging, and raised intellectually challenging questions that help me to think more critically. Dr. Wu has always opened her door to me and made her resources available to me. She and her postdoc, Dr. Yanqing Zhang, have patiently offered me countless technical support as well as life advices. I was very fortunate enough to rotate in Dr. Zhang's lab, and gained a deeper understanding of androgen receptor research and acquired molecular biology skills.

I was very grateful for the opportunity to rotate with Dr. Tianhua (Tim) Liu. Dr. Liu had dedicated himself to our collaborative project and I appreciated the training I received from him in the area of transcriptome analysis.

I was so lucky to be the first student in the Section of Endocrinology and Metabolism in Department of Medicine. I am very grateful to our Section Chief Dr. Vivian Fonseca for his translational input on my work and career advice. I also appreciate the help I received from our administrative staff, Jennifer, Cherie, and Porche. I will remember the days I spent in this collaborative environment and forever be proud to have been a member in the Section.

TABLE OF CONTENTS

LIST OF TABLES

LIST OF FIGURES

CHAPTER 1

Introduction

Primary Androgen Deficiency and Metabolic Dysfunction in the Male

In men, aging leads to gradual decline in the serum testosterone levels. A population-based observational study suggested that the prevalence of symptomatic testosterone deficiency (STD) increases with age in men, and is remarkably elevated in men over 70 years of age. It predicted that in 2025, STD will affect 6.5 million American men 30-79 years of age [1]. Low testosterone levels have long been known to negatively associate with central adiposity [2], and leads to impaired mitochondrial function, insulin resistance, and increased risk of T2D [3-7]. Patients with recurrent and metastatic prostate cancer receiving androgen deprivation therapy (ADT) belong to another group of men who are metabolically affected by low testosterone levels. Patients with ADT are at a greater risk of developing insulin resistance and hyperglycemia [8, 9]. An observational study with a population-based cohort revealed ADT with gonadotropin-releasing hormone (GnRH) agonists was associated with increased risk of T2D [10]. In another large observational study conducted in veterans, ADT led to significantly increased incidence (28%) of T2D [11].

Androgen replacement therapy (ART) on the other hand improves metabolic parameters in hypogonadal men. A double-blind, placebo-controlled study suggested that ART produced a significant reduction in glycated hemoglobin (HbA1c) level [12], and another study with ART improved glycemic control in T2D patients, and was associated with beneficial effect on insulin resistance [13]. A prospective observation pilot study in men with obesity-related secondary hypogonadism revealed that ART with long-acting intramuscular testosterone undecanoate improved glycemic control, β-cell function, and body composition in these patients [14].

Role of AR in Glucose Homeostasis in the Male

Androgens Prevent Visceral Fat Accumulation and Improves Insulin Sensitivity

The impact of testosterone deficiency on the development of visceral obesity, insulin resistance and metabolic syndrome in men is well established [2-4, 8, 15, 16]. There is an inverse correlation between total serum testosterone and the amount of visceral adipose tissue [2]. This is true in all situations of androgen deficiency, whether in the context of hypogonadism in older men [4], inherited testosterone deficiency as observed in Klinefelter's syndrome [17], or androgen deprivation during treatment for prostate carcinoma [8]. Thus, in men, high serum testosterone is associated with insulin sensitivity [3]. Of course, aromatization of testosterone into 17β-estradiol (E2) is critical to energy homeostasis in males, suggesting that testosterone functions as a prohormone in men to provide E2 for tissue metabolism. Indeed, orchidectomized male rodents treated with either testosterone or E2 remain lean, while those treated with the pure androgen DHT- that cannot be converted to E2- develop obesity demonstrating that following orchiectomy, the restoration of adiposity was due to testosterone conversion into E2 acting on estrogen receptors (ERs) [18]. This is also true in men for whom testosterone replacement suppresses adiposity, an effect that is blocked in the presence of an aromatase inhibitor [19]. In addition, human and rodent studies have revealed that mutations in the aromatase or the ERα genes increase visceral obesity in males further demonstrating the importance of estrogen in male energy metabolism [20]. Still, several lines of evidence demonstrate that in males, testosterone has anti-obesity properties mediated via AR actions. First, in men with genetic androgen resistance linked to CAG repeat polymorphisms in the AR gene- which decreases AR-mediated gene transcription- a low number of CAG repeats is independently associated with protective metabolic parameters such as low body fat mass and

plasma insulin, suggesting that intact AR transcription favors metabolic homeostasis [21]. Second, male mice with global deletion of the AR develop late onset visceral obesity with leptin resistance, insulin resistance, and increased lipogenesis in adipose tissue and liver [22, 23]. Furthermore, AR regulates adiponectin production. Serum adiponectin levels are high in hypogonadal men and are reduced by testosterone therapy [24]. Testosterone infusion also decreases adiponectin in mice [25]. This effect is at least partially mediated via AR since serum adiponectin concentrations are elevated in AR-deficient mice [22]. However, it is unclear whether AR suppression of adiponectin reflects increased adiponectin sensitivity, decreased adipocyte number, or improved adipose function.

Several lines of evidence suggest that the suppressing effect of testosterone on white adipose tissue (WAT) mass in males is indirectly mediated via AR signaling in skeletal muscle. First, in vitro, testosterone stimulates the commitment of pluripotent mesenchymal stem cells into myogenic lineage while at the same time suppressing the adipogenic lineage [26]. This AR-dependent pathway involves non-canonical Wnt signaling [27]. This androgenic anabolism induces the expression of IGF1, leading to nuclear accumulation of beta-catenin, a myogenic and anti-adipogenic stem cell factor [28]. Second, overexpression of AR selectively in muscle cells of transgenic male rats increases their lean mass via hypertrophy of type IIb muscle fibers which is associated with increased oxidative metabolism and metabolic rate[29]. This results in reduced adipocyte size and adipose tissue mass. Finally, and consistent with this model, male adipocyte-specific androgen receptor KO (ARKO) mice exhibit no increase in fat mass demonstrating that direct AR action in adipose tissue is not necessary for the control of fat mass [30]. Surprisingly, these mice show an increased production of leptin by adipose tissue without leptin resistance. Thus, activation of AR in skeletal muscle may indirectly decrease adipose tissue mass by increasing muscle oxidative metabolism or through the release of a circulating factor. However,

surprisingly, mice with myocyte-specific AR ablation have lower intra-abdominal fat. It should be noted that these mice exhibit a fast-to-slow fiber conversion, without major change in muscle mass and without affecting muscle strength, which could affect the adipose phenotype [31]. In summary, testosterone action prevents fat accumulation in males via a combination of ER (after aromatization in E2) and AR mediated effects. The AR suppression of adiposity could be mediated via AR signaling in skeletal muscle (**Figure 1**).

Testosterone Action in Skeletal Muscle Promotes Insulin Sensitivity in Males

The mechanism of insulin resistance following androgen deficiency probably also involves an alteration in skeletal muscle insulin sensitivity. Castration of male rats is followed by a marked insulin resistance in skeletal muscle under euglycemic, hyperinsulinemic clamp conditions [32]. Treatment with physiological doses of testosterone completely abolishes these perturbations in insulin sensitivity. Transcriptome analysis of skeletal muscle in mice demonstrates that testosterone regulates the expression of genes in glucose metabolism in a way that would promote insulin sensitivity [33]. The mechanism of AR deficiency-induced insulin resistance in skeletal muscle probably involves a decrease in the transcription factor, peroxisome proliferator-activated receptor-gamma coactivator alpha (PGC1α). Indeed, PGC1α stimulates mitochondrial biogenesis and skeletal muscle oxidative fibers and is thus a molecular marker of muscle insulin sensitivity. A decrease in PGC1a expression in skeletal muscle of T2D subjects is associated with insulin resistance [34]. Similarly, in men, low testosterone levels are associated with low PGC1a expression levels in muscle [3] and AR-deficient mice express low levels of PGC1a mRNA in tissues [22]. Thus, testosterone deficiency promotes insulin resistance
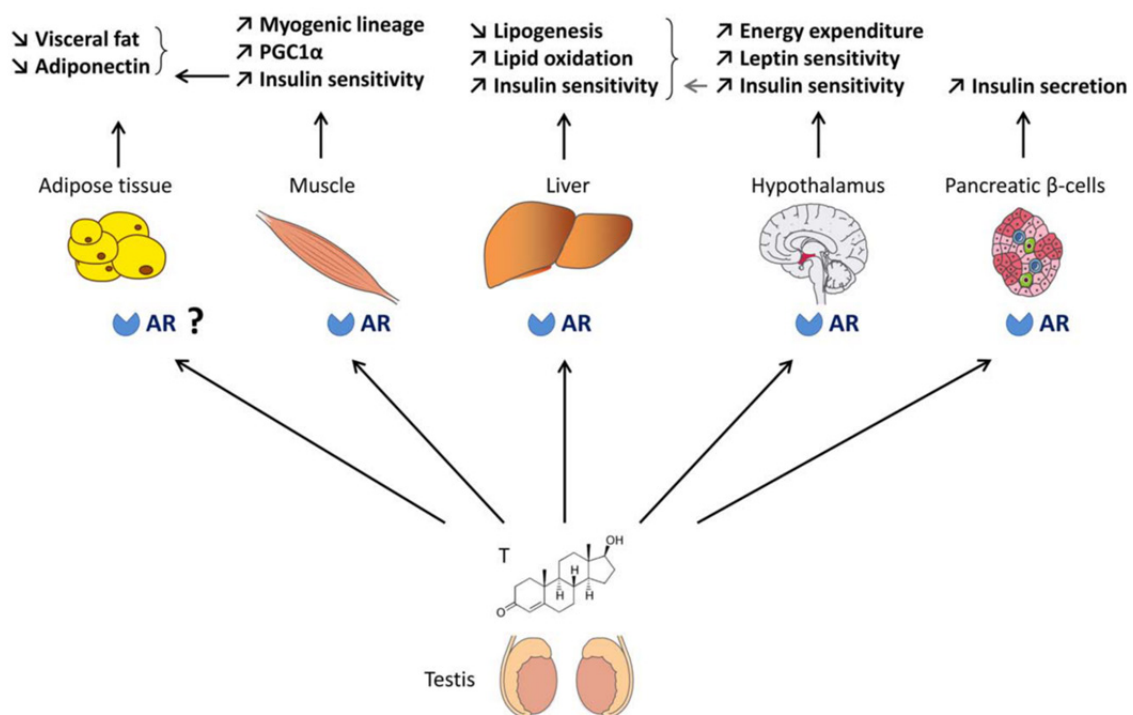
Figure 1. Proposed mechanism of androgen action via AR in males. In males, androgens promote glucose and energy homeostasis via actions on AR in skeletal muscle, liver, pancreatic β-cells, and metabolic centers in the hypothalamus. Androgen actions on adipose tissue could be indirectly mediated via AR actions in muscle.

in skeletal muscle at least partially via an AR dependent mechanism involving a decrease in PGC1a-mediated oxidative and insulin sensitive muscle fibers (**Figure 1**).

Androgen Actions in Liver Favors Lipid Hemeostasis and Insulin Sensitivity

Male hepatocyte-specific ARKO (HARKO) mice developed hepatic steatosis when fed a high-fat diet, but females did not [35]. Increased hepatic steatosis in these obese male HARKO mice resulted from decreased hepatic peroxisome proliferator-activated receptor α (PPARα) expression leading to decreased fatty acid oxidation and increased hepatic sterol regulatory element binding protein 1c leading to increased de novo lipid synthesis. This ultimately led to hepatic insulin resistance. Mice deficient in 5α -reductase type 1 (5αR1-/-), the enzyme that converts testosterone to the active androgen DHT, develop hepatic steatosis and show decreased hepatic expression of genes involved in insulin signaling when fed a Western diet [36]. Like the HARKO mice, male 5αR1-KO mice developed adiposity, hyperinsulinemia, hepatic steatosis, decreased mRNA transcript profiles for fatty acid b-oxidation, and increased genes for lipid storage. The nonselective 5α-reductase inhibitor finasteride induced hyperinsulinemia and hepatic steatosis in obese male Zucker rats, both intact and castrated [37]. These rodent studies are supported by the observation that low testosterone levels are associated with hepatic steatosis in men [38]. Together these studies show that AR actions in liver are important to prevent hepatic steatosis (**Figure 1**).

Central Androgen Actions Regulate Energy Homeostasis in Males

AR is more abundantly expressed in the brain of male rodents than that of females [39]. Male whole-body AR-deficient mice develop obesity without increase energy intake but with decreased locomotor activity. These mice also display reduced brown adipose tissue

thermogenesis which decreases energy expenditure [22]. AR also functions in the male hypothalamus to favor central leptin action (**Figure 1**). Indeed, in AR-deficient male mice, leptin fails to promote STAT3 nuclear localization in arcuate nucleus (ARC) neurons and does not suppress food intake or reduce body weight even before the onset of overt obesity [39]. Further, neuronal specific ARKO (NARKO) mice develop obesity, insulin resistance, and glucose intolerance. These mice show hypothalamic insulin resistance via activation of hypothalamic NFKB that increases inflammation [40]. Together, these observations demonstrate that in male rodents, AR is involved in the control of adipose tissue mass via central and peripheral effects.

Role of AR in β-cell Function and Insulin Secretion

Clinical study suggested an association of testosterone deficiency and insulin resistance and increased risk of T2D. Genetic mouse models were generated to discover the underlying mechanisms by which testosterone and its receptor, androgen receptor (AR), mediate β-cell function and insulin secretion. Global AR knockout mice developed reduced insulin resistance and impaired glucose tolerance, and when coupled with aging, it resulted in severe hyperinsulinemia and hyperglycemia [23]. In another study, global AR deficiency coupled with high fat diet exacerbated glucose tolerance and decreased glucose-stimulated insulin secretion (GSIS) [41] (**Figure 1**).

In our first study, to understand the role of AR in the β-cells specifically, we generated an inducible β-cell specific AR knockout (βARKO^{MIP}) mouse line by crossing AR^{lox} with MIP-CreERT transgenic mice [42]. We showed that the lack of AR signaling in the β-cells resulted in impaired insulin secretion, leading to glucose intolerance. DHT-activated AR potentiated GSIS in a similar manner to incretins, resulting in activation of adenylate cyclase (AC), increase in cAMP

accumulation, and PKA activation. DHT amplified both the endogenous and exogenous insulinotropic effect of GLP-1 to enhance GSIS.

In the second study, we explored the AR-dependent gene networks in β-cells and performed a high-throughput whole transcriptome sequencing (RNA-Seq) in islets from male βARKO$^{-/y}$ and control mice [43]. We identified 214 differentially expressed genes (DEGs), revealing alterations in β-cell genes involved in cellular inflammation/stress and insulin secretion. Accordingly, our subsequent pathway analysis and gene ontology analysis revealed significantly enriched pathways and biological processes involved mainly in insulin secretion, stress/growth factor signaling and inflammatory pathways, demonstrating the importance of androgen action in β-cell health in the male.

We investigate in the current third study the molecular mechanisms by which AR and GLP-1R collaboratively potentiate GSIS in male β-cells. DHT amplifies the islet-derived, not gut-derived, GLP-1 to induce GSIS in male mice. GLP-1R is essential for the AR signaling in the insulin secretion, but DHT-activated AR is not necessary for the action of the GLP-1. DHT does not amplify the insulinotropic effect of other ligands of G-protein coupled receptors (GPCRs) coupling to Gαs and activating AC, for example GIP and glucagon, and shows the specificity towards GLP-1. Consistently, DHT increases GLP-1 induced cAMP production but not that of GIP and glucagon, and it signals via a cAMP/PKA/EPAC pathway and the activation of mTOR pathway to amplify GSIS.

CHAPTER 2

Extranuclear Action of Androgen Receptor Potentiates Glucose-Stimulated Insulin Secretion

Overview

Testosterone action is mediated by the androgen receptor (AR), a ligand-activated transcription factor. The extent to which the AR plays a role in β-cell failure in testosterone deficient males is unknown. Remarkably, we currently have no insight on the role of the AR in β-cell function in males. These issues are highly relevant to the health of aging men because novel antidiabetic androgen therapies that do not increase risk of prostate growth could have a substantial public health impact.

We investigated the role of the AR in β-cell function in the male using β-cell-specific AR knockout mice and cultured mouse and human islets. We show that the β-cell AR is important for testosterone potentiation of glucose-stimulated insulin secretion (GSIS) in male mice as well as in human islets. This AR-dependent pathway involves a rise in islet cAMP and the activation of protein kinase A, which amplifies the effect of GLP-1 on GSIS. We identify the AR as a physiological enhancer of β-cell function via the cAMP pathway, a finding that has clinical and pharmacological implications for the prevention of T2D in aging men.

Materials and Methods

Transgenic Mouse Generation

βARKO$^{-/y}$ mouse were generated by crossing B6.Cg-Tg (Ins2-cre)25Mgn/J (AR$^{+/Y}$, Cre$^{+/-}$, RIP-Cre) and AR$^{lox/+}$, Cre$^{-/-}$. RIP-Cre (Jackson Laboratory) carries a construct composed of a 668 bp fragment of rat insulin II promotor, Cre recombinase with a nuclear localization sequence, and a 2.1 kb fragment from human growth hormone gene. This mouse strain will specifically overexpress cre in the pancreatic β cells, and when used in "Cre-lox" system and combined with mice carrying floxed alleles, it leads to pancreatic specific knockout of these targeted alleles. AR$^{lox/lox}$ mouse, carrying the AR gene with floxed exon 2 on their X chromosome, was a kind gift from Dr. Guido Verhoeven from Catholic University of Leuven, and its generation and characterization had been described [44]. NARKO$^{-/-}$ mice were generated by crossing ARlox$^{+/-}$ with the Syn-Cre$^{+/-}$ mice (Jackson Laboratory) as described [40]. To generate βARKO^{MIP} mice we crossed AR$^{lox/lox}$ mice with the Ins1-Cre/ERT (MIP-Cre$^{+/-}$) transgenic mouse (Jackson Lab). We induced Tamoxifen (Tam) inactivation of AR after puberty following a 5-day treatment with Tam (75mg/Kg). All studies were performed with the approval of Northwestern University and Tulane University Animal Care and Use Committees in accordance with the NIH Guidelines.

Western Diet

Mice were weaned onto a customized diet designed to be high in saturated fat and simple sugars (sucrose and fructose) to mimic a western diet (30% AMF; 14.9% Kcal protein, 33.2% Kcal carbohydrates, 51.9% Kcal fat; Harlan Teklad) for 9 weeks.

Metabolic studies

Blood glucose was measured from tail vein blood using a True Metrix glucometer (Trividia Health). Insulin (Linco Research and Millipore) and glucagon (ALPCO) were measured in serum by ELISA. For IP-GTT (2 g/kg) and GSIS (3 g/kg), mice were fasted overnight before glucose injection. For IP-ITT, mice were fasted for 6 hours prior to insulin injection (0.75 U/kg). Pancreas insulin concentration was measured from acid ethanol extract as described [45].

Immunohistochemistry and β-cell mass quantification

Insulin and glucagon staining as well as β-cell mass measurement from pancreas sections were performed as described [45]. For AR staining of human islets, and islets from βARKO$^{-/y}$, βARKO^{MIP} and their respective controls, sections were incubated with primary antibody rabbit anti-AR (PG-21, 1:100, Millipore). Secondary antibody goat biotinylated anti-rabbit (1:200; Linco) and Alexa 568 tyramide signal amplification kit (TSA, Molecular Probes) was used for signal amplification. For AR staining in the hypothalamus, tissues were fixed in 10% formalin at 4 ^{0}C and stored in 30% sucrose until sectioning in 20 µm sections. Sections were incubated with primary antibody anti-AR (N20, 1:250, Santa Cruz). Secondary goat biotinylated anti-rabbit antibody was visualized using the VECTASTAIN Elite ABC kit (Vector Laboratories). Images were captured at x20 magnification using a fluorescent microscope (Nikon Eclipse E400). LNCaP and INS-1 cells were treated with vehicle or DHT (10^{-8} M) for 40 minutes, followed by fixation in 4% paraformaldehyde. LNCaP cells were incubated in the anti-AR antibody (N20, 1:200, Santa Cruz), and then in the goat anti-rabbit secondary antibody (1:400). INS-1 cells were incubated in the anti-AR antibody (N20, 1:200, Santa Cruz). The signal was amplified using TSA. The images were taken using a Nikon A1 confocal microscope.

Subcellular fractionation

The LNCaP and INS-1 cells were treated with DHT for 20 minutes, 40 minutes, 1 hour, 3 hours, and 8 hours. Subcellular fractionation was performed by first extracting the cytosolic proteins with dilution buffer, followed by extracting the nuclear protein fractions with lysis buffer. Cytosolic and nuclear protein fractions were normalized to GAPDH and Histone H3 respectively.

Islet isolation and insulin secretion in static incubation

Islet isolation was performed following pancreatic duct injection with collagenase as described [45]. For measurement of insulin secretion, islets were hand-picked under a dissection microscope, and treated with DHT (10^{-8} M; Steraloids), or vehicle (95% ethanol) for 48 hrs. Insulin release from islets was measured as described [45]. For experiment with inhibitors, islets were treated with flutamide (10^{-8} M; Sigma-Aldrich, St. Louise, MO) or H-89 (10μM;Cell Signaling).

Islet perfusion

A perifusion system (Biorep Technologies) was used to determine the insulin biphasic response. Briefly, batches of 60 mouse islets were perifused at 37 °C, at a flow of 100 μL/min. Islets were first equilibrated for 60 min with KRB solution containing 2.8 mM glucose, then stimulated for 30 min with KRB solution contained either DHT (10^{-8} M) or vehicle (95 % ethanol) and 16.7 mM glucose. Samples were collected in a 96-well plate and insulin concentration was determined by ELISA (Millipore).

Luciferase assay

LNCaP cells were transfected with ARR3-tk-luciferase reporter, containing three repeats of androgen response element(ARE)s in tandem, upstream of the minimal tk enhancer fused to the luciferase reporter [46], or control plasmids containing renilla luciferase reporter gene using TurboFect transfection reagent (Thermo Scientific) and 48 hours prior to the treatment. On the experiment day, cells were lysed, and dual-luciferase reporter assay system (Promega) was used to measure firefly and renilla luciferase activity sequentially. The ratio of firefly and renilla luciferase reading was calculated to indicate the ability of DHT and ADC to activate ARE-mediated luciferase expression.

ATP and cAMP measurements

Intracellular ATP concentrations were measured in 10 islets per condition treated with either vehicle or DHT (10^{-8} M) for 30 minutes using EnzyLight^{TM} ATP assay and ADP assay (BioAssay Systems) according to the manufacturer's instructions. Islets were lysed to release ATP and ADP, and luminescence was measured on a luminometer (BioTek) and quantified to ATP and ADP standards. cAMP levels were determined in mouse islets pre-treated with vehicle, DHT (10^{-8} M), flutamide (10^{-8} M), or DHT plus flutamide for 30 min in the presence of 200uM 3-isobutyl-1-methylxanthine (IBMX). Islets were lysed, and the supernatant was collected to measure the intracellular cAMP level with cyclic AMP XP® Assay Kit (Cell Signaling) according to the manufacturer's instructions.

Measurement of cytoplasmic calcium and perifusion

Islet $[Ca^{2+}]_i$ was measured with the Ca^{2+} sensitive dye fura-*2* acetoxymethyl ester (Molecular Probes) as described [47]. Mouse islets were plated on coverslips and dye-loaded

with fura-2. Fluorescence imaging was performed using a Nikon Eclipse TE2000-U microscope equipped with an epifluorescent illuminator (Sutter instruments), a CoolSNAP HQ2 camera (Photometrics) and Nikon Elements software (Nikon). The $[Ca^{2+}]_i$ ratios of emitted fluorescence intensities at excitation wavelengths of 340 and 380 nm ($F$340/$F$380) were determined every 5 s with background subtraction. A perifusion system (Biorep Technologies) containing DHT (10^{-8} M) or vehicle (95 % ethanol) 2.8 and 16.7 mM glucose was used to determine biphasic response.

Food intake measurement

Animals were housed individually for 1 week to accommodate to the new environment. Food intake was measured daily for 1 week following accommodation.

Induction of experimental diabetes

Mice were exposed to a single intraperitoneal (IP) injection of 150 mg/kg of STZ (Sigma Aldrich, St. Louis, MO) to induce diabetes. Blood glucose was measured every 48 h following STZ injection. At day 8 following STZ injection, insulin was assessed and pancreases were processed for measurement of pancreatic insulin concentration.

IP-Insulin tolerance test

For ip-ITT, mice were morning fasted for 6 hrs prior to insulin injection (0.75 U/kg). At the completion of treatment (12-13 weeks of age) pancreases were dissected and processed for measurement of pancreatic insulin concentration and β-cell mass.

Quantification of relative AR Expression

The images were captured with Nikon Eclipse Ti-S microscope, and the quantification of AR expression was performed using NIS-Elements Advanced Research software. The mean AR intensity was quantified from islets of pancreas sections from 4 BARKO[MIP] and 3 AR[lox] MIP-CreERT. All values were normalized to the average of the AR[lox] MIP-CreERT group (as 100%), and the results were shown as the relative AR expression.

ADC synthesis

All reagents were used as purchased. CH_3CN, THF, and CH_2Cl_2 used in reactions were dried using a solvent delivery system (neutral alumina column). Compounds and materials were supplied from the sources indicated: radiolabeled R1881 ([3H]R1881, [17-methyl-3H]methyltrienolone, 17alpha- hydroxy-17-methyl-estra-4,9,11-trien-3-one, 70-87 Ci mmol^{-1}, PerkinElmer) and R1881 for radiometric evaluation of synthesized S-GTx-007 and its analogs (PerkinElmer, MA), LBD (ligand binding domain) of androgen receptor (Invitrogen, Grand Island, NY), 4-cyano-3-(trifluoro)aniline (Lancaster, Ward Hill, MA), (2R)-3-bromo-2-hydroxy-2-methylpropanoic acid (Obiter research, Champaign, IL), PAMAM generation-6 dendrimer (ethylene diamine core), 4-nitro-3-(trifluoro)aniline, glutaric anhydride, 4-aminophenol, *N*-acetylethylenediamine, thionyl chloride, N,N'-dicylohexylcarbodiimide, N-hydroxysuccinimide (Aldrich, Milwaukee WI), Amicon® Ultra centrifugal filter (Milipore, Bedford, MA). S-GTx-007 (or S-4) and analog of S-GTx-007(agonist to androgen receptor) was prepared according to a modified literature procedure [48, 49].

Proton ^{1}H NMR spectra were recorded on a Varian Inova-500 at 500 MHz with the deuterated solvent noted. Carbon ^{13}C NMR spectra were obtained on a Varian Inova-500 at 126 MHz with the deuterated solvent noted. MALDI-TOF (Matrix Assisted Laser Desorption

Ionization-Time Of Flight) mass analysis (2,5-dihydroxybenzoic acid, DHB, as a matrix) and High- and low-resolution electron-ionization electrospray ionization mass spectra were obtained using Voyager-DE™ STR and a Q-TOF Ultima API (Waters Co. Ltd), respectively.

(R)-3-Bromo-2-hydroxy-2-methyl-N-(4-cyano-3-(trifluoromethyl)phenyl)propanamide (I): This compound was synthesized according to the literature method: To the (2R)-3-bromo-2-hydroxy-2-methylpropanoic acid (300 mg, 1.64 mmol) in CH_3CN (10 mL) was added dropwise thionyl chloride (290 mg, 2.46 mmol) at around -10 °C. After stirring for an additional 2 hr under the same temperature, trimethylamine (414 mg, 4.10 mmol) was added into the resulting mixture for 10 min at -15 to -20 °C. Subsequently a solution of 4-cyano-3-(trifluoro)aniline (270 mg, 1.45 mmol) in acetonitrile (5 mL) was added into the reaction mixture at the same temperature, and the reaction temperature was allowed to warm up to rt to accelerate the reaction. Once the aniline disappeared on SiO_2 TLC, the solvent was evaporated. The residue was extracted with EtOAc (20 mL x 3), dried over $MgSO_4$, and loaded onto SiO_2 column chromatography. Elution with a mixture of EtOAc and n-hexane (25:75, v/v) provided the title compound as a dark yellowish solid (447 mg, 88%). ^{1}H NMR (500 MHz, $CDCl_3$) δ 1.64 (s, 3H), 3.41 (s, 1H), 3.58 (d, J = 10.5 Hz, 1H, CH<u>H</u>), 3.98 (d, J = 10.5 Hz, 1H, C<u>H</u>H), 7.80 (d, J = 8.5 Hz, 1H), 8.04 (dd, J = 2.0, 8.5 Hz, 1H), 8.12 (d, J = 8.5 Hz, 1H), 9.11 (s, 1H, NH). [^{13}C NMR (126 MHz, $CDCl_3$) δ 25.07, 41.06, 75.80, 104.80, 115.76, 117.71 (q, $^3J_{C-F}$ = 4.5 Hz), 122.26, 122.31 (q, $^1J_{C-F}$ = 273.4 Hz), 134.28 (q, $^2J_{C-F}$ = 33.2 Hz), 136.12, 141.61. 172.21]. HRMS (ESI) m/z calcd for $C_{12}H_{11}BrF_3N_2O_2$ (M^++1) 350.9956, found 350.9968.

4-Propionamidophenol (II): The mixture of *p*-aminophenol (1.09 g, 10.0 mmol) and glutaric anhydride (1.15 g, 10.0 mmol) in THF-CH_2Cl_2 (20 mL, 1:1, v/v) at rt was sonicated for 5 min to form a precipitate. The title compound was collected by filtration as an off-white solid (1.8 g, 80.7%) and used without further purification. ^{1}H NMR (500 MHz, CD_3OD) δ 1.96 (quintet, J = 7.5

Hz, 2H), 2.38 (t, J = 7.5 Hz, 2H), 2.39 (t, J = 7.5 Hz, 2H), 6.72 (d, J = 9.0 Hz, 2H), 7.31 (d, J = 9.0 Hz, 2H). ^{13}C NMR (126 MHz, CDCl$_3$) δ 21.08, 33.00, 35.56, 115.00, 122.22, 130.45, 154.18, 172.29, 175.74. HRMS (ESI) m/z calcd for C$_{11}$H$_{14}$N$_4$O$_4$ (M$^+$+1) 224.0923, found 224.0924.

Benzyl 5-((4-hydroxyphenyl)amino)-5-oxopentanoate (III): To the solution of 4-propionamidophenol (223 mg, 1.0 mmol) and K$_2$CO$_3$ (378 mg, 2.7 mmol) in DMF (10 mL) at rt was added benzyl chloride (126 mg, 1.0 mmol). The resulting solution was further stirred 2 hr more and poured into water, followed by extraction with EtOAc (10 mL x 3), dried over MgSO$_4$, and loaded onto a SiO$_2$ column chromatography to separate out the title compound (280 mg, 89%) as an off-white powder with the solvent mixed with EtOAc and n-hexane (40:60, v/v).

^{1}H NMR (500 MHz, CDCl$_3$ + CD$_3$OD) δ 1.95 (quintet, J = 7.5 Hz, 2H), 2.28 (t, J = 7.5 Hz, 2H), 2.40 (t, J = 7.5 Hz, 2H), 5.05 (s, 2H), 6.68 (d, J = 8.5 Hz, 2H), 7.21 (d, J = 8.5 Hz, 2H), 7.25-7.30 (m, 5H). ^{13}C NMR (126 MHz, CDCl$_3$) δ 21.10, 33.46, 36.03, 66.65, 115.53, 122.29, 128.36, 128.49, 128.75, 130.23, 135.85, 153.78, 171.40, 173.81. HRMS (ESI) m/z calcd for C$_{18}$H$_{20}$NO$_4$ (M$^+$+1) 314.1392, found 314.1392.

Benzyl (S)-5-((4-(2-hydroxy-3-((4-cyano-3-(trifluoromethyl)phenyl)amino)-2-methyl-3-oxopropoxy)phenyl)amino)-5-oxopentanoate (IV): The mixture of **I** (100 mg, 0.28 mmol), **III** (135 mg, 0.43 mmol), and K$_2$CO$_3$ (77 mg, 0.56 mmol) in DMF (10 mL) was stirred for 8 hr. To the reaction mixture was added **I** (48 mg, 0.13 mmol) again. After stirring 4 hr more, deionized water (20 mL) and EtOAc (20 mL) were added into the reaction mixture. The EtOAc layer was separated out and aqueous layer was extracted twice more with EtOAc (20 mL x 2). The EtOAc layer was dried over MgSO$_4$, concentrated under vacuum, and loaded onto SiO$_2$ column for chromatography. Elution with the mixture of EtOAc and n-hexane (60:40, v/v) afforded the title compound (129 mg, 39%) as a colorless powder.

^{1}H NMR (500 MHz, CDCl$_3$ + CD$_3$OD) δ 1.64 (s, 3H), 2.04 (quintet, J = 8.0 Hz, 2H), 2.36 (t, J = 8.0 Hz, 2H), 2.46 (t, J = 8.0 Hz, 2H), 3.93 (d, J = 9.0 Hz, 1H, CH<u>H</u>), 4.36 (d, J = 9.0 Hz, 1H, C<u>H</u>H), 5.11 (s, 2H), 6.77 (d, J = 9.0, 2H), 7.32 (d, J = 9.0, 2H), 7.75 (d, J = 8.5 Hz, 1H), 7.94 (dd, J = 2.0, 8.5 Hz, 1H), 8.12 (d, J = 2.0 Hz, 1H). HRMS (ESI) m/z calcd for C$_{30}$H$_{29}$N$_3$O$_6$F$_3$ (M$^+$+1) 584.2008, found 584.2010.

(**S**)-5-((4-(2-hydroxy-3-((4-cyano-3-(trifluoromethyl)phenyl)amino)-2-methyl-3-oxopropoxy)phenyl)amino)-5-oxopentanoic acid (**V**): The methanol solution (5 ml) of **IV** (40 mg, 0.07 mmol) and catalytic amount of 10% Pd-C was charged with 30 psi hydrogen and shaken for 2 hr at rt. Filtration through Celite and evaporation provided the title compound (31 mg, 92%) as an colorless powder. ^{1}H NMR (500 MHz, CDCl$_3$ + CD$_3$OD) δ 1.39 (s, 3H), 1.82 (quintet, J = 9.0 Hz, 2H), 2.20 (t, J = 9.0 Hz, 2H), 2.22 (t, J = 9.0 Hz, 2H), 3.82 (d, J = 11.5 Hz, 1H, CH<u>H</u>), 4.16 (d, J = 11.5 Hz, 1H, C<u>H</u>H), 6.70 (d, J = 11.5 Hz, 2H), 7.26 (d, J = 11.5 Hz, 2H), 7.67 (d, J = 10.5 Hz, 1H), 7.88 (dd, J = 2.5, 10.5 Hz, 1H), 8.08 (d, J = 2.5 Hz, 1H). HRMS (ESI) m/z calcd for C$_{23}$H$_{21}$N$_3$O$_6$F$_3$ (M$^+$-1) 492.1382, found 492.1383.

2,5-dioxopyrrolidin-1-yl (**S**)-5-((4-(2-hydroxy-3-((4-isocyano-3(trifluoromethyl)phenyl) amino)-2-methyl-3-oxopropoxy)phenyl)amino)-5-oxopentanoate (**VI**). Compound **V** (9.0 mg, 0.02 mmol), N-hydroxysuccinimide (2.0 mg, 0.02 mmol), and catalytic amount of 4-N,N-dimethylpyridine was suspended in CH$_2$Cl$_2$ (5 mL). To the resulting solution was added DCC (3.7 mg, 0.02 mmol) at rt and stirred for 1 hr. The precipitated N, N'-dicyclohexylurea was filtered off to afford the title compound (11 mg). The obtained compound was used without further purification. ^{1}H NMR (500 MHz, CDCl$_3$) δ 1.57 (s, 3H), 2.19 (quintet, J = 7.0 Hz, 2H), 2.45 (t, J = 7.0 Hz, 2H), 2.71 (t, J = 7.0 Hz, 2H), 2.89 (brs, 4H, -OC-CH$_2$CH$_2$-CO-), 3.95 (d, J = 10.5 Hz, 1H, CH<u>H</u>), 4.41 (d, J = 10.5 Hz, 1H, C<u>H</u>H), 6.83 (d, J = 10.0 Hz, 2H), 7.43 (d, J = 10.0 Hz, 2H), 7.79 (d, J = 10.0

Hz, 1H), 7.86 (s, 1H), 7.95 (dd, J = 2.5, 10.0 Hz, 1H), 8.11 (d, J = 2.5 Hz, 1H), 9.18 (s, 1H). HRMS

(ESI) m/z calcd for $C_{27}H_{26}N_4O_8F_3$ (M^++1) 591.1703, found 591.1702.

Androgen-dendrimer conjugation (VII): PAMAM dendrimer generation 6 (ethylene diamine

core, 5% methanol solution, 400 mg) was diluted with triple the volume of methanol in

preparation for a reaction. To the solution of PAMAM G6 (net 20 mg) was added **VI** (5.0 mg, 8.5

μmol) in DMF (100 μL). The resulting solution was sonicated for 20 min at rt. Once the NHS ester

(**VI**) disappeared on the SiO_2 TLC (EtOAc eluent), the reaction mixture was transferred into

Amicon membrane filter (30K MW cutoff) and centrifuged 6 times at ~500 X g with methanol

solution, as described elsewhere. [50]. After washing, the residual aliquot was transferred to 3-

mL glass vial, dried under a gentle stream of nitrogen, and then prepared as a stock solution

with the mixture of methanol and DI water (1:5, v/v). MALDI-TOF (DHA matrix) Mn 62,389, Mw

64,089, PDI 1.03. (Reference PAMAM G6 was measured as Mn 46,167, Mw 47,209, PDI 1.02).

To label the conjugate with Cy5, the conjugate in a mixture of methanol and water (1:5, v/v,

net weight 1.25 mg) was diluted with pH 7.0 phosphate buffer (100 μL) followed by the addition

Cy5-NHS (0.15 mg, 0.19 μmol) in DMSO (50 μL) and sonication for 20 min at rt. The resulting

solution was transferred to the 30K MWCO Amicon membrane filter for purification, centrifuged

with pH 7.0 phosphate buffer three time and DI water three times until no more Cy5 was

detected in filtrate. The final aliquot was dried under a gentle stream of nitrogen and prepared

as a stock solution with the mixture of methanol and DI water (1:5, v/v). MALDI-TOF (DHA

matrix) Mn 67,794, Mw 69346, PDI 1.02.

Androgen receptor binding assays

Relative binding affinities were determined by competitive radiometric binding assays

with 10 nM [³H]R1881 as tracer, as a modification of methods previously described. The source

of AR was purified, recombinant rat, ligand binding domain purchased from Invitrogen. Incubations were done at 0 °C for 18–24 h, and hydroxyapatite (Bio-Rad) was used to absorb the purified receptor-ligand complexes. The binding affinities are expressed as relative binding affinity (RBA) values, where the RBA of R1881 is 100%; under these conditions, the Kd of R1881 for AR is ca. 0.6 nM. The determination of these RBA values is reproducible in separate experiments with a CV of 0.3.

Statistical analysis

Results are presented as mean ± SEM as specified in figures. All statistical analyses were performed using the unpaired Student's *t* test. A P value less than 0.05 was considered statistically significant. * $P<0.05$, ** $P<0.01$.

Results

Generation of βARKO$^{-/y}$ mice

To explore the role of AR in β-cell function, we generated a β-cell-specific AR knockout (βARKO$^{-/y}$) mouse using the Cre-loxP strategy and crossing AR$^{lox/y}$ mice with RIP-Cre transgenic mice. A previous report showed that mice expressing the RIP-Cre transgene developed glucose intolerance and impaired insulin secretion [51]. It is therefore recommended that studies involving crosses between floxed mice and RIP-Cre mice use the RIP-Cre as the control group rather than the littermate floxed or wild type mice. We also observed that RIP-Cre mice were hyperglycemic compared to littermate AR$^{lox/y}$ mice and to a lesser extent compared to wild type mice (**Figure 2.1**). Thus, we used RIP-Cre mice as the control group. We confirmed recombination of the AR allele in islets from male βARKO$^{-/y}$ mice by the presence of the excised 404 bp fragment (**Figure 2.2A**). Immunostaining for AR showed cytosolic AR expression in islet β-cells from control mice and confirmed elimination of the AR protein in islets from male βARKO$^{-/y}$ (**Figure 2.2B**). Since gene manipulations using RIP-Cre transgenic mice are reported to promote recombination in nutrient neurons [51], we investigated whether recombination of AR had occurred in hypothalamic neurons of βARKO$^{-/y}$ mice. We observed recombination of the AR allele in hypothalamus of male βARKO$^{-/y}$ mice with the presence of the excised 404 bp fragment (**Figure 2.3A**). Accordingly, male βARKO$^{-/y}$ mice displayed a significant decrease in AR protein expression in the arcuate nucleus (ARC) and ventromedial hypothalamus (VMH) (**Figure 2.3B–D**). We confirmed the presence of the non-recombined 952 bp AR allele in all other tissues of the βARKO$^{-/y}$ mice (**Figure 2.4A**) where AR protein expression was not altered (**Figure 2.4B**). Although AR expression was decreased in hypothalamus, βARKO$^{-/y}$ mice showed no alteration in food intake or body weight between 12 and 20 weeks of age (**Figure 2.5**).

A

B
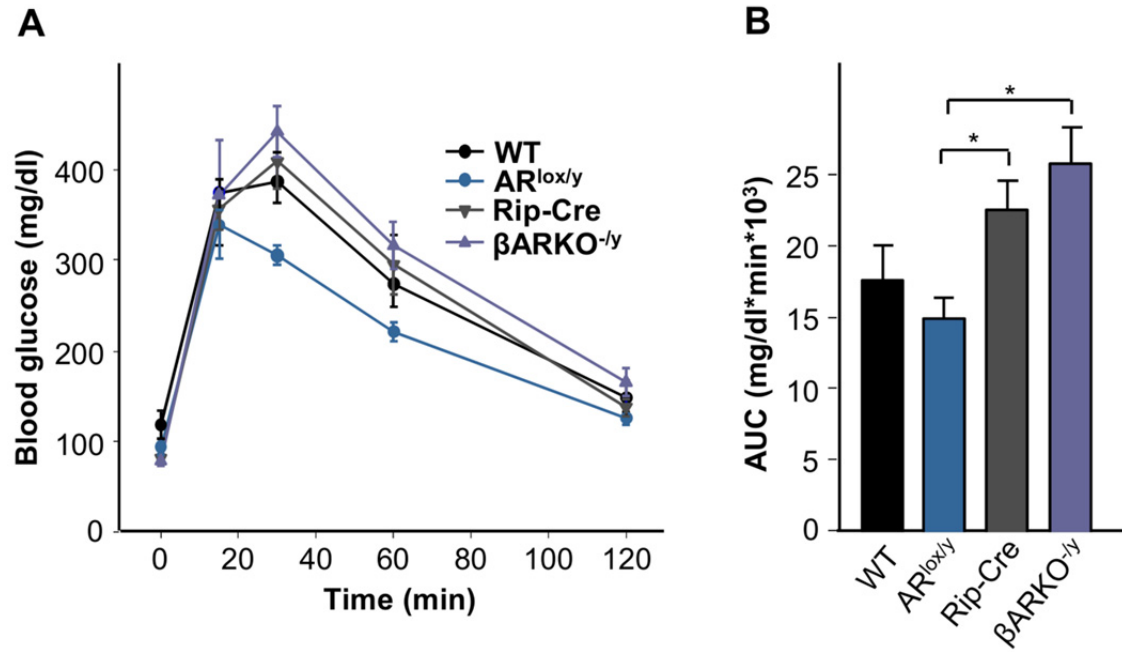
Figure 2.1. **(A)** IP-Glucose tolerance test (2g/kg) and **(B)** area under the curve for glucose from

(**A**) in 12 week old mice. Values represent the mean ± SEM. * P < 0.05.
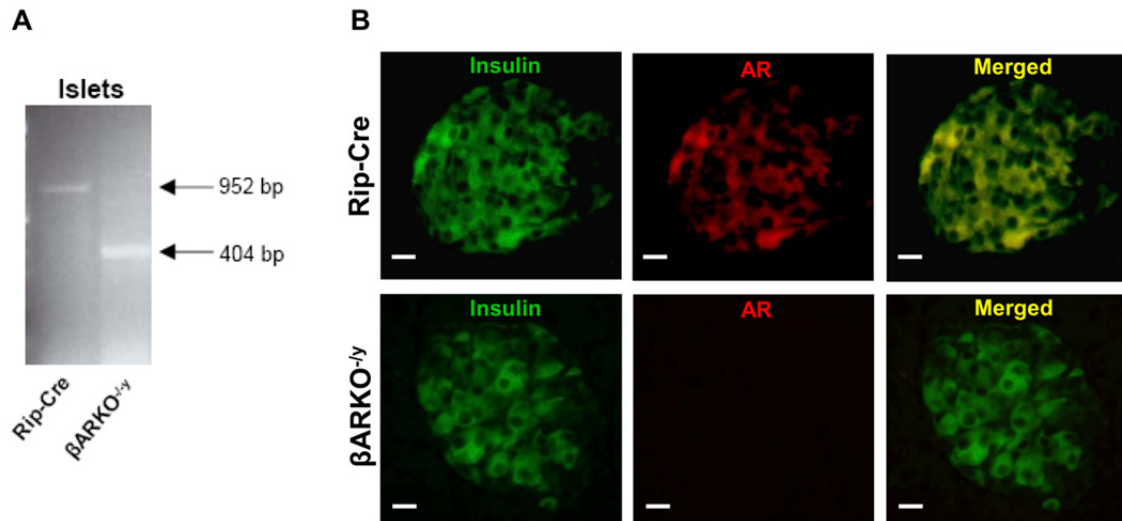
Figure 2.2. **(A)** PCR showing the recombined 404 bp fragment of the *ar* allele in islets from male βARKO$^{-/y}$. **(B)** Pancreas section showing AR immunofluorescent staining (red) in β-cells co-localizing with insulin (green) in control mice and confirming successful AR deletion in βARKO$^{-/y}$ islets (the scale bar represents 10μm).
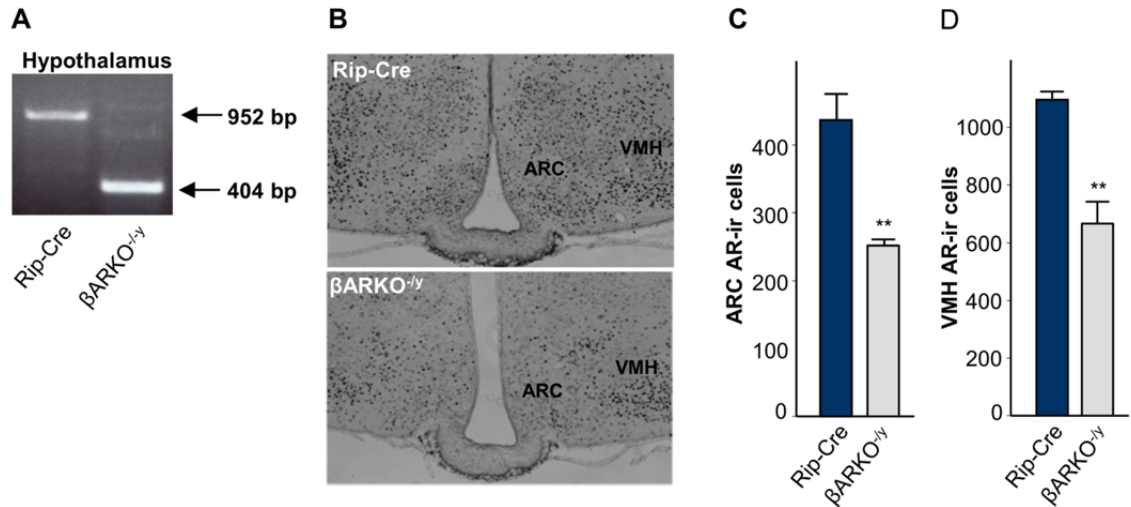
Figure 2.3. **(A)** PCR showing recombination of AR allele in hypothalamus. **(B)** IHC staining and quantification of AR immunoreactivity in **(C)** the arcuate nucleus (ARC) and **(D)** ventromedial hypothalamus (VMH) of control and βARKO$^{-/y}$ mice. Results are representative of 3-5 mice. Values represent the mean ± SEM. **P < 0.01.
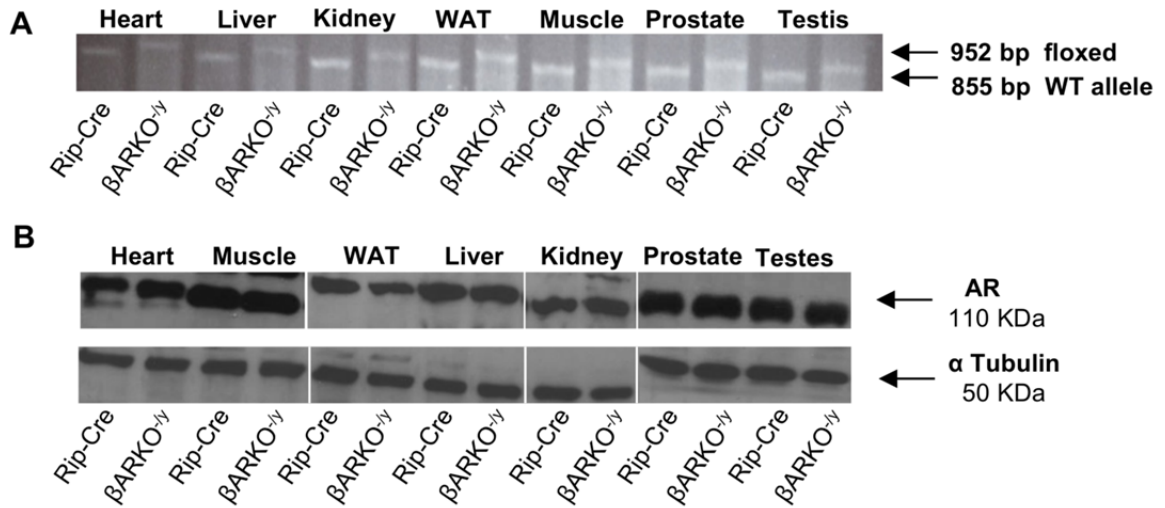
Figure 2.4. **(A)** PCR showing the specific DNA fragment of the non-recombined *Ar* allele for each group in non-islet tissues (n = 3). **(B)** Western blot showing AR protein expression in non-islet tissues of βARKO$^{-/y}$ mice at 12 weeks of age.
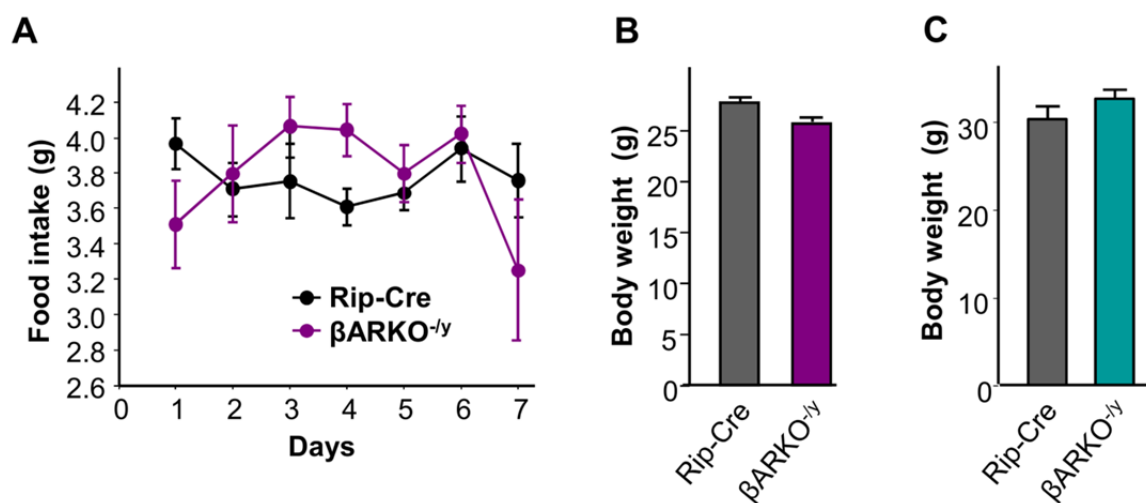
Figure 2.5. **(A)** Daily food intake (n = 10). **(B)** Body weight measured at 12 weeks of age (n = 20).

(C) Body weight measured at 20 weeks of age (n=16).

Male βARKO^{-/y} mice exhibit β-cell dysfunction and glucose intolerance

We assessed glucose homeostasis in male control and βARKO$^{-/y}$ mice at 12 weeks of age. This point is before the development of late onset obesity and insulin resistance observed in mice globally lacking AR [22] or selectively in neurons [40]. On normal chow, βARKO$^{-/y}$ mice showed no alteration in fed or fasting blood glucose or in fed insulin levels (**Figure 3.1A-C**). However, they showed decreased fasting insulin concentrations (**Figure 3.1D**). Following an intraperitoneal (IP) glucose challenge, βARKO$^{-/y}$ mice exhibited decreased basal and GSIS (**Figure 3.2A**) that resulted in glucose intolerance compared to controls (**Figure 3.2B**). Despite their deficient insulin secretion, βARKO$^{-/y}$ mice had similar islet architecture, β-cell mass, and pancreatic insulin concentration as controls (**Figure 3.3**). Control and βARKO$^{-/y}$ mice also exhibited similar insulin sensitivity during an insulin tolerance test (ITT) (**Figure 3.4**), and had similar serum glucagon concentrations (183±36 and 169±27 pg/ml, controls and βARKO$^{-/y}$, respectively, mean ±SE). To investigate whether AR deficiency in β-cells synergizes with a second β-cell stress *in vivo* to alter β-cell function, we induced metabolic stress in male control and βARKO$^{-/y}$ mice by feeding them a western diet for 9 weeks. After this challenge, βARKO$^{-/y}$ mice displayed reduced fasted and fed serum insulin concentrations compared to control mice (**Figure 3.5B & E**) and developed hyperglycemia in both the fed and fasted states (**Figure 3.5A & D**). As a result, the insulin deficiency index (insulin/glucose) was more pronounced in βARKO$^{-/y}$ mice (**Figure 3.5C & F**). It followed that western diet-fed βARKO$^{-/y}$ mice showed decreased GSIS and developed glucose intolerance (**Figure 3.6**) relative to controls. However, following western diet feeding, βARKO$^{-/y}$ mice still showed no alteration in β-cell mass or pancreatic insulin concentrations (**Figure 3.7**). In addition, βARKO$^{-/y}$ and control mice on western diets had similar insulin sensitivity following an ITT (**Figure 3.8**). Note that female islets exhibited lower AR expression than males (**Figure 3.9**), and female βARKO$^{-/-}$ mice showed no alteration in GSIS
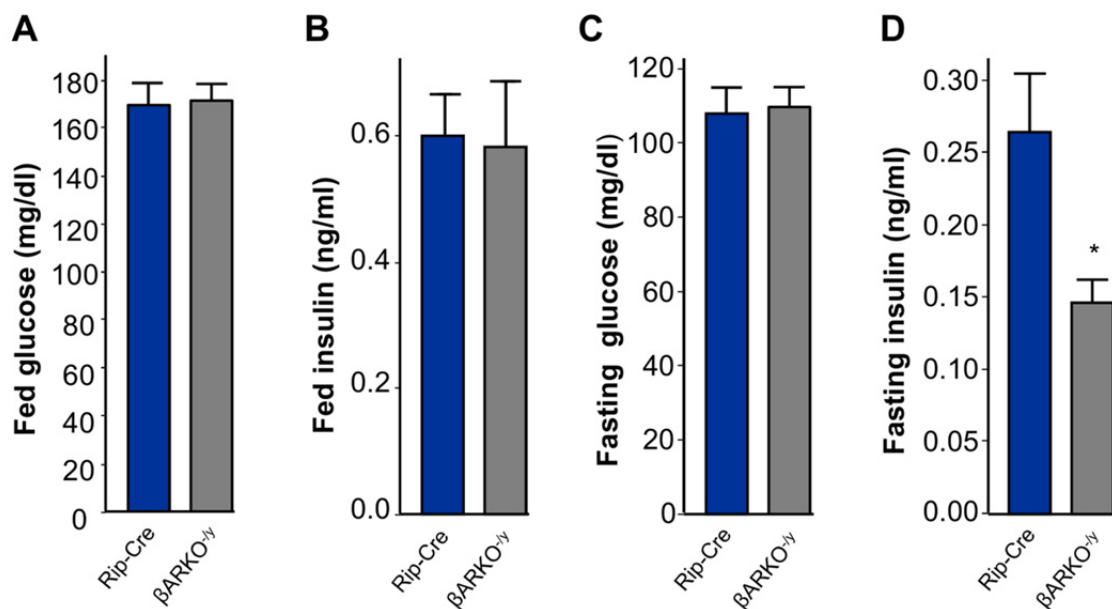
Figure 3.1. Data are from mice fed a normal chow. **(A)** Random fed blood glucose. **(B)** Random fed serum insulin. **(C)** Fasting blood glucose. **(D)** Fasting serum insulin. Values represent the mean ± SEM. * P < 0.05.
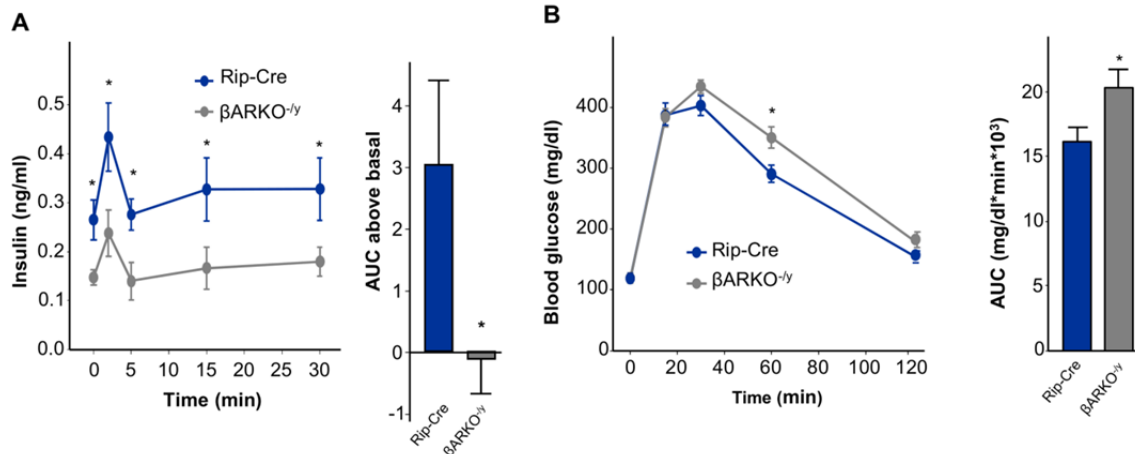
Figure 3.2. Data are from mice fed a normal chow. **(A)** IP-GSIS (3 g/kg) with insulin area under the curve (AUC). **(B)** IP-GTT (2 g/kg) with glucose AUC (n= 12-15). Values represent the mean ± SEM. * P < 0.05.
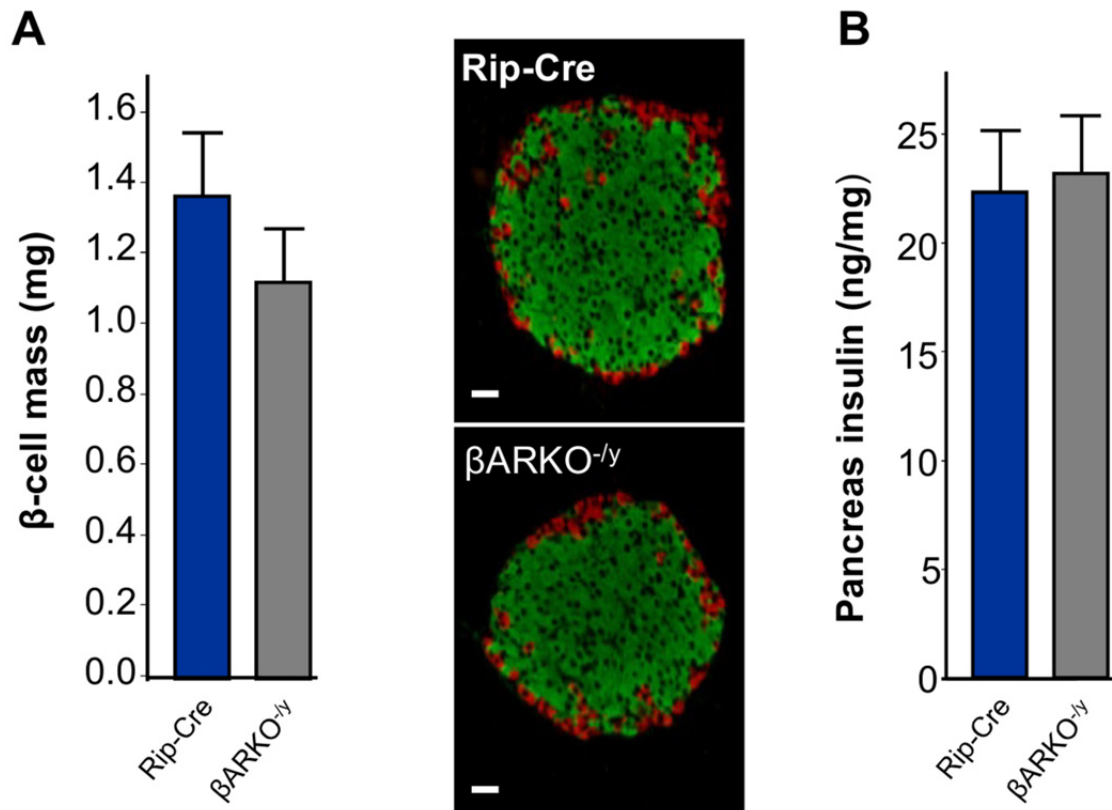
Figure 3.3. Data are from mice fed a normal chow. **(A)** β-cell mass quantification and representative pictures of islets stained with insulin (green) and glucagon (red) (the scale bar represents 10µm). **(B)** Pancreas insulin content.
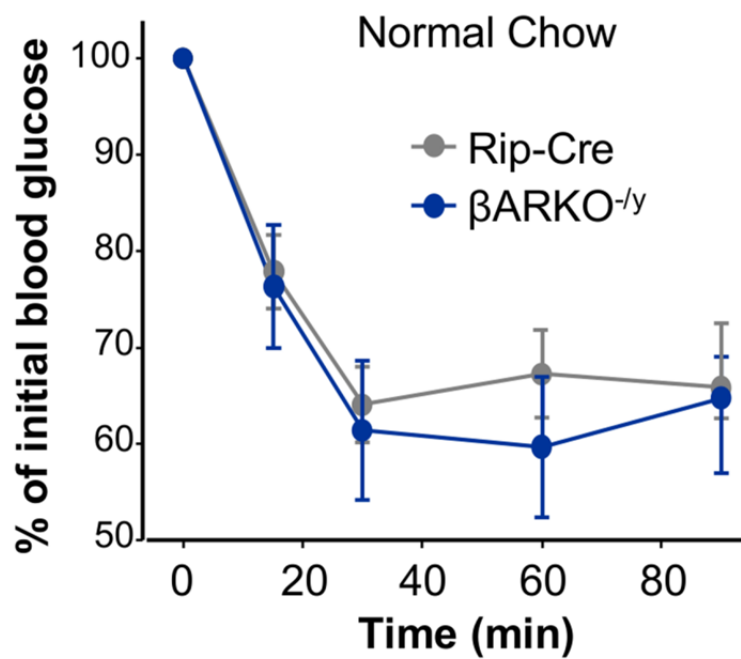
Figure 3.4. IP-insulin tolerance test (ITT) was performed following 6 hr fasting in mice fed on a

normal chow (n = 12).
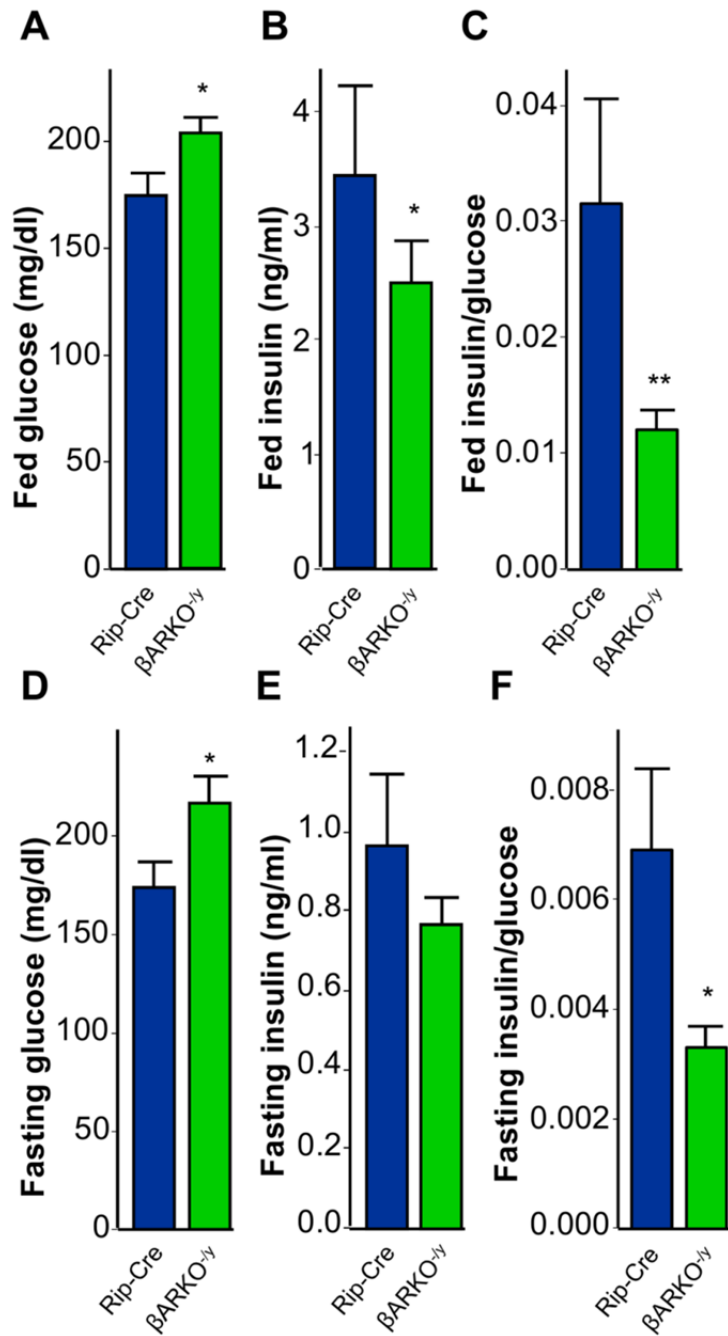
Figure 3.5. Data are from mice fed on a western diet for 9 weeks. **(A)** Random fed blood glucose following 9 weeks western diet feeding. **(B)** Fed insulin levels. **(C)** Fed index of insulin deficiency (insulin/glucose). **(D)** Fasting blood glucose. **(E)** Fasting insulin levels. **(F)** Fasting index of insulin deficiency. Values represent the mean ± SEM. *P < 0.05, **P < 0.01.
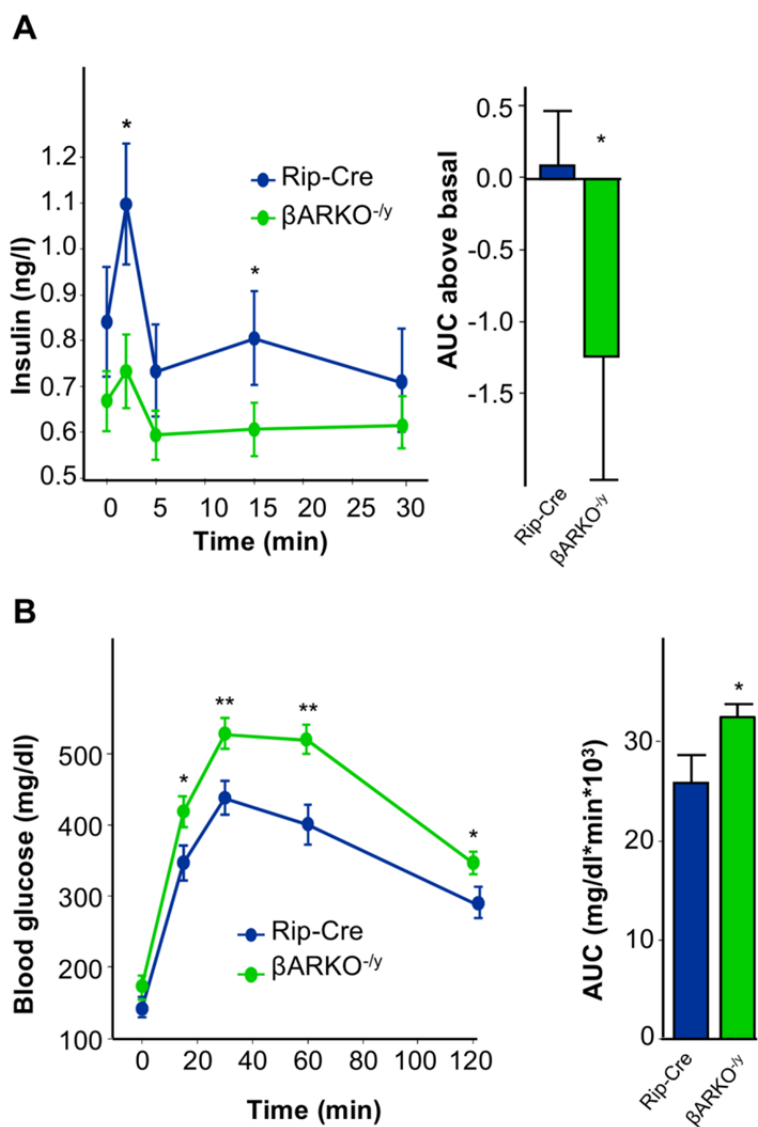
Figure 3.6. Data are from mice fed on a western diet for 9 weeks. **(A)** IP-GSIS (3 g/kg) with insulin AUC. **(B)** IP-GTT (2 g/kg) with glucose AUC. Values represent the mean ± SEM. *P < 0.05, **P < 0.01.
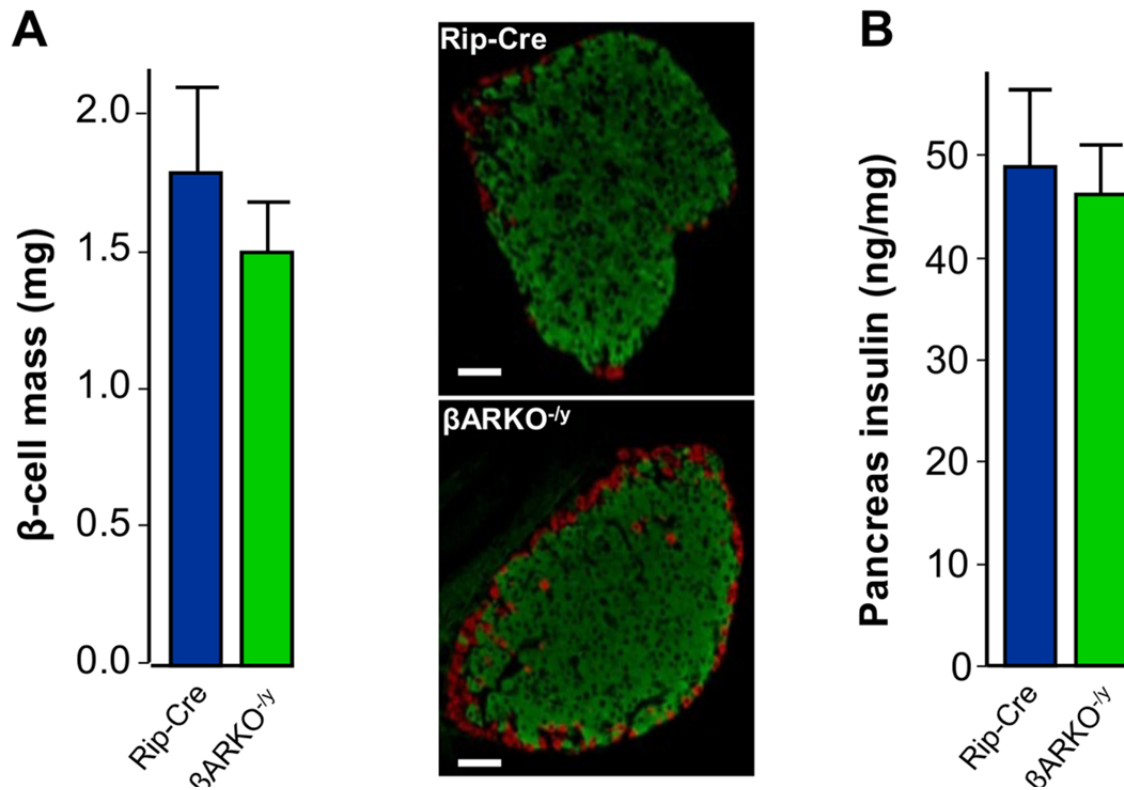
Figure 3.7. Data are from mice fed on a western diet for 9 weeks. **(A)** β-cell mass quantification and representative pictures of islets (the scale bar represents 10μm). **(B)** Pancreatic insulin content. Mice were studied at 12 weeks of age (n = 12-14) and pancreas were removed at 14 weeks of age.
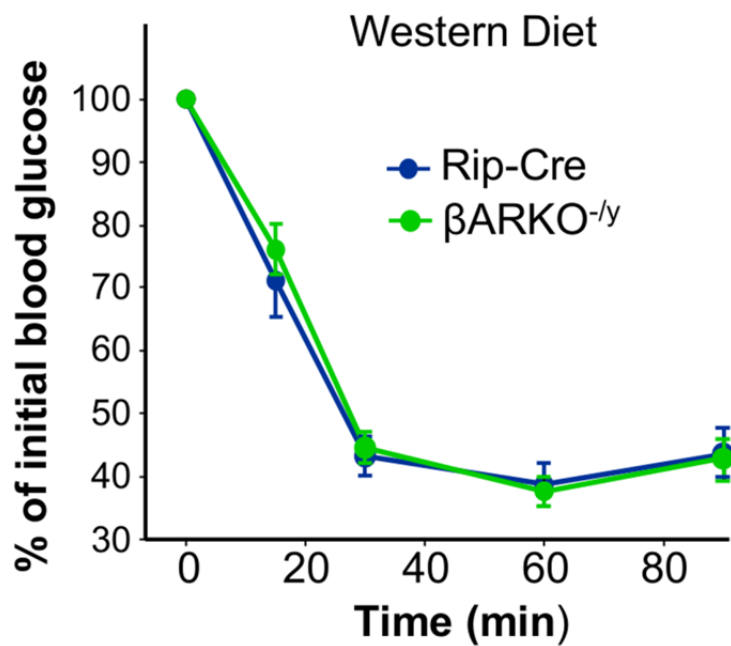
Figure 3.8. IP-ITT was performed following 6 hr fast in mice fed on a western diet (n = 16-18).
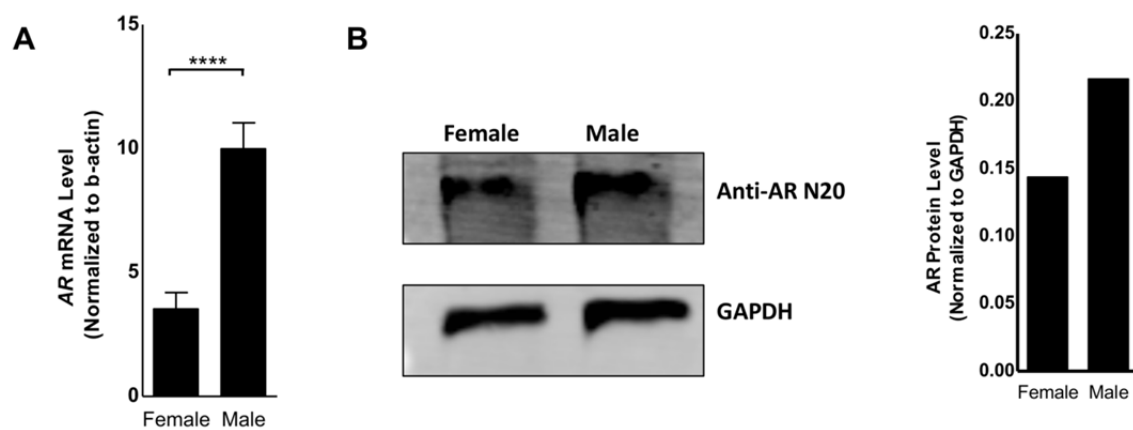
Figure 3.9. **(A)** *Ar* mRNA level and **(B)** AR protein expression level in female and male islets.

and GTT either on a normal chow (**Figure 3.10**) or western diet (**Figure 3.11**). We then examined whether AR deficiency in male β-cells synergizes with additional β-cell stress induced by streptozotocin (STZ) to alter β-cell survival. We observed no increased predisposition to STZ in male βARKO$^{-/y}$ mice (**Figure 3.12**). Thus, βARKO$^{-/y}$ mice developed altered GSIS, which was exacerbated following western diet feeding but without alteration in β-cell mass or increased predisposition to STZ-induced insulin-deficient diabetes.

AR deficiency in neurons does not alter β-cell function in male mice

Innervation of islet β-cells regulates insulin secretion by afferent signals arising from the hypothalamus [52]. To determine whether AR hypothalamic deletion contributes to the metabolic phenotype of male βARKO$^{-/y}$ mice, we generated a neuronal AR knockout mouse (NARKO$^{-/y}$) by crossing AR$^{lox/y}$ mice with synapsin-Cre transgenic mice that selectively express Cre in neuronal cells [53]. We confirmed decreased AR expression in brains of male NARKO$^{-/y}$ mice with normal AR expression in other non-neuronal tissues (**Figure 4.1**). Male NARKO$^{-/y}$ mice showed no alteration in fasting and fed blood glucose or in insulin levels, observations that were similar when the mice were on normal chow (**Figure 4.2**) or on a western diet (**Figure 4.3**). Importantly, unlike male βARKO$^{-/y}$, male NARKO$^{-/y}$ mice showed no alteration in GSIS and retained similar glucose tolerance and insulin sensitivity compared to controls on both normal chow and western diet (**Figure 4.4** & **Figure 4.5** and **Figure 4.6**). To further eliminate the possibility that the defect in GSIS observed in male βARKO$^{-/y}$ mice derives from the partial AR hypothalamic deletion, we generated a second β-cell specific ARKO model (βARKO^{MIP}) by crossing our AR^{lox} mice with the MIP-CreERT1^{Lphi} (MIP-CreERT) transgenic mouse that lacks Cre activity in the hypothalamus [54]. The MIP-CreERT transgenic mouse, however, has limitations because of transgene-driven expression of human growth hormone leading to decreased
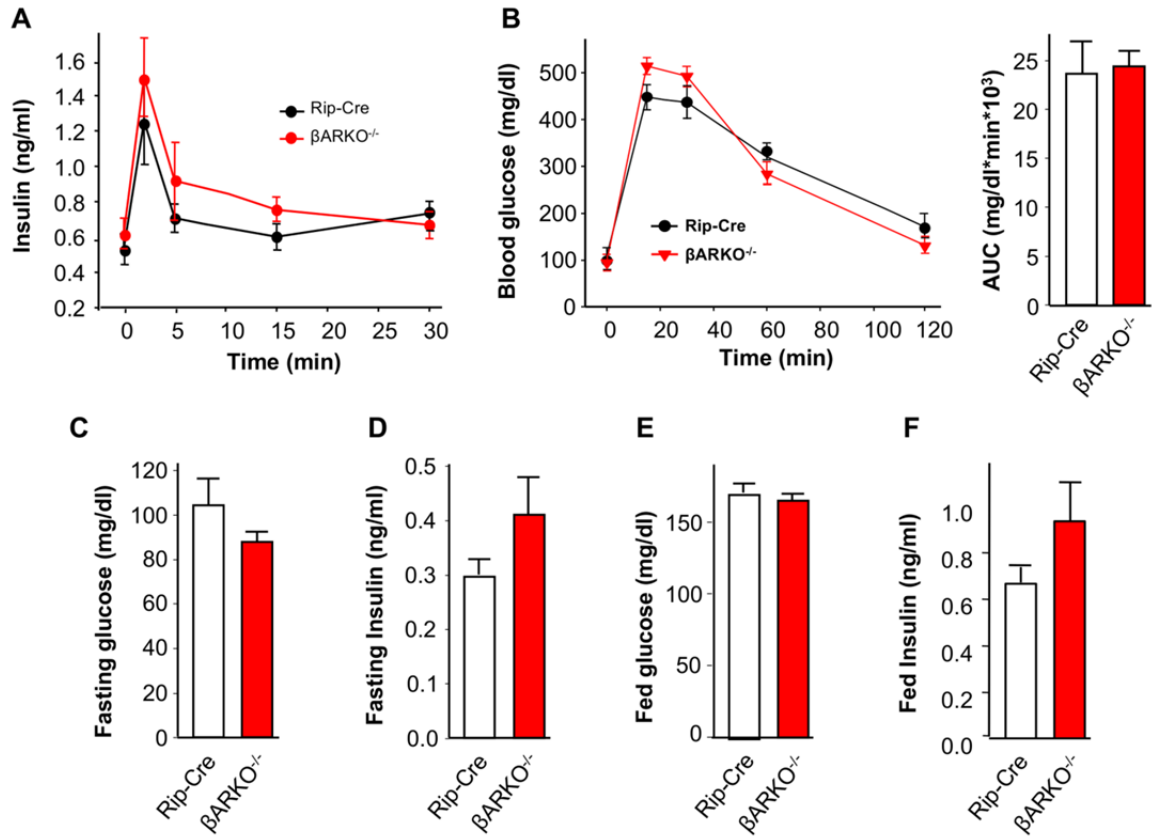
Figure 3.10. Data are from female mice fed on a normal chow **(A-F). (A)** IP-GSIS (3 g/kg). **(B)** IP-GTT (2 g/kg) with glucose AUC. **(C)** Fasting blood glucose. **(D)** Fasting insulin. **(E)** Random fed glucose. **(F)** Random fed insulin.
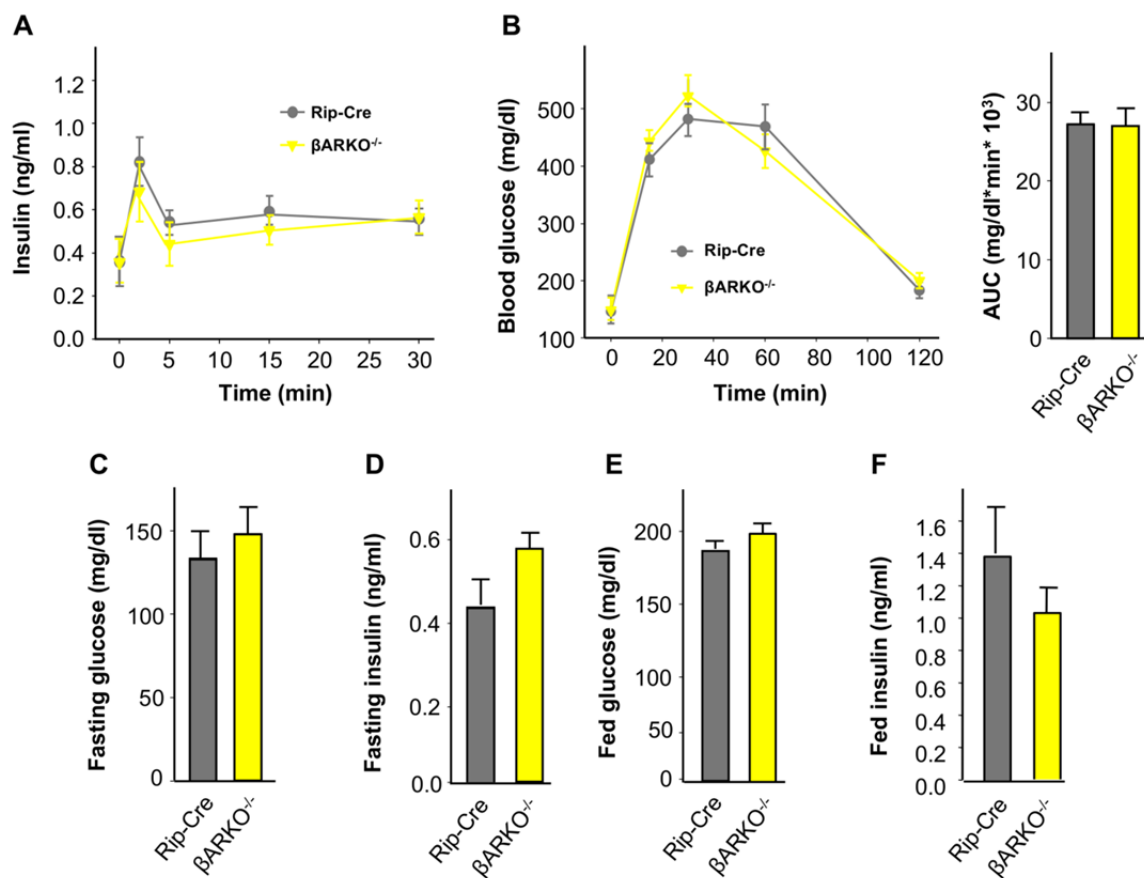
Figure 3.11. Data are from female mice fed on a western diet **(A-F). (A)** IP-GSIS (3 g/kg). **(B)** IP-GTT (2 g/kg) with glucose AUC. **(C)** Fasting blood glucose. **(D)** Fasting insulin. **(E)** Random fed glucose. **(F)** Random fed insulin.
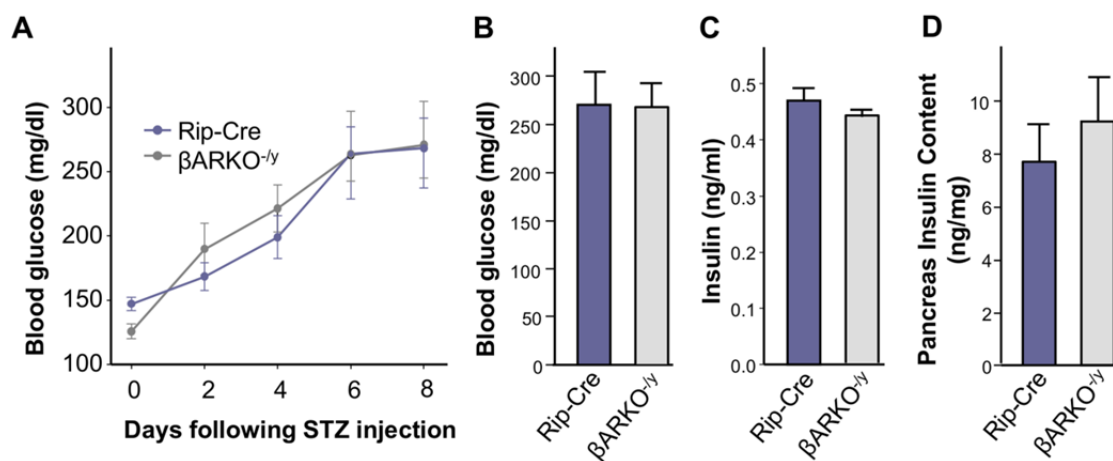
Figure 3.12. **(A)** Blood glucose following STZ-induced diabetes (100 mg/kg). **(B)** Blood glucose at day 8 (post STZ). **(C)** Serum insulin at day 8 (post STZ). **(D)** Pancreas insulin concentration.

A

Brain

← AR 110 KDa

← α tubulin 50 KDa

AR$^{lox/y}$ NARKO$^{-/y}$

B

| Heart | Liver | Pancreas | WAT | Kidney | Muscle | Prostate | Testes | Epididymis |

← AR 110 KDa

← α tubulin 50 KDa

AR$^{lox/y}$ NARKO$^{-/y}$ AR$^{lox/y}$ NARKO$^{-/y}$ AR$^{lox/y}$ NARKO$^{-/y}$ AR$^{lox/y}$ NARKO$^{-/y}$ AR$^{lox/y}$ NARKO$^{-/y}$ AR$^{lox/y}$ NARKO$^{-/y}$ AR$^{lox/y}$ NARKO$^{-/y}$ AR$^{lox/y}$ NARKO$^{-/y}$ AR$^{lox/y}$ NARKO$^{-/y}$
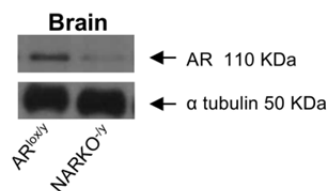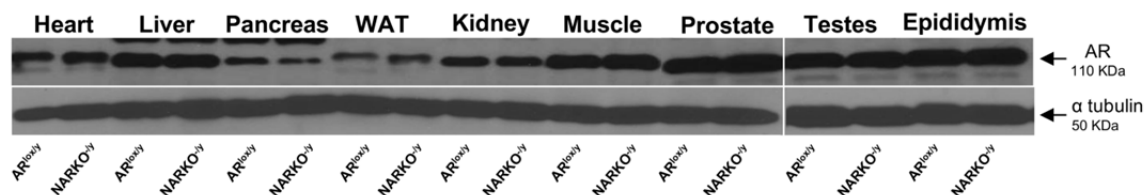
Figure 4.1. **(A)** AR protein expression in whole brain from AR$^{lox/y}$ and NARKO$^{-/y}$ mice was quantified by western blotting. **(B)** Western blot showing AR protein expression in other tissues of AR$^{lox/y}$ and NARKO$^{-/y}$ mice at 12 weeks of age.
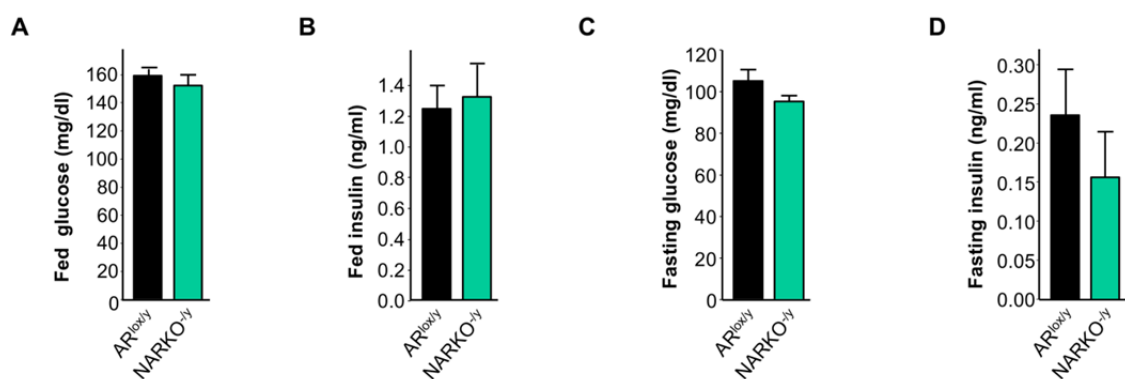
Figure 4.2. Data are from 12 week-old NARKO$^{-/y}$ mice fed on a normal chow (n = 12-15): **(A)** Random fed blood glucose. **(B)** Random fed serum insulin. **(C)** Fasting blood glucose. **(D)** Fasting serum insulin.
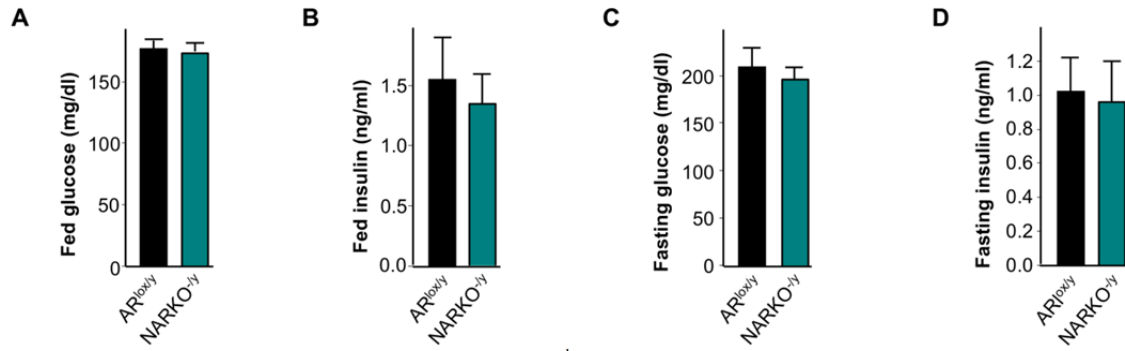
Figure 4.3. Data are from 12 week-old NARKO$^{-/y}$ mice fed on a western diet for 9 weeks (n = 12-15): **(A)** Random fed blood glucose following 9 weeks western diet feeding. **(B)** Fed insulin levels. **(C)** Fasting blood glucose. **(D)** Fasting insulin levels.
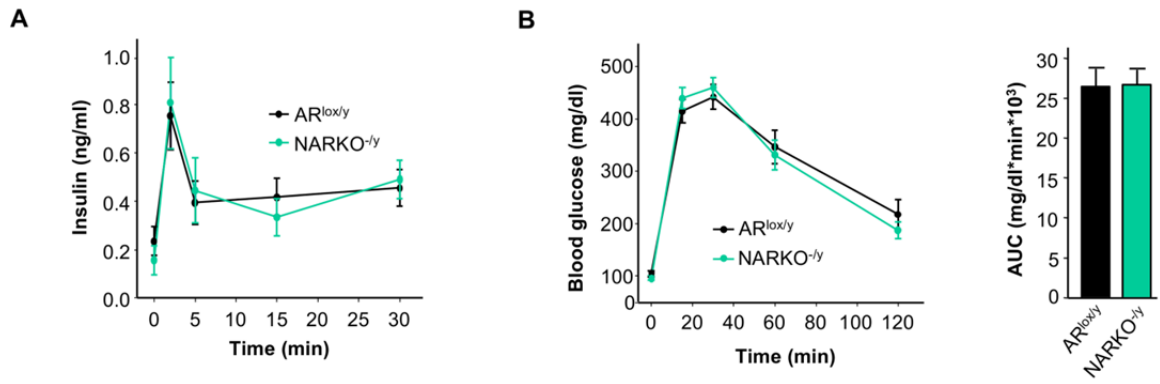
Figure 4.4. Data are from 12 week-old NARKO[-/y] mice fed on a normal chow (n = 12-15): **(A) IP-GSIS (3 g/kg). (B)** IP-GTT (2 g/kg) with glucose AUC.
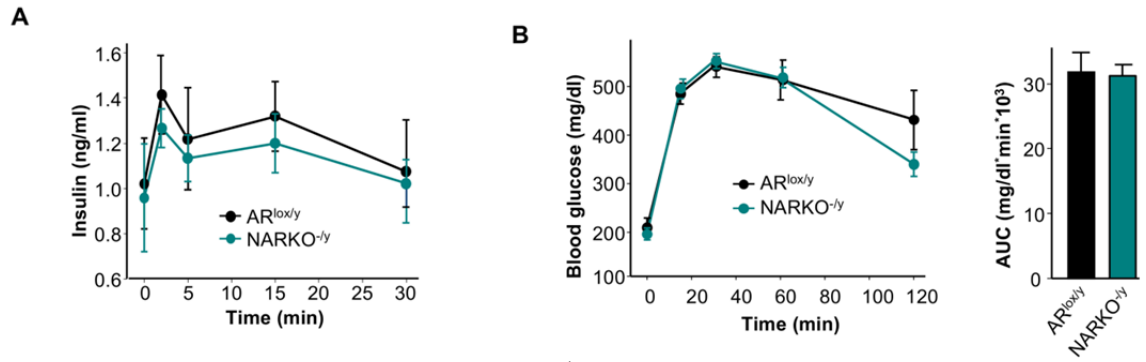
Figure 4.5. Data are from 12 week-old NARKO[-/y] mice fed on a western diet for 9 weeks (n = 12-15): **(A)** GSIS (3 g/kg). **(B)** GTT with glucose AUC. Data are from 20-week old βARKO[MIP] mice fed a western diet for 8 weeks.
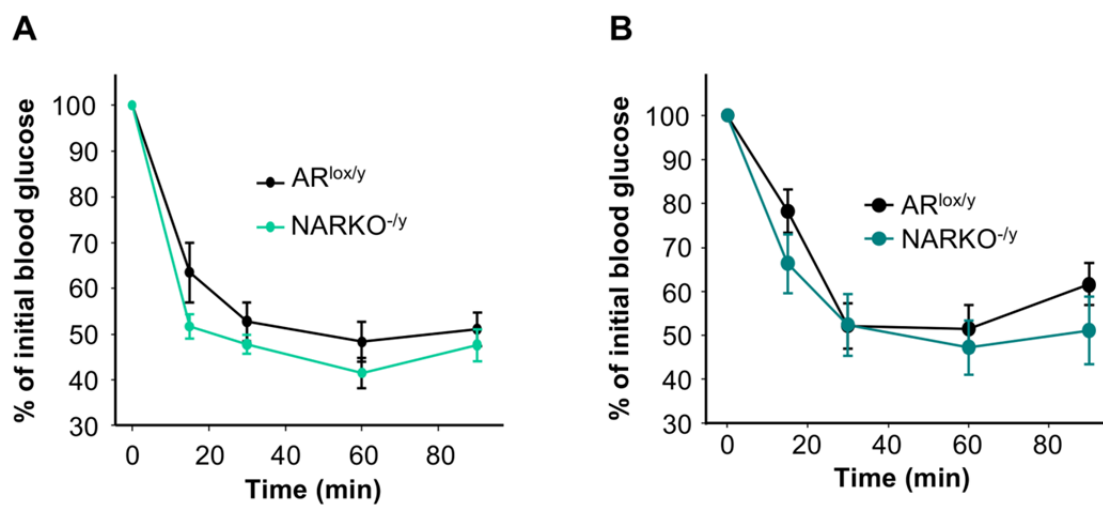
Figure 4.6. **(A)** IP-insulin tolerance test was performed following 6 hr fasting in mice fed on a normal chow (n = 12). **(B)** Insulin tolerance test was performed following 6 hr fasting in mice fed on a western diet (n = 12).

glucagon secretion and improved insulin sensitivity [55]. Therefore, we used AR^{lox} MIP-CreERT mice (without Tam injection) as controls of βARKO^{MIP}. AR^{lox} (with Tam) and AR^{lox} MIP-CreERT (without Tam) displayed similar glucose tolerance (**Figure 4.7**). Tam-induced recombination was induced in adult AR^{lox} MIP-CreERT mice to obtain βARKO^{MIP} mice. Characterization of the βARKO^{MIP} confirmed the selective AR deletion in β-cells (**Figure 4.8A**), but βARKO^{MIP} β-cells exhibited incomplete recombination leading to a 60% decrease in AR expression (**Figure 4.8B**). Despite these limitations, upon exposure to a western diet, βARKO^{MIP} mice exhibited decreased fasting insulin and blunted GSIS following an IP glucose challenge that resulted in glucose intolerance, compared to controls (**Figure 4.9**). The insulin sensitivity remained similar between the two groups (**Figure 4.10**). Taken together, these observations confirm that elimination of AR in β–cells in mice produces a defect in GSIS leading to glucose intolerance.

AR deficiency in β-cells alters GSIS from male islets

To determine whether the altered insulin secretion of βARKO$^{-/y}$ mice was an islet-cell autonomous effect, we studied GSIS in static incubation in cultured islets from male control and βARKO$^{-/y}$ mice that were fed normal chow. Consistent with the importance of AR in GSIS observed *in vivo*, at 16.7 mM glucose, control islets exposed to the natural AR agonist dihydrotestosterone (DHT) showed increased GSIS compared to those exposed to vehicle. The stimulatory effect of DHT on GSIS was abolished in βARKO$^{-/y}$ islets (**Figure 5.1A**). Notably, in all groups of mice, only a minor increase in GSIS was observed when glucose was increased from 2.8 to 16.7 mM, probably as a consequence of the deleterious effect of the RIP-Cre transgene on islet function [51]. Islets from control and βARKO$^{-/y}$ mice fed a western diet showed a modest and non-significant increase in GSIS over basal, which probably resulted from the combined deleterious effect of the RIP-cre transgene and western diet on islet function (**Figure 5.1B**).
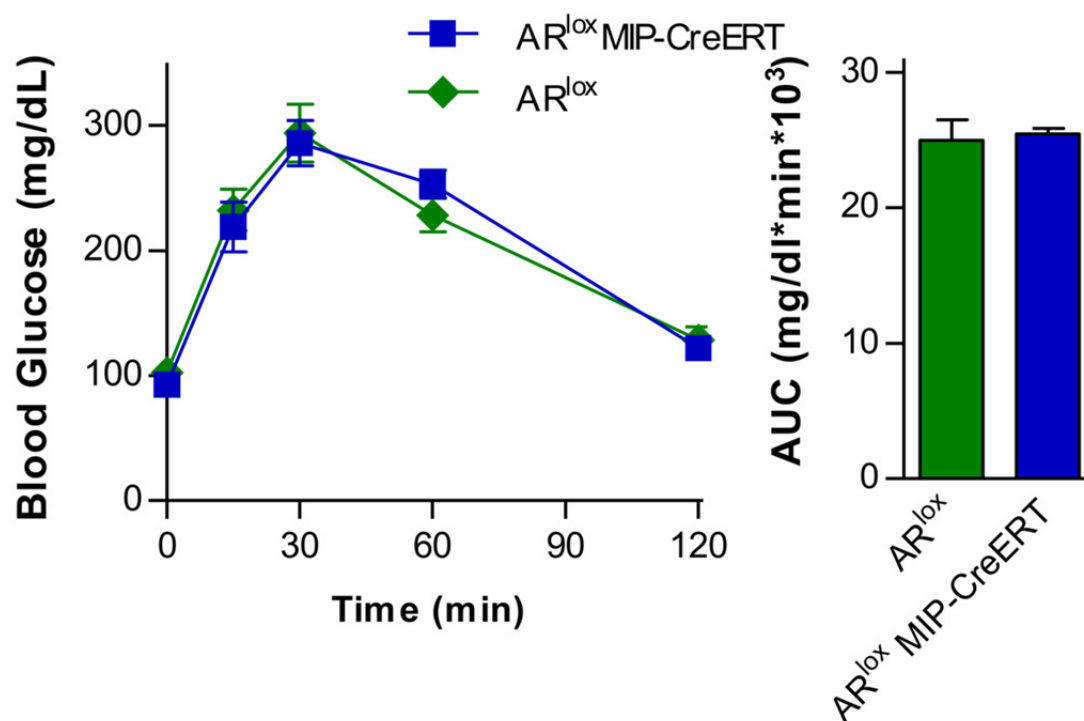
Figure 4.7. IP-Glucose tolerance test (2g/kg) and AUC for glucose from 18 week old mice.

A

B
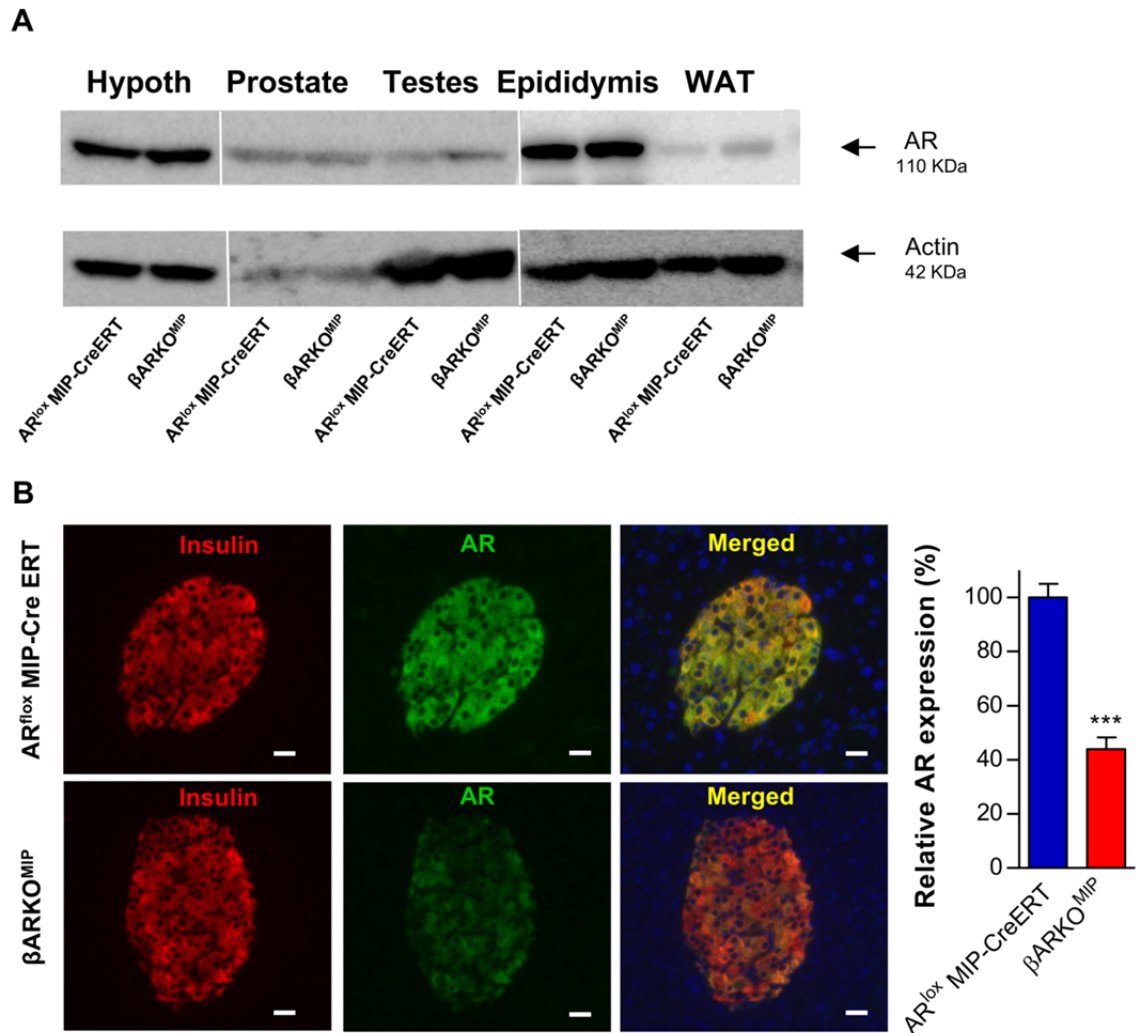
Figure 4.8. **(A)** Western blot showing AR expression in hypothalamus (Hypoth) and in various other tissues of AR^{lox} MIP-CreERT and βARKO^{MIP}. **(B)** Pancreas section showing AR immunofluorescent staining (green) in β-cells co-localizing with insulin (red) in βARKO^{MIP} and control mice, and quantification of relative AR expression in βARKO^{MIP} compared to the control (the scale bar represents 10μm).
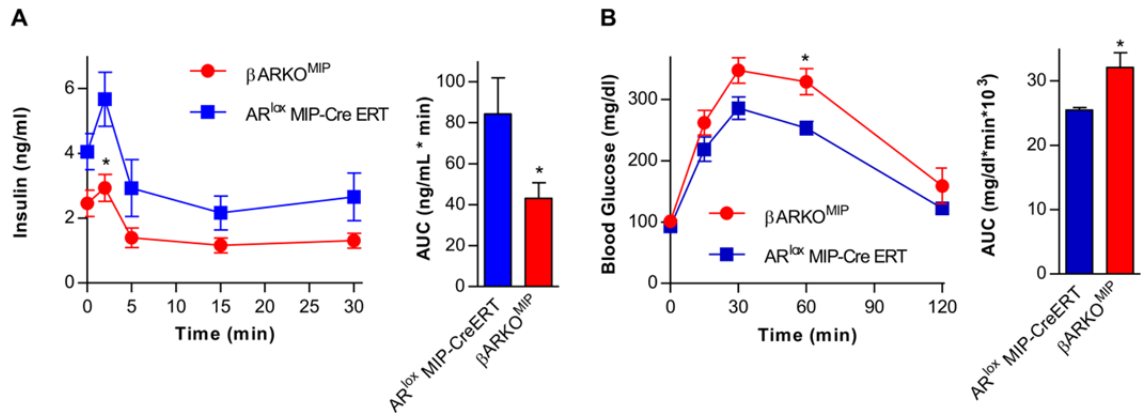
Figure 4.9. **(A)** IP-GSIS (3g/kg) with insulin AUC (n= 5-6). **(B)** IP-GTT with glucose AUC (n= 5-6).

Values represent the mean ± SEM. *P < 0.05.
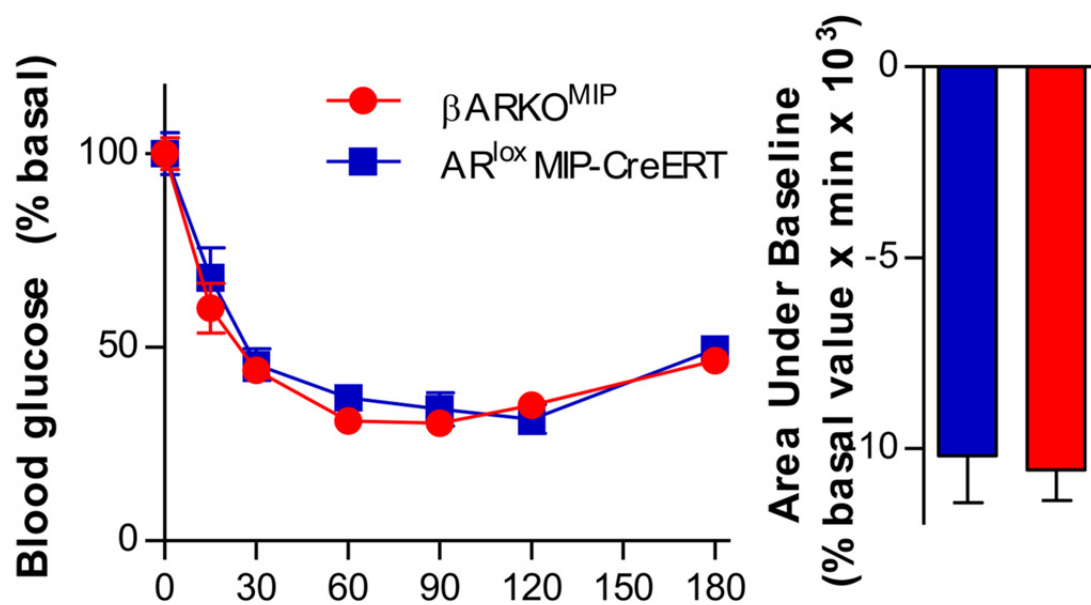
Figure 4.10. IP-insulin tolerance test was performed following 6 hr fasting in mice fed on a western diet (n = 5-6). Values represent the mean ± SEM.
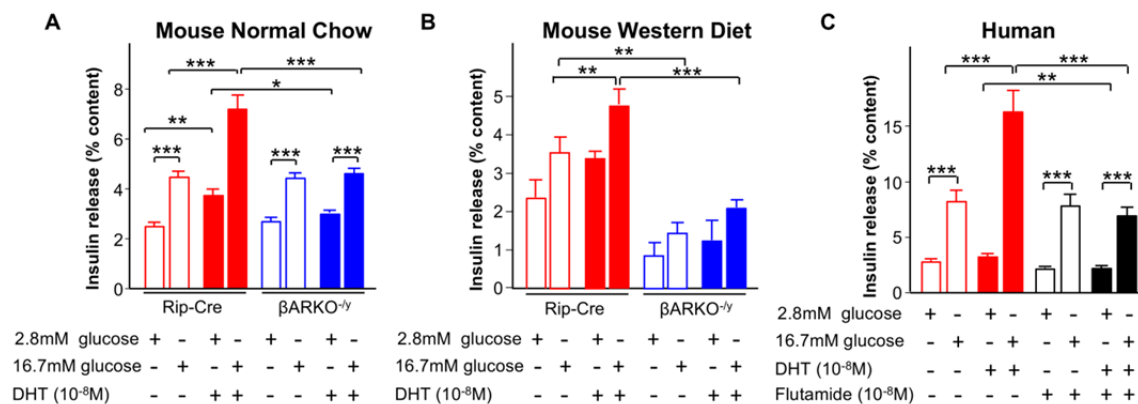
Figure 5.1. **(A)** GSIS measured in static incubation in islets from the indicated mice fed a normal chow and treated with vehicle or DHT (10^{-8} M) *in vitro* for 48 hours prior to static incubation. **(B)** GSIS measured in static incubation in islets from mice fed a western diet for 9 weeks and treated with vehicle or DHT (10^{-8} M) *in vitro* prior to static incubation. **(C)** GSIS measured in static incubation in male human islets treated with vehicle, DHT, or flutamide.

However, at 16.7 mM glucose, control islets exposed to DHT showed increased GSIS compared to vehicle-exposed islets (**Figure 5.1B**). Importantly, compared to control islets, βARKO$^{-/y}$ islets exhibited decreased insulin secretion at both 2.8 and 16.7 mM glucose (**Figure 5.1B**).

We translated these findings to male human islets. Exposure of human islets to a physiological concentration of DHT enhanced insulin secretion in the presence of 16.7 mM glucose, an effect that was abolished by antagonizing AR with flutamide (**Figure 5.1C**). Neither DHT, nor AR genetic elimination, nor pharmacological inhibition affected islet insulin content in mouse or human islets (**Figure 5.2**). To study dynamic insulin secretion *in vitro*, male control and βARKO$^{-/y}$ islets were placed in a perifusion system. In this setting, insulin secretion in response to glucose is characterized by a bi-phasic pattern [56]. The first phase is a rapid and marked, but transient elevation in the secretory rate. The second phase is characterized by a gradual increase in secretion that lasts as long as the glucose stimulus is present. Following DHT stimulation, control islets exhibited enhanced first and second phase insulin secretion compared to vehicle treatment (**Figure 5.3A** and **5.3C-E**). In contrast, the increased first phase was not observed in βARKO$^{-/y}$ islets (**Figure 5.3B** and **5.3C-E**). Further, βARKO$^{-/y}$ islets exhibited aberrant early second phase-insulin secretion (**Figure 5.3E**) and lower global insulin secretion than control islets (**Figure 5.3C-E**).

Extranuclear AR actions enhance GSIS

The AR is a classical ligand-activated nuclear receptor that regulates the expression of target genes through binding to an androgen response element on the promoter of target genes [57-59]. Nongenomic actions of AR are thought to account for rapid, transcription-independent effects of androgens [60]. However, these nongenomic androgen effects have been observed only *in vitro* and await functional validation in animal models. In mouse prostate – a classical
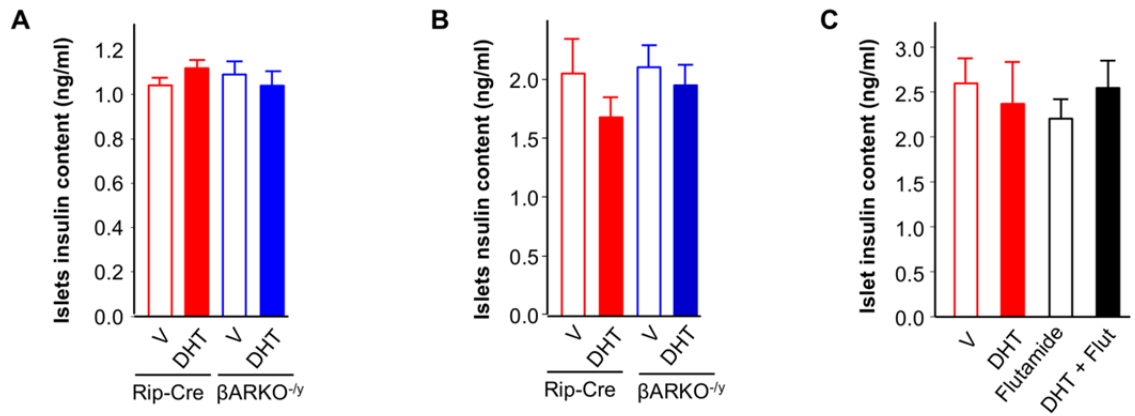
Figure 5.2. **(A)** Islet insulin content from Figure 4.1A. **(B)** Islet insulin content from Figure 4.1B. **(C)** Islet insulin content from Figure 4.1C. Data in Figure 4.1 & 4.2 are from 10 mouse islets or 5 human IEQ per condition (n = 6-8 independent wells). Human islet donors were two Caucasian males under 50 years of age and with a BMI between 25 and 27.
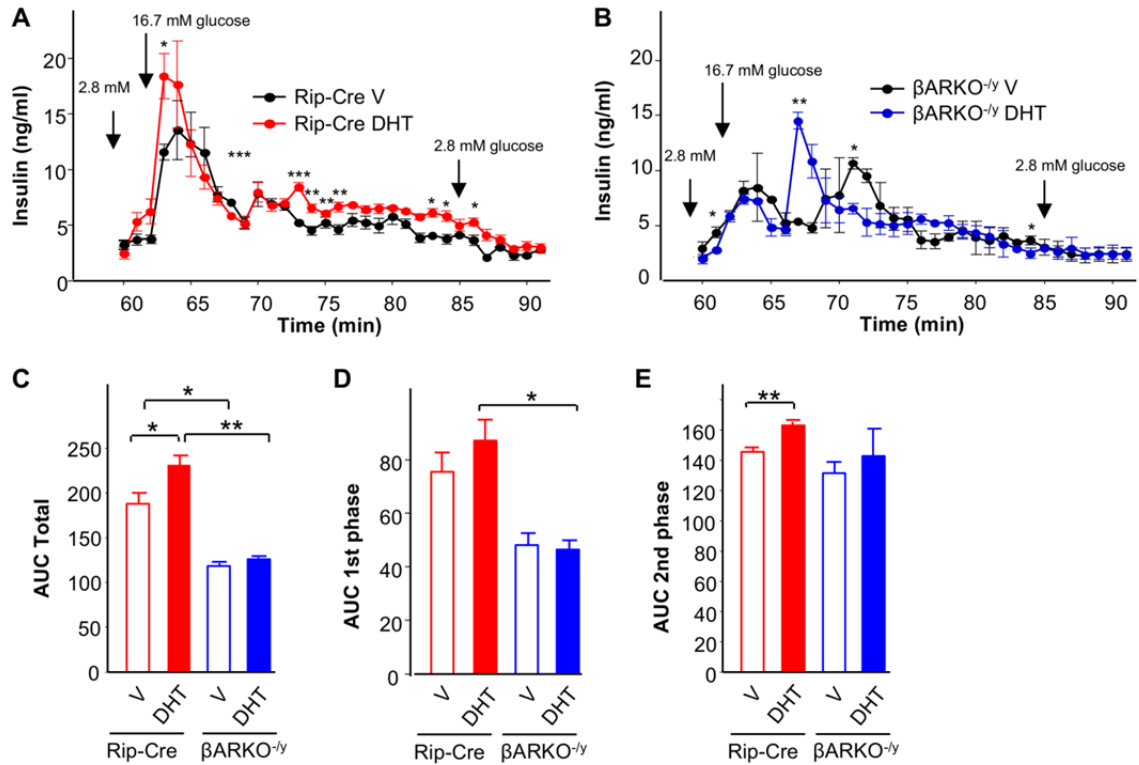
Figure 5.3. **(A)** GSIS during islet perifusion from Rip-Cre mice and **(B)** βARKO$^{-/y}$ mice. **(C)** Total AUC from GSIS (60 to 90min). **(D)** AUC from the 1st phase GSIS (60 to 65min). **(E)** AUC from the 2st phase GSIS (65 to 90min). Islets were isolated from 12-14 weeks old mice and perifused in batches of 60 islets per group. Values represent the mean ± SEM. *P < 0.05, **P = 0.01.

androgen target tissue – AR immunohistochemical staining showed nuclear localization (**Figure 6.1A**). In male mouse pancreatic islets and in male human islets; however, AR colocalized with insulin in a predominant extranuclear localization (**Figure 6.2A & C and Figure 6.1B**) and was not observed in α-cells (**Figure 6.2B**). We studied AR subcellular localization by confocal microscopy following binding of DHT in human prostate adenocarcinoma LNCaP cells — a classical model of AR nuclear actions — and in INS-1 rat insulin-secreting cells. In the absence of DHT, AR signal was predominantly extranuclear in LNCaP and INS-1 cells. As expected, upon DHT stimulation, AR underwent nuclear translocation in LNCaP cells (**Figure 6.3A**). In contrast, following DHT stimulation, AR remained predominantly in the extranuclear compartment of INS-1 cells (**Figure 6.3B**). Similar findings were observed in the MIN-6 mouse insulin-secreting cells (**Figure 6.1C**). We next studied AR subcellular localization by subcellular fractionation. Confirming results obtained by microscopy, in LNCaP cells, DHT produced a robust nuclear translocation of AR starting at 20 min and sustained for at least 8h (**Figure 6.4A**). In contrast, in INS-1 cells, DHT produced a weak nuclear translocation of AR and the activated AR remained mainly in the cytosolic fraction (**Figure 6.4B**).

Mechanism of AR potentiation of GSIS in pancreatic β-cells

Having established that ligand-activated AR exhibits a preferential extranuclear location in β-cells, we sought to determine whether this extranuclear location is instrumental in stimulating GSIS. To this end, we synthesized a novel androgen dendrimer conjugate (ADC) that selectively activates extranuclear AR signaling pathways, but remains outside the nucleus (**Table 1** and **Figure 7.1**). We successfully used a similar estrogen dendrimer conjugate to validate the function of extranuclear estrogen receptors in β-cell function and survival [45, 61-64]. We confirmed that unlike DHT, ADC 1) cannot increase AR-dependent gene transcription in cells
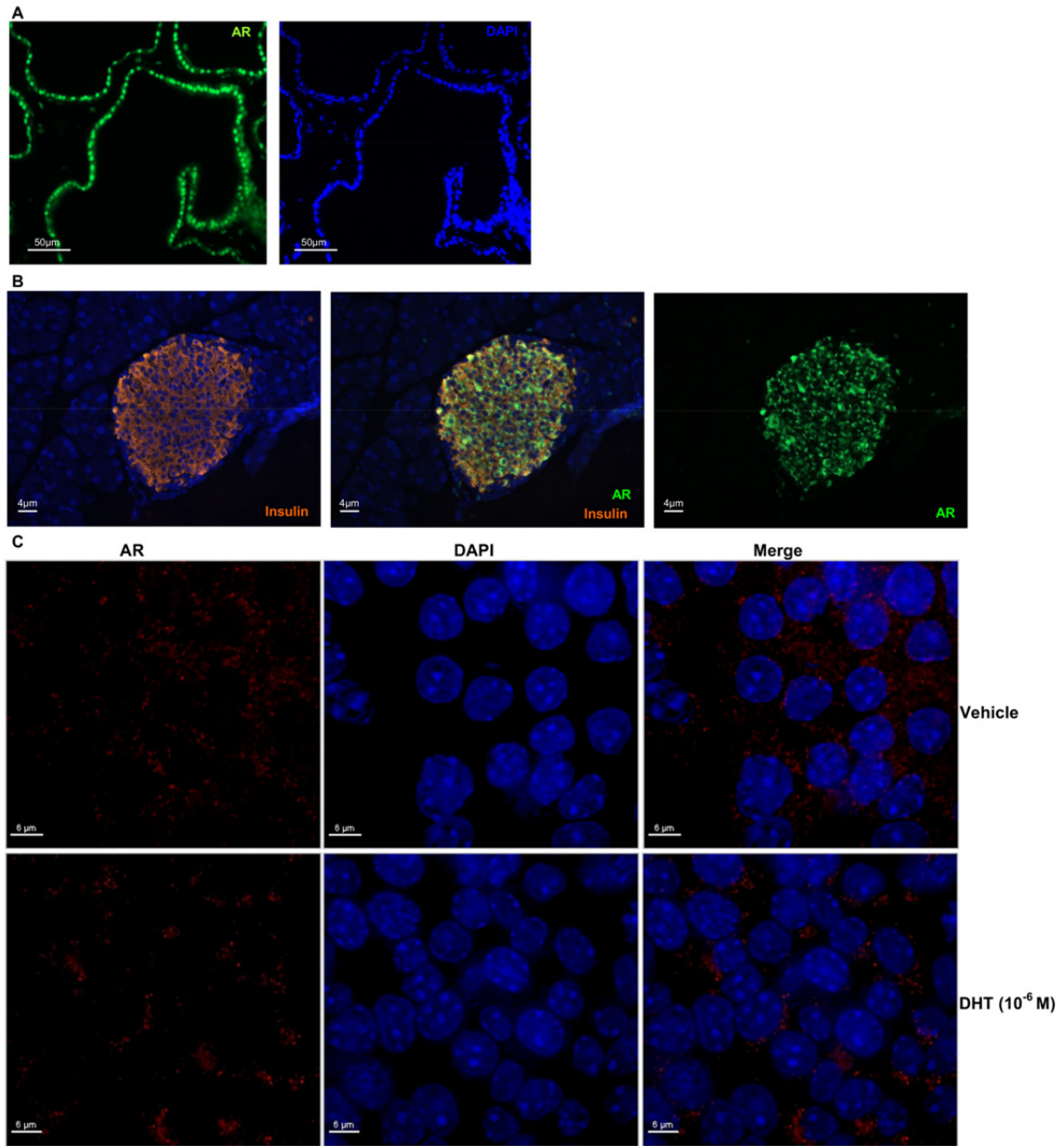
Figure 6.1. **(A)** A mouse prostate depicting AR (green) immunofluorescent staining and DAPI (blue). **(B)** Male mouse pancreatic islet with immunofluorescent staining with insulin (orange), AR (green), and DAPI (blue). **(C)** MIN-6 insulin-secreting cell showing immunofluorescent staining of AR (Red) following DHT stimulation.
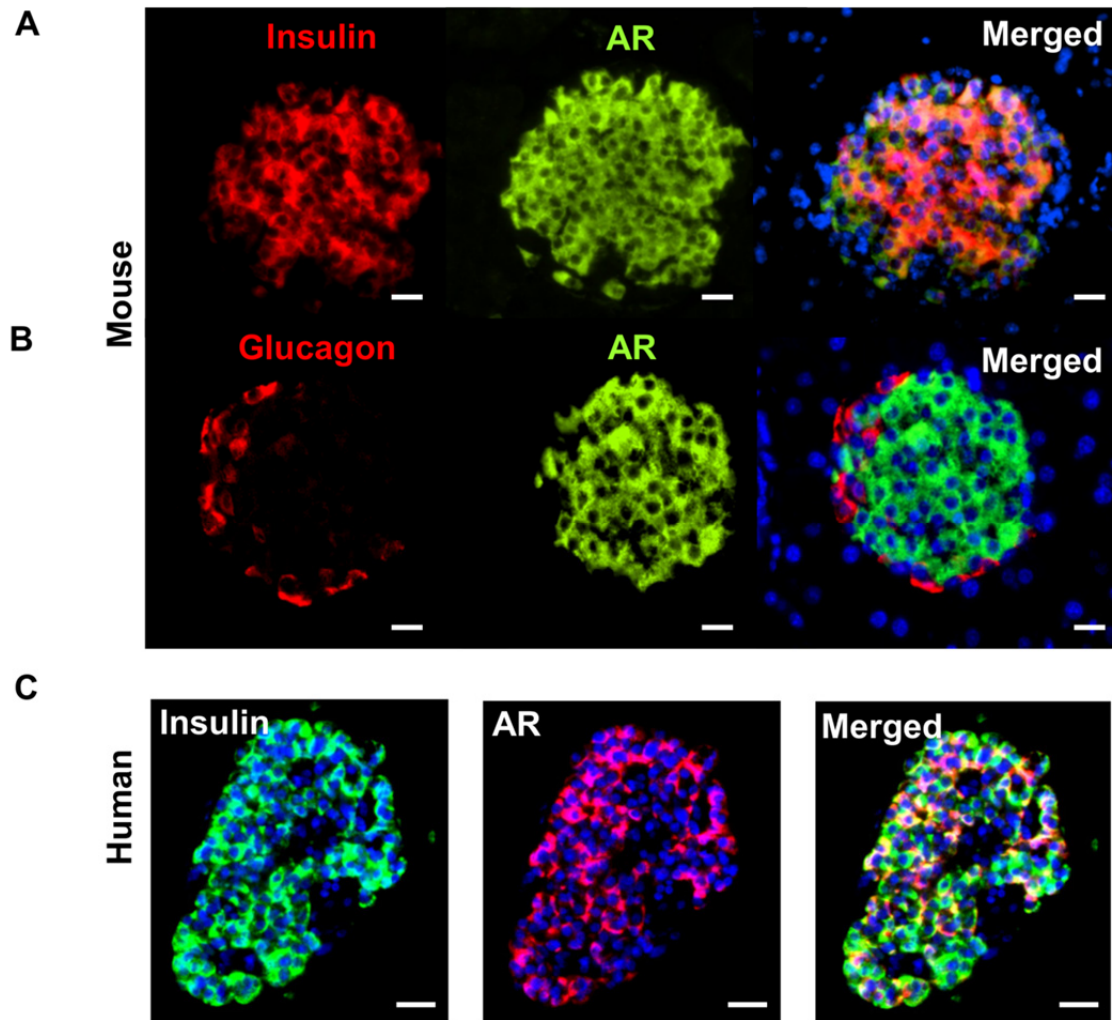
Figure 6.2. **(A-B)** Mouse pancreas section showing an islet with AR immunofluorescent staining (green) in β-cells colocalizing with insulin (red) and DAPI (blue) merged images (the scale bar represents 10µm). **(C)** Human islet showing AR (green) expression (the scale bar represents 20µm).
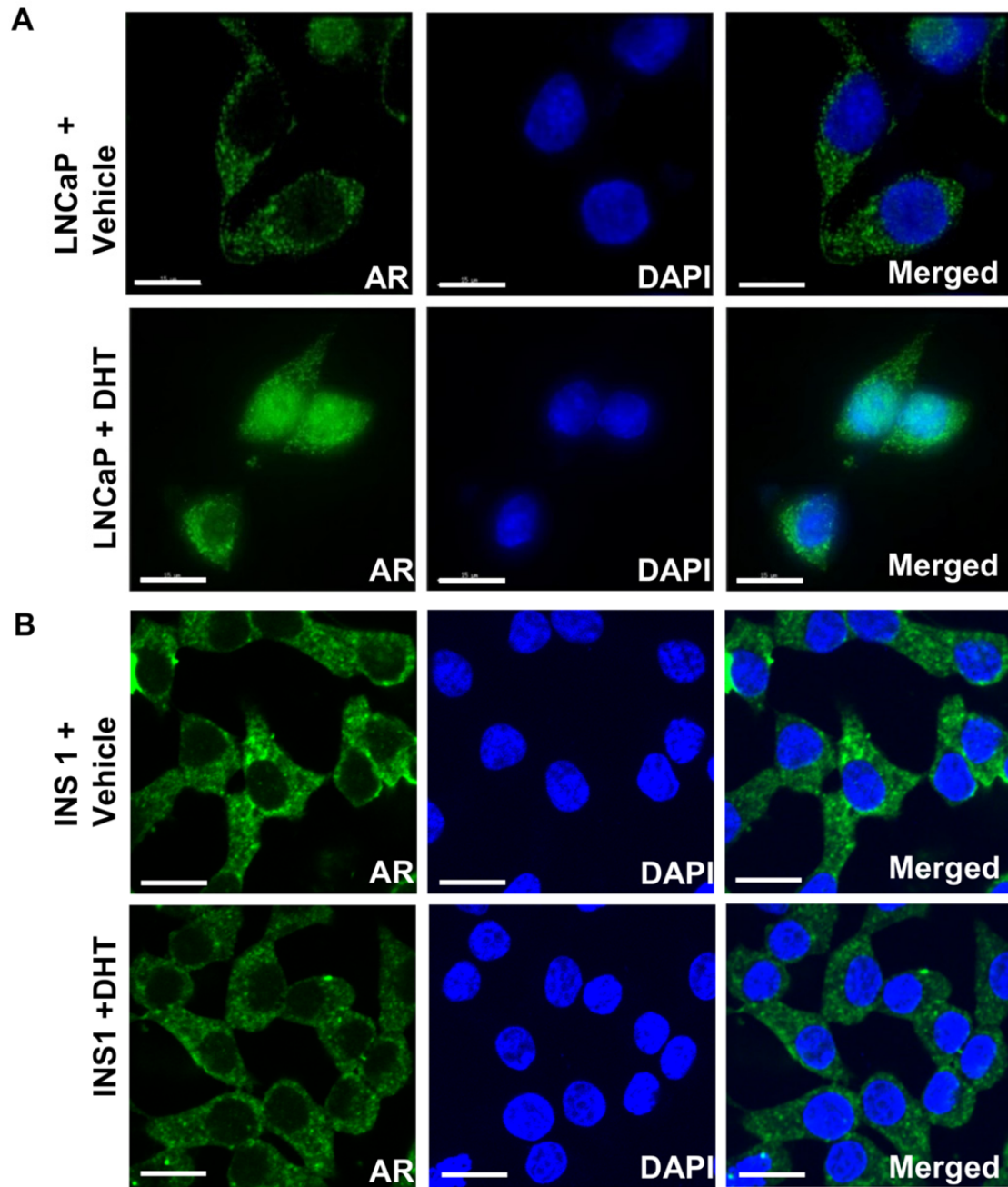
Figure 6.3. Immunofluorescent staining of AR (green) in **(A)** LNCaP cell and **(B)** INS-1 cell treated with Vehicle or DHT for 40 minutes and imaged by confocal microscopy (the scale bar represents 15μm).
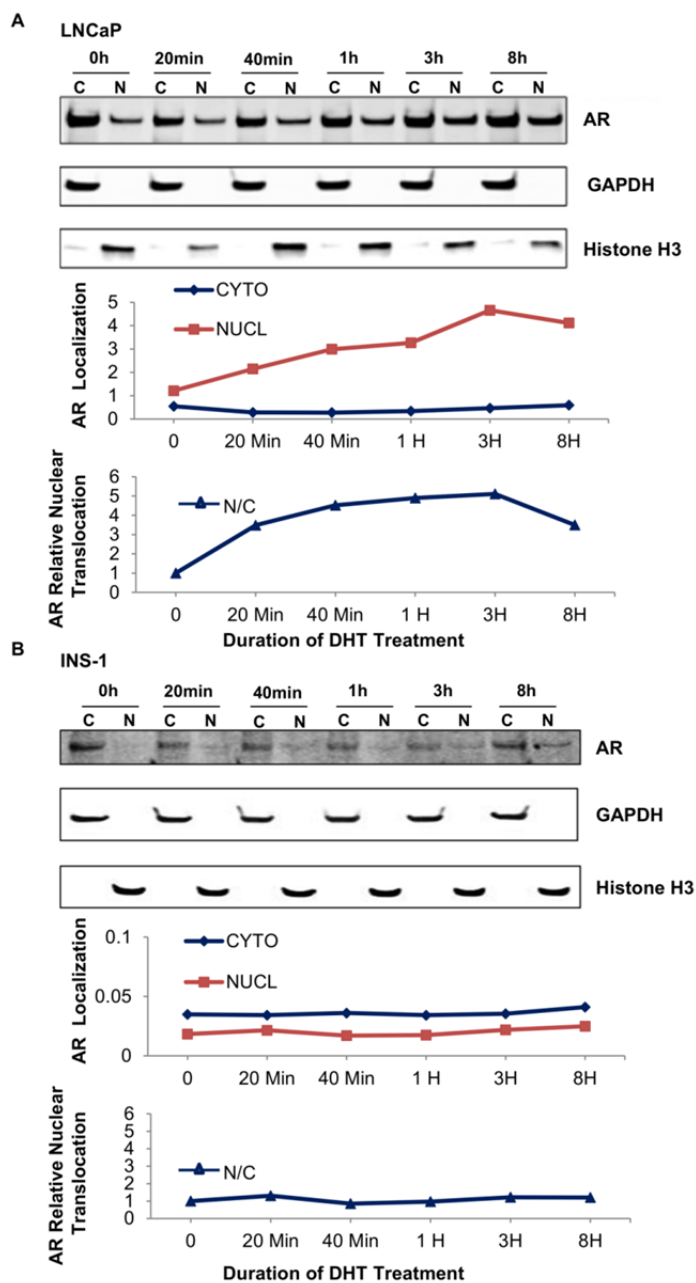
Figure 6.4. **(A)** LNCaP cells and **(B)** INS-1 cells treated with DHT at the indicated time points, followed by subcellular fractionation. Upper panels show representative immunoblots of AR, GAPDH (cytosolic marker), Histone H3 (nuclear marker) expression. Middle panels: AR cytosolic and nuclear localizations were quantified by dividing AR expression by the expression of the respective markers. Lower panels: AR relative nuclear translocation was calculated as the ratio of nuclear (N) over cytosolic (C) AR expression. N = 3 independent experiments.

Name	Structure	Relative Binding Affinity to R1881
Androgen Dendrimer Conjugate (ADC)		0.272
Dendrimer		0.813
ADC-Cy5		0.832
Dendrimer-Cy5		0.016

Table 1. Compound structure and relative binding affinity (RBA) to R1881. AR agonist was conjugated to a PAMAM dendrimer (gray circle) through a tether to create androgen dendrimer conjugate (ADC), and it was then labeled with Cy5 to produce ADC-Cy5. The table shows the structure and RBA of each compound.
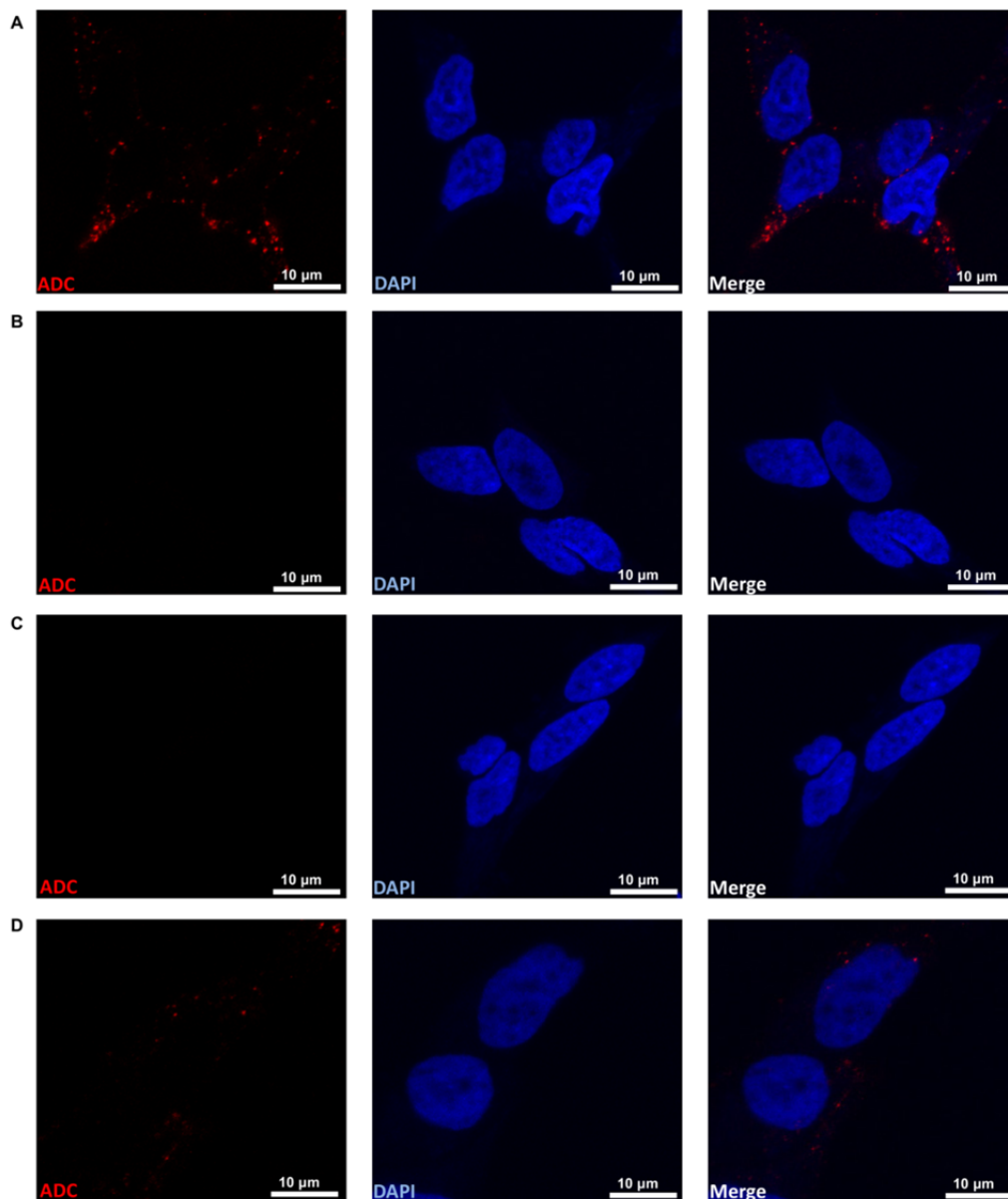
Figure 7.1. In **(A)**-**(D)**, LNCaP cells were treated with the indicated compounds for 4 hours (the scale bar represents10µm). **(A)** Treatment with 100 nM ADC-Cy5 showed exclusively extranuclear fluorescent signal. **(B)** Treatment with 30 nM dendrimer-Cy5 showed no fluorescence, indicating there was no uptake of dendrimer without the ligand. **(C)** Treatment with 100nM ADC non fluorescent control. **(D)** Treatment with 100 nM ADC-Cy5 in the presence of 50-fold excess of the potent AR ligand R1881 shows a marked decrease in the fluorescent signals, demonstrating specific AR binding of ADC.

transfected with a reporter construct containing an androgen response element (ARE) (**Figure 7.2A**), and 2) cannot increase the expression of the prostate specific antigen, an AR target gene containing an ARE [65] (**Figure 7.2B**). In contrast, in cultured mouse and human islets, selectiveextranuclear activation of AR using ADC was as efficient as DHT in enhancing GSIS (**Figure 7.3**).

The observation that ligand-activated extranuclear AR stimulates GSIS in β-cells led us to hypothesize that in these cells, DHT-activated AR interacts with membrane or cytosolic molecules to enhance GSIS. GSIS is triggered by glucose metabolism that leads to increased ATP/ADP ratio, the closure of ATP sensitive K^+ channels that is followed by membrane depolarization, opening of Ca^{2+} channels, and influx of intra-cellular calcium $[Ca^{2+}]_i$ [66]. Using male WT islets exposed to KCl at low glucose to depolarize the cell membrane, we investigated whether AR acts through K_{ATP} channels and membrane depolarization independently of glucose metabolism. As expected, KCl-treated islets showed increased insulin secretion (**Figure 7.4**). However, we observed no further effect of DHT on insulin secretion, an observation demonstrating that AR does not potentiate insulin secretion triggered by depolarization alone (**Figure 7.4**). We next investigated whether AR activation could stimulate glucose metabolism (and therefore ATP generation) and subsequent $[Ca^{2+}]_i$ influx. Increasing glucose concentration from 2.8 to 11 and 16.7 mM increased ATP concentration in male WT mouse islets (**Figure 7.5A**). However, exposure to DHT did not result in a further increase in ATP concentration in these islets (**Figure 7.5A**). Similar results were obtained when we quantified the ATP/ADP ratio (**Figure 7.5B**). Consistent with these findings, at 11mM glucose, DHT did not significantly increase ATP concentration in control or βARKO$^{-/y}$ islets (**Figure 7.5C**). However, it is important to stress that βARKO$^{-/y}$ islets displayed decreased ATP concentration compared to control islets (**Figure 7.5C**).

A

B
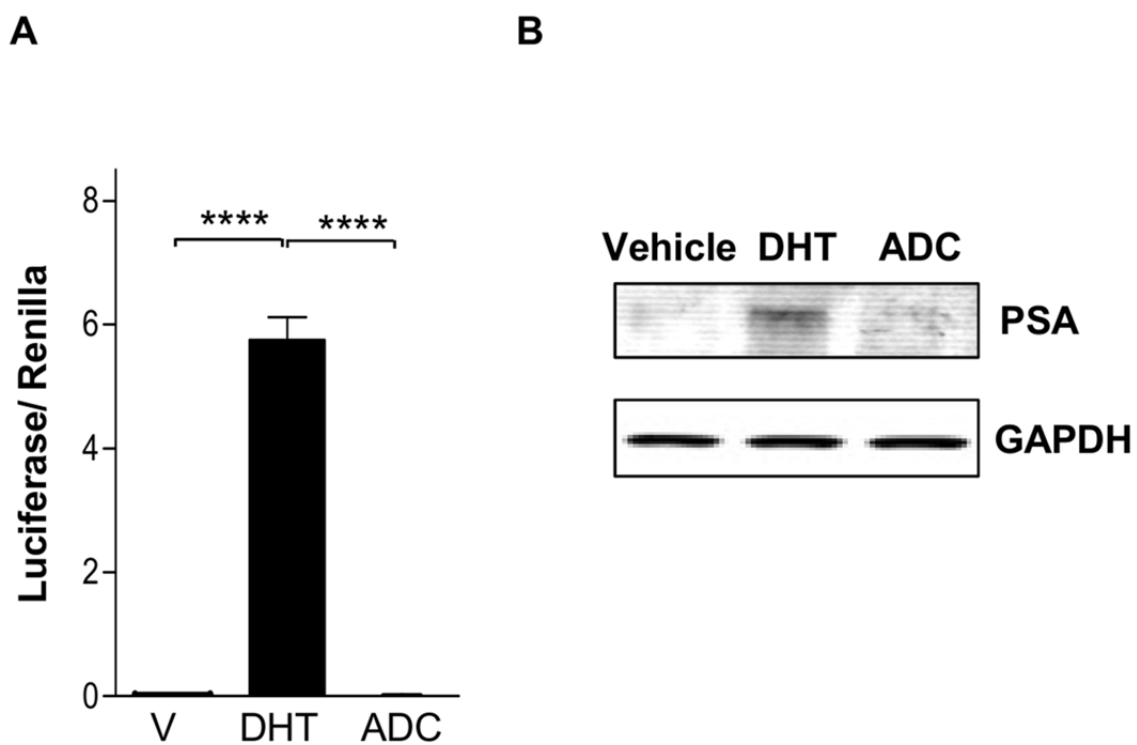
Figure 7.2. **(A)** Luciferase activity measured in LNCaP cells following a 6 hours treatment by DHT

(10^{-8} M) and ADC (10^{-7} M) (n=4 independent wells). **(B)** PSA protein expression inn LNCaP cells

after 2 days of DHT and ADC treatment.
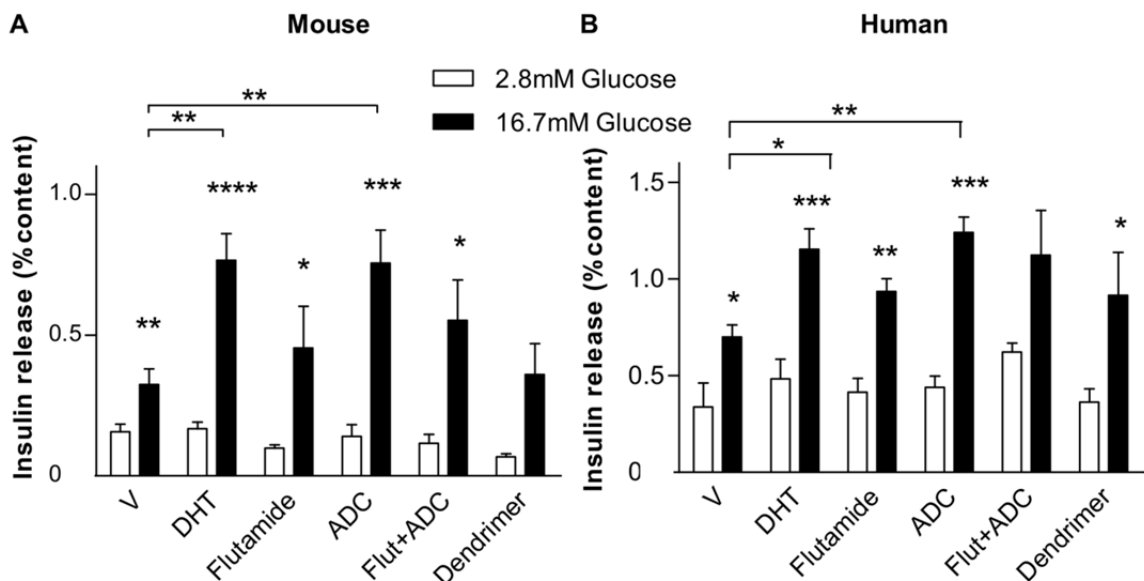
Figure 7.3. **(A)** GSIS measured in static incubation in WT male mouse islets treated with vehicle, DHT (10^{-8} M), flutamide (10^{-8} M), ADC (10^{-7} M), and ADC plus flutamide, dendrimer (concentration adjusted to ligand concentration in ADC) *in vitro* for 40 minutes. Results from 2 experiments (n= 6 independent wells). **(B)** GSIS measured in static incubation in male human islets treated with vehicle, DHT (10^{-8} M), flutamide (10^{-8} M), ADC (10^{-7} M), and ADC plus flutamide, dendrimer *in vitro* for 40 minutes. Results from 2 experiments (n= 6 independent wells). Human donors were a male Caucasian aged 28 with BMI 18.6 and a male Latino aged 61 with BMI 25.8. The results were the average from 2 different donors/experiments. 10 mouse islets or 10 IEQ were used per condition.
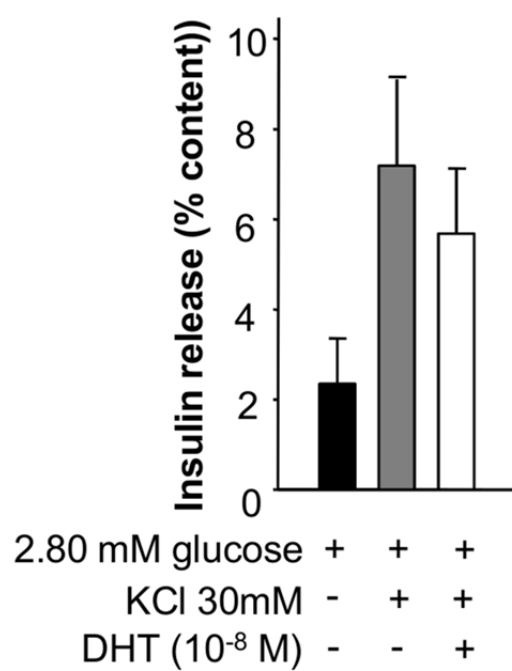
Figure 7.4. Effect of DHT on insulin secretion at low glucose and KCl (30 mM) during a 30 min stimulation (n = 6 independent wells, 10 mouse islets were used per condition).
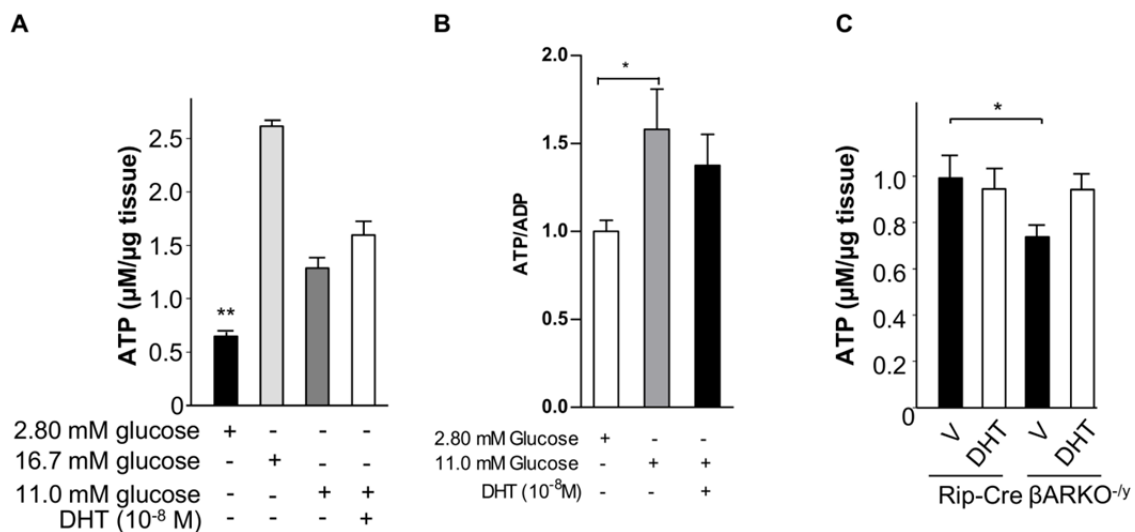
Figure 7.5. **(A)** ATP concentration measured on lysates from WT male islets following stimulation with glucose and DHT for 30 min (n = 10 independent wells, at least 3 experiments). **(B)** ATP/ADP measured on WT male islets after treatment with 10 nM DHT for 30 minutes (n = 4 independent wells, and 2 independent experiments). **(C)** ATP levels measured on islets from male RIP-Cre and βARKO$^{-/y}$ islets following 30 min DHT stimulation and at 11mM glucose.

We then explored whether DHT could increase $[Ca^{2+}]_i$ influx. Consistent with results for ATP concentration, raising glucose concentration increased $[Ca^{2+}]_i$ influx in both control and βARKO$^{-/y}$ islets (**Figure 7.6**). However, consistent with results for ATP content, DHT did not further increase $[Ca^{2+}]_i$ in control or βARKO$^{-/y}$ islets (**Figure 7.6**). Notably, at high glucose, as in the case of ATP concentration, βARKO$^{-/y}$ islets exhibited decreased $[Ca^{2+}]_i$ compared to control islets (**Figure 7.6**). Thus, DHT increased insulin secretion without increasing glucose metabolism or $[Ca^{2+}]_i$ influx. We interpreted the decreased ATP and $[Ca^{2+}]_i$ in βARKO$^{-/y}$ islets as consequences of glucose desensitization leading to decreased glucose metabolism and ATP production. Indeed, genes involved in dedifferentiation of β-cells secondary to hyperglycemia (GK, GLUT2) were downregulated in glucose intolerant male βARKO$^{-/y}$ islets compared to controls. In contrast, these genes were not decreased in islets from normoglycemic female βARKO$^{-/-}$ mice (**Table 2**).

The finding that DHT acting on AR enhanced GSIS without increasing cellular ATP generation or $[Ca^{2+}]_i$ influx suggested to us that AR activation amplifies GSIS by acting downstream and augmenting the Ca^{2+} signal. Incretins like glucagon-like peptide-1 (GLP-1) potentiate GSIS by increasing β-cell concentrations of cyclic adenosine monophosphate (cAMP) [67]. We explored the effect of DHT on cAMP production in islets from male mice. In control male islets, DHT increased cAMP production by approximately two fold (**Figure 8.1A**). In contrast, the effect of DHT in increasing cAMP levels was not observed in βARKO$^{-/y}$ islets (**Figure 8.1A**) or in WT islets treated with the AR antagonist flutamide (**Figure 8.1B**), an observation demonstrating its dependence on AR. Note that in these experiments, DHT-induced cAMP production was independent from phosphodiesterase (PDE) inhibition since DHT increased cAMP concentration over vehicle in islets preincubated with PDE inhibitors. An increase in intracellular cAMP concentration activates the cAMP-dependent protein kinase A (PKA) [68].
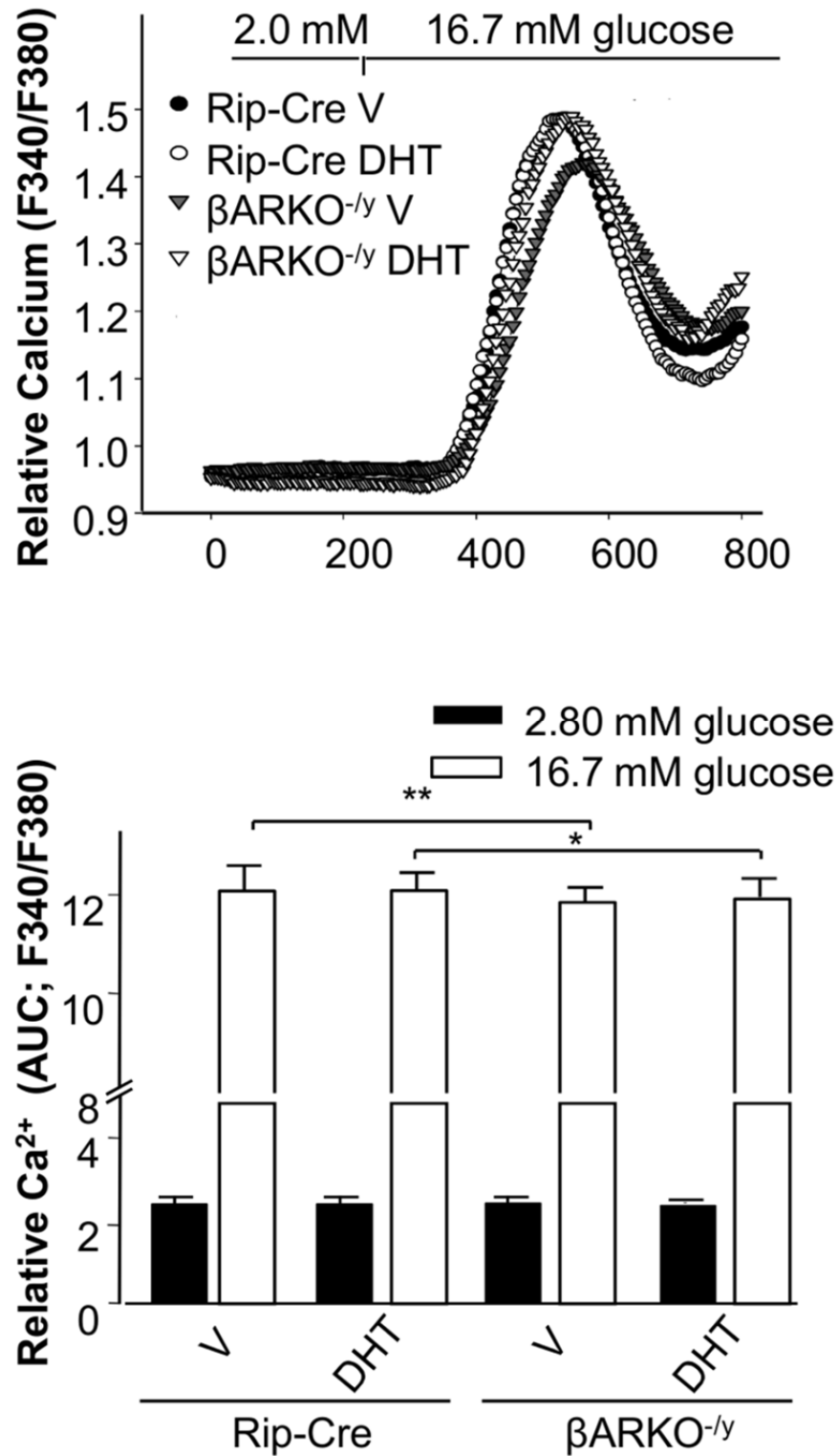
Figure 7.6. Intracellular Ca^{2+} influx in isolated mouse islets from Rip-Cre and βARKO$^{-/y}$ mice (left)

and corresponding AUC (right) from the indicated glucose concentrations.

Gene	M Rip-Cre	M βARKO$^{-/y}$	p-value	F Rip-Cre	F βARKO$^{-/-}$	p-value
Ins2	1.0 ±0.32	0.29 ±0.14	0.14	1.0 ±0.12	1.00 ±0.12	0.97
Glut2	1.0 ±0.26	0.26 ±0.06	0.05	1.0 ±0.05	0.92 ±0.08	0.43
Ucp2	1.0 ±0.37	0.63 ±0.34	0.13	1.0 ±0.13	1.00 ±0.23	0.87
Gck	1.0 ±0.49	0.23 ±0.10	0.04	1.0 ±0.07	1.30 ±0.06	0.01
Hk1	1.0 ±0.11	0.97 ±0.08	0.84	1.0 ±0.09	0.90 ±0.11	0.85
Gcg	1.0 ±0.00	0.74 ±0.00	0.21	1.0 ±0.20	0.92 ±0.09	0.69

Table 2. Differentially expressed genes in βARKO$^{-/y}$ and its control. Islets were isolated from male and female βARKO mice and from their respective controls. The indicated mRNA expression levels were quantified by qPCR.
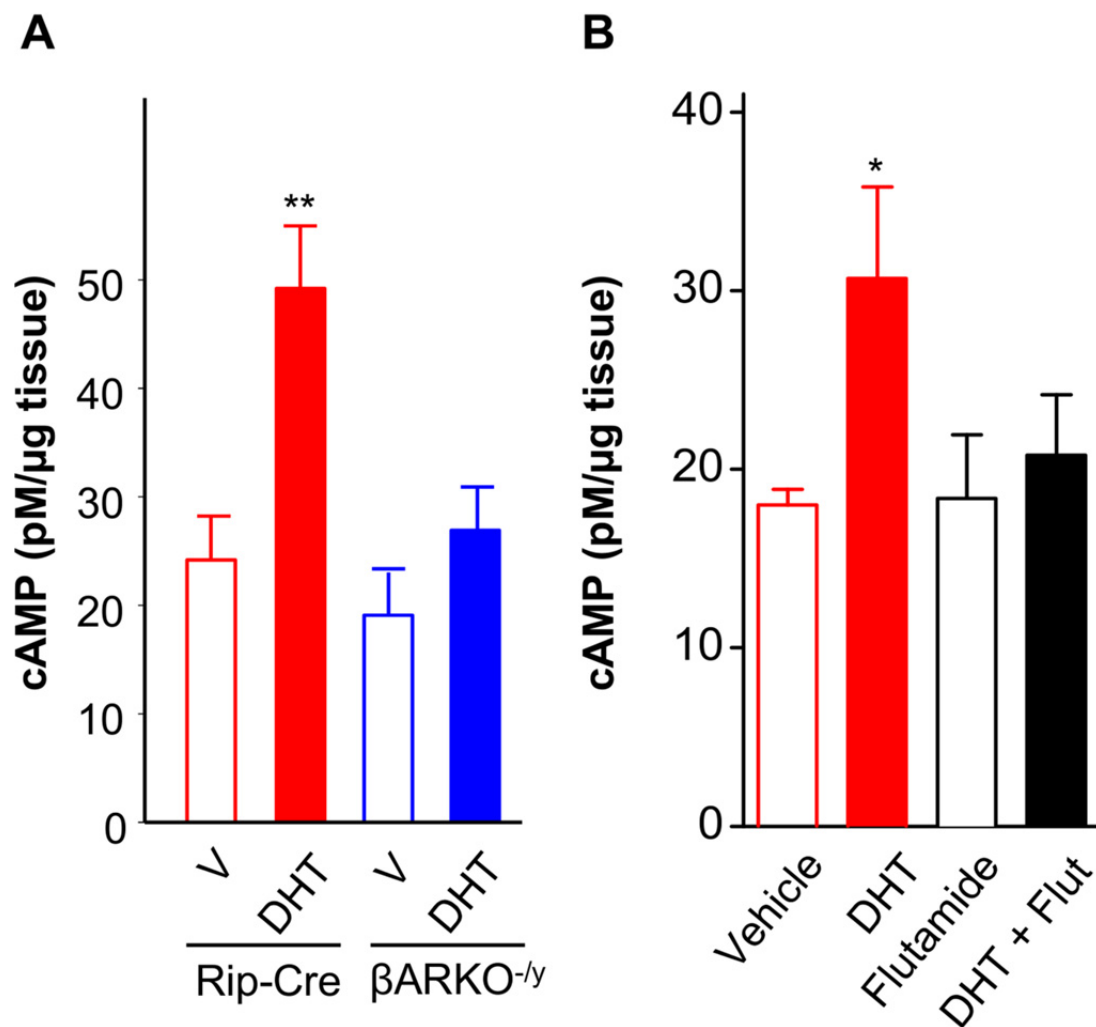
Figure 8.1. **(A)** cAMP concentrations measured in the indicated male mouse islets stimulated with DHT (10^{-8}M) for 30 min. cAMP was measured by an enzyme-linked immunoassay. Results from 3 experiments (n = 6 independent wells). **(B)** cAMP measured in WT male islets treated with vehicle, DHT (10^{-8} M), flutamide (10^{-8} M), and DHT plus flutamide, supplemented with 200uM IBMX in each condition. Results from 2 experiments (n = 3 independent wells)

To determine whether DHT-mediated potentiation of GSIS was dependent on PKA activation, we used H-89, the PKA inhibitor. While DHT potentiated GSIS in cultured WT male islets, the DHT effect was ablated in the presence of H-89 (**Figure 8.2A**). Further, activation of PKA leads to phosphorylation of the cAMP response element-binding protein (CREB). In male mouse islets, DHT exposure produced a rapid phosphorylation of CREB (**Figure 8.2B**). Thus, AR activation by DHT potentiates GSIS in a cAMP and PKA-dependent manner.

Interestingly, the insulinotropic effect of DHT observed in mouse and human islets was not observed in INS-1 cells (**Figure 8.3A**) despite the fact that INS-1 cells express AR (**Figure 6**), suggesting that the insulinotropic effect of DHT requires a secreted factor, produced by islet non-β-cells, that acts on β-cells in a paracrine manner. Therefore, we explored the hypothesis that AR action in β-cells amplifies GLP-1R signaling to increase cAMP production, thus potentiating the insulinotropic action of GLP-1. We reasoned that because GLP-1 is produced by cultured islet α-cells [69, 70], DHT enhances GSIS in cultured islets (which produce GLP-1) but not in cultured INS-1 cells (which do not produce GLP-1). Consistent with this hypothesis, in mouse and human islets **(Figure 8.4A)** and in INS-1 cells (**Figure 8.3B**), DHT amplified the insulinotropic effect of GLP-1 on GSIS. To explore the possibility that DHT amplification of GSIS requires a functional GLP1-R, we studied the effect of DHT in the presence of the selective GLP1-R antagonist exendin (9-39) and in absence of exogenous GLP-1 [71]. The effect of DHT in amplifying GSIS was abolished in the presence of exendin (9-39) (**Figure 8.4B**). Together, these studies demonstrate that DHT amplifies the insulinotropic effect of exogenous and islet-derived GLP-1 and this effect requires a functional GLP-1R.
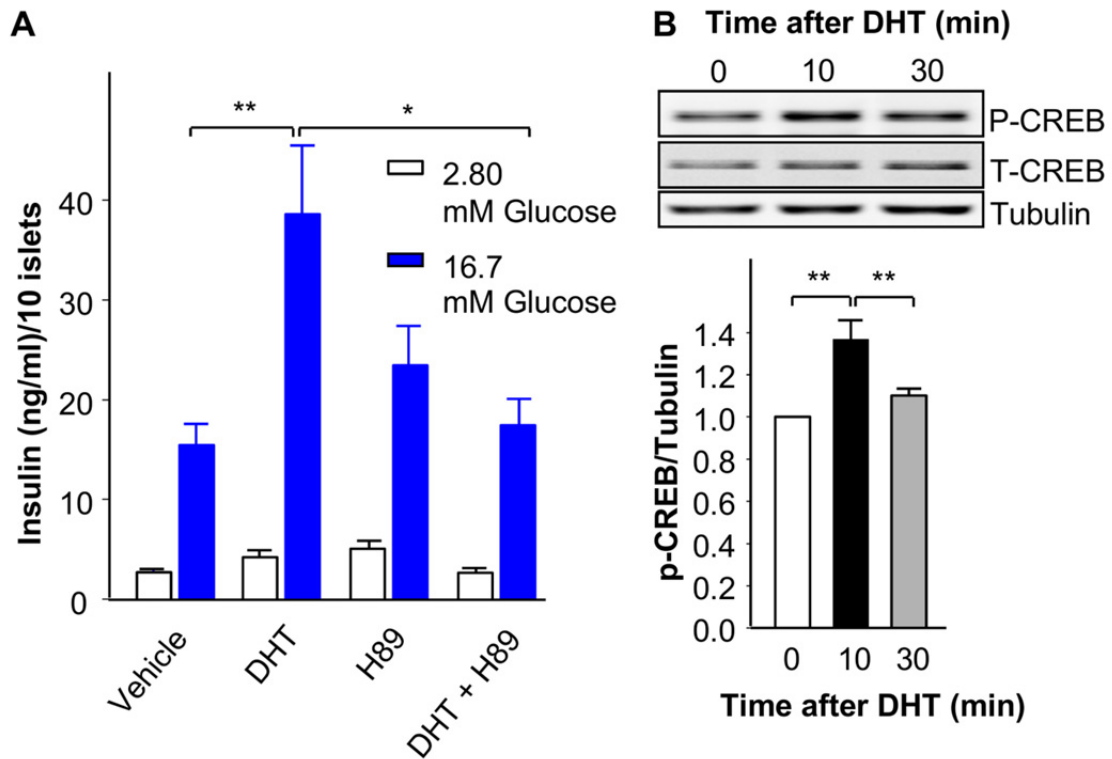
Figure 8.2. **(A)** GSIS measured in static incubation in islets from WT male mice treated with vehicle or DHT (10^{-8}M) in vitro for 48 hours and H89 (10µM) 30 minutes prior to stimulation. Results from 4 experiments (n= 12 independent wells). **(B)** Phosphorylation of CREB measured by western blotting in WT male islets treated with DHT for 10 and 30 min. Blots are representative of 3 experiments. Islets were isolated from mice 12-14 weeks of age. Values represent the mean ± SEM. *P < 0.05, **P = 0.01.
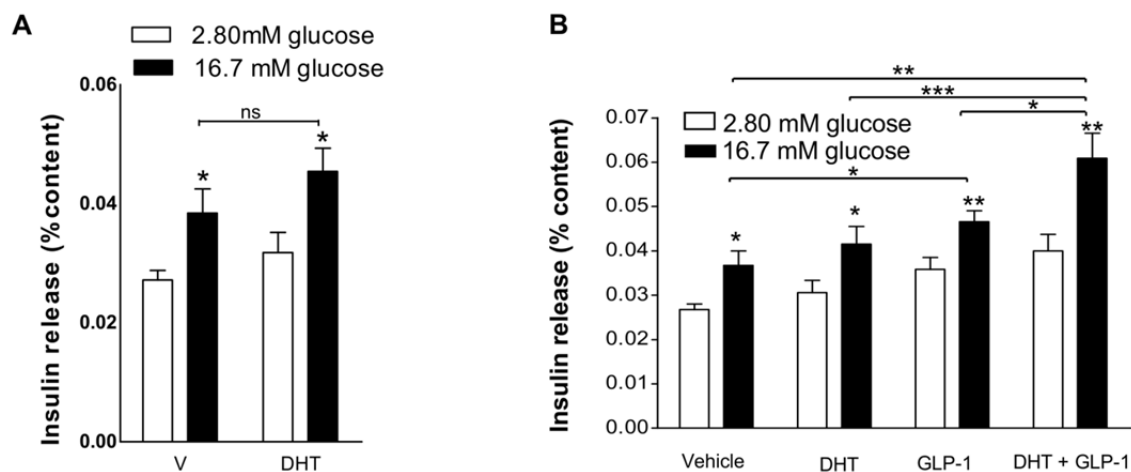
Figure 8.3. **(A)** INS-1 cells were treated with 10 nM DHT for 40 minutes. (n = 3 independent wells, and 4 independent experiments). **(B)** GSIS measured in static incubation in INS-1 cells treated with vehicle, DHT (10^{-8} M), GLP-1 (10^{-8} M), or DHT plus GLP-1. Values represent the mean ± SEM. *P < 0.05, **P = 0.01, ***P = 0.0001.
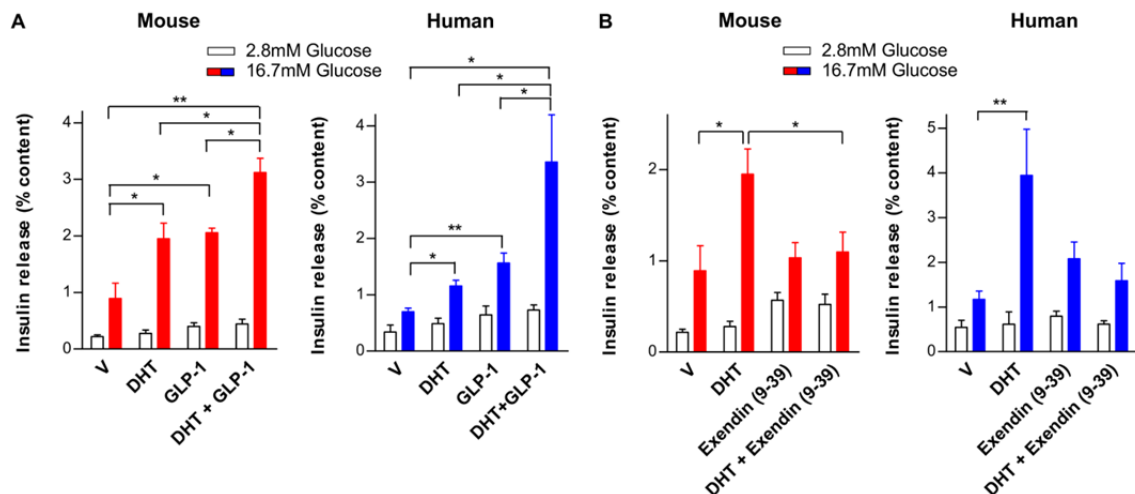
Figure 8.4. **(A)** GSIS measured in static incubation in WT male mouse islets (left) and male human islets (right) treated with vehicle, DHT (10^{-8} M), GLP-1 (10^{-8} M), or DHT plus GLP-1. Results from 2 experiments (n= 6 independent wells). Human donors were a male Latino aged 61 with BMI 25.8 and a male Caucasian aged 53 with BMI 33. The results were the average from 2 different donors/experiments. **(F)** GSIS measured in static incubation in WT male mouse islets and male human islets treated with vehicle, DHT (10^{-8} M), Exendin (9-39) (10^{-7} M), or DHT plus Exendin (9-39). Results from 2 experiments (n= 6 independent wells). Human donor was a male Caucasian aged 53 with BMI 33. The results were a representative experiment from 2 different donors.

Discussion

To study the role of testosterone in β-cells *in vivo*, we generated a mouse with conditional elimination of AR in these cells. Although male βARKO$^{-/y}$ mice also exhibit decreased AR expression in hypothalamus, the insulin-secretory defect observed in these mice results from the loss of AR in β-cells. This is supported by the following evidence: First, abnormalities observed in male βARKO$^{-/y}$ mice are reproduced in isolated male βARKO$^{-/y}$ islets and in human islets exposed to an AR antagonist, demonstrating that this defect is secondary to the loss of AR in the islets. Second, the insulin-secretory defect observed in male βARKO$^{-/y}$ mice is not observed in male mice that selectively lack AR in neurons. Finally, and most importantly, a second βARKO^{MIP} mouse exhibiting selective and inducible β-cell AR elimination in adulthood recapitulates the impaired GSIS leading to glucose intolerance.

A critical finding of this study is that AR deficiency in β-cells of male mice impairs GSIS which produces glucose intolerance because activation of β-cell AR is required to enhance both first and second phase GSIS. Importantly, the insulinotropic function of the AR is present in human islets at physiological concentrations of testosterone. Together, these observations suggest that (1) testosterone is necessary for normal GSIS in men, and (2) men with androgen deficiency display a deficit in GSIS that predisposes them to T2D.

Early studies showing binding of androgen to a nuclear protein in prostate [72] followed by the cloning of the AR and analysis of its structure [57-59] led to the establishment of a paradigm in which AR acts as a nuclear ligand-activated transcription factor. Indeed, in prostate, AR *is maintained in the cytosol in an inactive complex by heat-shock proteins Upon ligand binding, AR homodimerizes and translocates to the nucleus* [73]. In β-cells, however, AR is mostly localized in an extranuclear compartment where it remains sequestrated following androgen stimulation. When male cells are permanently exposed to DHT *in vivo*, AR is localized

in the nucleus of prostate cells. In contrast, under the same conditions, AR is observed in the extranuclear compartment of islet β-cells. The nongenomic actions of AR are thought to account for the rapid, transcription-independent effects of androgens [60]. However, to date, these nongenomic effects of androgens have been observed only *in vitro* and therefore await validation *in vivo* in animal models.

We previously described novel extranuclear actions for estrogen receptors (ERs) in β-cells [45, 61-64]. Unlike the nuclear ER that acts as a ligand-activated transcription factor in breast and uterine cells, extranuclear ERs protect pancreatic islet β-cell function and survival via cytosolic interactions with kinases and transcription factors. The current study provides the first evidence of rapid androgen action via an extranuclear AR involved in the pathophysiology of insulin secretion. This novel androgen action is observed at physiological concentration of the hormone, is validated *in vivo,* and most importantly, it is found in human tissue.

In β-cells, GSIS is driven by glucose metabolism that generates ATP [74] and triggers $[Ca^{2+}]_i$ influx. Testosterone activation of the AR increases GSIS independently of increases in glucose metabolism and $[Ca^{2+}]_i$ influx. Rather, AR activation increases GSIS from β-cells by producing cAMP and activating the cAMP-dependent PKA pathway. Consistent with AR signaling via a PKA pathway, transgenic mice with enhanced PKA catalytic activity in pancreatic islets [75, 76] exhibit increased GSIS but — like male βARKO$^{γ/-}$ mice — show no change in β-cell mass or insulin synthesis. A previous report suggested that testosterone stimulates islet insulin mRNA and content [77]. However, we found no evidence of AR stimulation of insulin synthesis. Because the authors used testosterone (which is converted into estrogen), the effect they described was likely due to testosterone aromatization to estrogen acting on ERs [61].

Incretins, like GLP-1 and exendin 4, restore first-phase and enhance second phase insulin release in humans with T2D [78, 79]. Most of these incretin effects in β-cells require activation

of the cAMP-dependent PKA pathway via the G protein-coupled receptor (GPCR) of GLP-1 [80], which activates the adenylate cyclase (AC) to trigger cAMP production. We observe that in cultured mouse and human islets, the insulinotropic effect of testosterone is abolished by pharmacological inhibition of the GLP-1R in absence of exogenous GLP-1, demonstrating that the AR requires an active GLP-1R to enhance GSIS and enhances the effect of islet-produced GLP-1. Accordingly, AR activation by testosterone also amplifies the insulinotropic effect of exogenous GLP-1 in these islets. Therefore, the testosterone-AR pathway could act as an incretin sensitizer in β-cells. In the future, the effect of testosterone in amplifying the insulinotropic action of other ligands of Gs-linked GPCR, like glucagon or glucagon inhibitory polypeptide, deserves investigation. Interestingly, cultured islets from βARKO$^{-/y}$ mice previously exposed to a western diet secrete less insulin than controls. This suggests that AR is also necessary for islet adaption to metabolic stress. Further studies are also needed to address this issue. The mechanism through which we propose AR stimulates GSIS in male β-cells is summarized **Figure 9**.

The biological basis for androgen stimulation of insulin secretion and the integration of androgenic and metabolic signals in males is likely to be anabolic since both testosterone and insulin are anabolic hormones. In contrast to males, AR deficiency in β-cells of female mice does not alter GSIS. Females have lower AR expression in β-cells compared to males, an observation that likely promotes weaker androgen signaling [81]. In addition, females exhibit lower serum and tissue androgen concentrations than are necessary to activate the AR [16]. We therefore interpret the absence of phenotype of βARKO$^{-/-}$ female mice as a consequence of the evolution of females' lower dependence on AR activation and signaling.

This study has clinical ramifications. *S*elective androgen receptor modulators (SARMs) are a novel class of androgen receptor ligands. The goal of SARMs is to provide androgen therapy
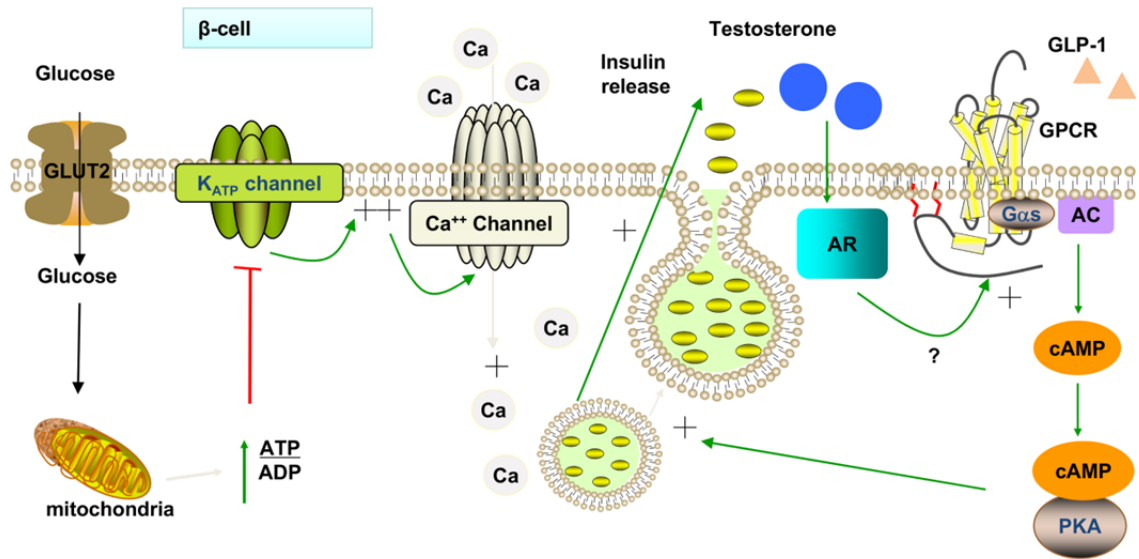
Figure 9. Proposed mechanism of AR stimulation of GSIS in β-cells. Testosterone activation of AR in β-cell indirectly activates a GPCR coupled with Gαs at the plasma membrane. This stimulates AC and cAMP production leading to PKA activation, thus amplifying the glucose signal on insulin exocytosis.

for age-related functional decline with customized anabolic activity on muscle and bone, but without androgenic action in the prostate [82]. Our work suggests that androgen deficiency-induced T2D is at least partially due to a loss of androgen stimulation of GSIS in β-cells. Designing SARMs with AR agonistic activity in β-cells could represent a novel strategy to prevent androgen deficiency-related glucose dysregulation in men.

In conclusion, AR action is required in males' β-cells for GSIS. This study identifies the AR as a novel β-cell receptor and enhancer of β-cell function via the cAMP-dependent pathway and has important clinical and pharmacological implications for prevention of T2D in aging men.

CHAPTER 3

Androgen Receptor-deficient Islet β-cells Exhibit Alteration in Genetic Markers of Insulin Secretion and Inflammation. A Transcriptome Analysis in the Male Mouse

Overview

To assess the role of AR in β-cell function in the male, we previously generated male mice lacking AR selectively in β-cells (βARKO$^{-/y}$). These mice develop decreased glucose-stimulated insulin secretion (GSIS) without alteration in β-cell mass but producing glucose intolerance [42]. When these mice are exposed to a western diet, they are hyperglycemic and hypoinsulinemic in the fasted and fed states. We reported that testosterone action on AR β-cells amplifies the insulinotropic action of GLP-1 on its receptor via a cAMP-dependent protein kinase-A pathway [42]. Thus, androgen deficiency predisposes to T2D via the combination of loss of androgen action in peripheral tissues producing insulin resistance and loss of androgen action in β-cells producing β-cell failure to compensate for insulin resistance [42, 83, 84].

To gain further insight on the role of AR in male β-cells though AR-dependent gene networks, we performed a high throughput whole transcriptome sequencing (RNA-Seq) in islets from male βARKO$^{-/y}$ and control mice.

Materials and Methods

Generation of Mutant Mice

The βARKO⁻/ʸ mouse was generated by crossing mice carrying the AR gene with floxed exon 2 on their X chromosome (AR^lox) with transgenic mice with the Cre recombinase expression under rat insulin II promoter (RIP-Cre, Jackson Laboratory) as previously described [42].

Islet Isolation and RNA Preparation

Islet isolation was performed following pancreatic duct injection with collagenase as previously described [45]. Islets were isolated from 3 male ARlox⁻/ʸ mice and 3 RIP-Cre mice and immediately frozen in liquid nitrogen (**Figure 10**). Mice were at 12-week of age at the time of islet isolation, and were fed on the normal chow. The metabolic parameters of mice at the same age were previously described [42]. Total RNA was extracted using RNeasy Maxi Kit (Qiagen) following the manufacturer's recommendations, and the samples were sent to NUseq Core, Northwestern University for RNA sequencing.

RNA-Seq Analysis

The quality of DNA reads, in FASTQ format, was evaluated using FastQC (http://www.bioinformatics.babraham.ac.uk/projects/fastqc/). Adapters were removed and reads of inadequate quality were filtered. The raw read data was processed largely following the procedure described in [85]. Briefly, the reads were aligned to the *Mus musculus* genome (mm10) using TopHat (v2.0.8b). Subsequently, the aligned reads, in conjunction with a gene annotation file for mm10 obtained from the University of California Santa Cruz (UCSC) website (http://genome.ucsc.edu/), were used to determine RNA expressions of annotated genes using Cufflinks (v2.1.1).
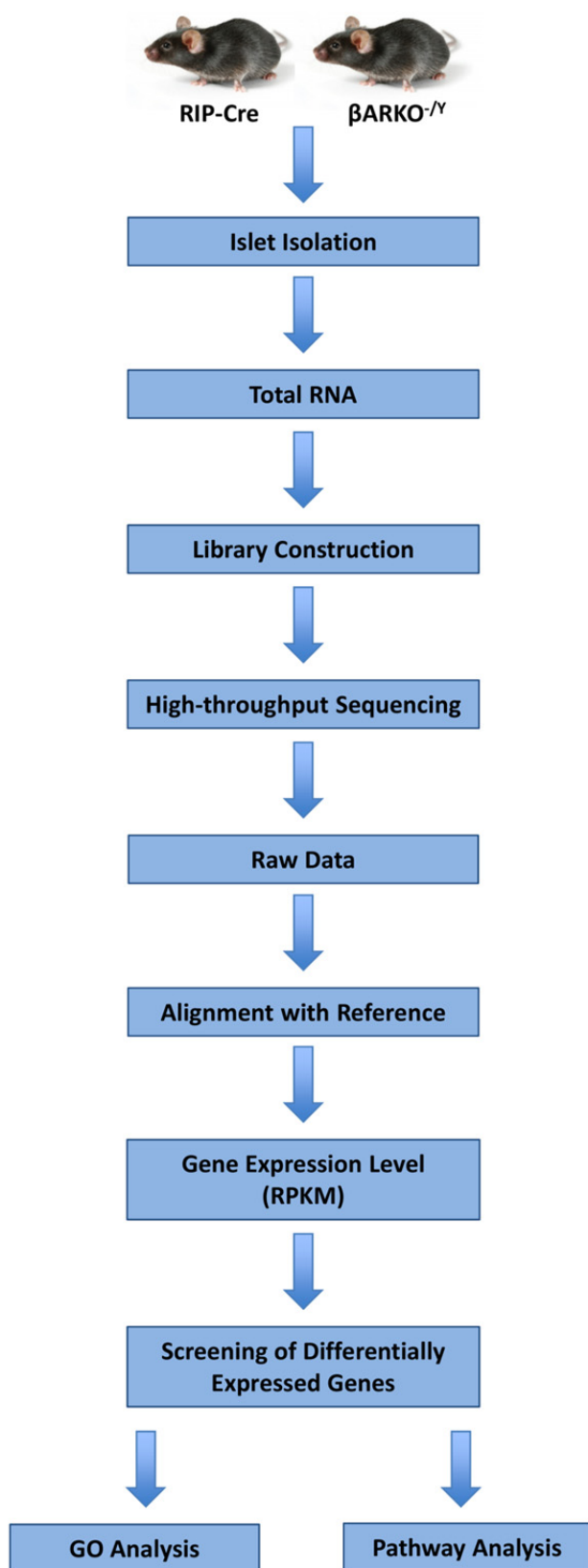
Figure 10. Flow chart of the RNA-Seq experiment

Single-Gene Analysis

For a transcript g, the expression level is estimated by the number of reads (C_g) mapped to the region of the transcript normalized by the length (L) of the transcript in nucleotides and the total number (N) of mapped reads of the mouse genome. If we use kilobase as the unit for L and million reads as the unit for N, this estimation is called <u>r</u>eads <u>p</u>er <u>k</u>ilobase of transcript per <u>m</u>illion mapped reads (RPKM), which is the most widely used RNA-seq normalization method [86]. The individual transcript files generated by Cufflinks for each sample were merged into a single gene annotation file, which was then used to perform a DE analysis with the Cufflinks routine, Cuffdiff. Significant DEGs were determined by Cuffdiff using the procedure described in [85] based on a Benjamini-Hochberg false discovery rate (FDR) threshold of 0.05 [87]. Results of such differential expression analysis were processed with CummeRbund [85]. The significant DEGs were separated into those that were up-regulated and those that were down-regulated.

Quantitative Reverse Transcription PCR (qRT-PCR)

Total RNA was extracted from MIN6 cells with RNeasy Plus Mini Kit (Qiagen) following the manufacturer's instructions. The quality and concentration of RNA were assessed by NanoDrop Spectrophotometer (Thermo Scientific). RNA was reverse transcribed into cDNA using iScript cDNA Synthesis Kit (Bio-Rad). Quantification of targeted genes was performed using iTaq™ Universal SYBR® Green Supermix (Bio-Rad) and the iCycler iQ™ Real Time PCR Detection System (Bio-Rad). Ct values were normalized to TBP and the relative gene expression was calculated with the $2^{-\Delta\Delta}$Ct method. Gene-specific KiCqStart™ primers were purchased from Sigma-Aldrich as listed in Supplemental Table 1.

Pathway and Gene Ontology (GO) Analysis

The list of 312 (225 up- and 87 down-regulated) significant DEGs (FDR < 0.05) were analyzed by applying (i) GeneCodis3 (http://genecodis.cnb.csic.es) [88] and (ii) GeneTrail (http://genetrail.bioinf.uni-sb.de/) [89] software tools to identify significantly enriched Kyoto Encyclopedia of Genes and Genomes (KEGG) pathways and GO categories by over-representation analysis.

Statistical Analysis

Results are presented as mean ± SEM in Fig. 4. All statistical analyses were performed using the unpaired Student's *t* test. A P value less than 0.05 was considered statistically significant. ** P<0.01, *** P<0.001.

Results

Single-Gene Analysis

A total of 23,179 genes were annotated with RefSeq IDs. Of these, a fold change (FC) (defined as the relative ratio of gene expression between βARKO$^{-/y}$ to control islets) could be computed for 22,061 genes. Among these genes, 312 differentially expressed genes (DEGs) (225 up- and 87 down-regulated) were discovered at a false discovery rate (FDR) < 0.05. At FDR < 0.05 and FC > 2, a total of 214 significant DEGs (158 were up- and 56 down-regulated) were identified (Supplemental Table 2). Of these DEGs, 66 were associated with inflammation and stress (53 up- and 13 down-regulated) (**Table 3**), and 56 were associated with β-cell insulin secretion including metabolism, cAMP-PKA signaling, ion channels, Ras-related protein/GTPase, glucose metabolism, membrane polarization, and secreted factor (44 up- and 12 down-regulated) (**Table 4**). Thus, in βARKO$^{-/y}$ islets, 31% of the DEGs were associated with β-cell inflammation and stress, and 26% with insulin secretion (**Figure 11**). We validated a set of individual gene expression results by qRT-PCR in cultured MIN-6 insulin-producing cells treated with the pure AR agonist dihydrotestosterone (DHT) (**Figure 12**).

Mirroring the results obtained in control and βARKO$^{-/y}$ islets, DHT suppressed the mRNA for hepatokine fibroblast growth factor 21 (*Fgf21*), the innate immune molecule lipocalin 2 (*Lcn2*), syntrophin, gamma 2 (*Sntg2*), G-protein-coupled receptor (GPR) 26 (*Gpr26*), and *Gpr119*. No effect of DHT was observed for dual oxidase 2 (*Duox2*), and the transient receptor potential cation channel, subfamily C, member 4 (*Trpc4*).

Pathway Analysis

Gene expression analyzed on a gene-by-gene basis ignores the underlying biological structure and diminishes the power of analysis, obscuring the presence of important biological

Gene Symbol	Full Name	RefSeq ID	Fold Change	FDR-adjusted p-value	Annotation
Wfdc2	WAP four-disulfide core domain 2	NM_026323	11.09	4.24E-02	Inflammation
Lcn2	lipocalin 2	NM_008491	10.04	4.28E-03	Inflammation
Mmp7	matrix metallopeptidase 7	NM_010810	7.80	1.02E-02	Inflammation
Gbp11	predicted gene, EG634650; guanylate-binding protein 11; RIKEN cDNA 5830443L24 gene	NM_001039647	7.17	4.28E-03	Inflammation
Cxcl5	similar to LPS-induced CXC chemokine; chemokine (C-X-C motif) ligand 5	NM_009141	6.16	4.28E-03	Inflammation
Fgf21	fibroblast growth factor 21	NM_020013	4.72	4.28E-03	Stress
Gbp10	predicted gene, EG634650; guanylate-binding protein 10; RIKEN cDNA 5830443L24 gene	NM_001039646	4.69	4.28E-03	Inflammation
Cxcl10	chemokine (C-X-C motif) ligand 10; similar to Small inducible cytokine B10 precursor (CXCL10) (Interferon-gamma-induced protein CRG-2) (Gamma-IP10) (IP-10) (C7)	NM_021274	4.51	4.28E-03	Inflammation
Gbp4	predicted gene, EG634650; guanylate-binding protein 4	NM_001256005	4.34	4.28E-03	Inflammation
Sftpd	surfactant associated protein D	NM_009160	4.11	4.28E-03	Inflammation
Gbp9	predicted gene, EG634650; guanylate-binding protein 9, cDNA sequence BC057170	NM_172777	4.10	4.28E-03	Inflammation
Sostdc1	sclerostin domain containing 1	NM_025312	3.86	4.28E-03	Stress
Gbp8	predicted gene, EG634650; guanylate-binding protein 10; RIKEN cDNA 5830443L24 gene	NM_029509	3.80	4.28E-03	Inflammation
Gsta4	glutathione S-transferase, alpha 4	NM_010357	3.67	1.77E-02	Stress
Matn2	matrilin 2	NM_016762	3.44	4.28E-03	Inflammation
Col5a2	collagen, type V, alpha 2	NM_007737	3.43	4.28E-03	Stress
Noxa1	NADPH oxidase activator 1	NM_001	3.41	4.24E-02	Stress

		163626			
Gbp6	IFI16	NM_194 336	3.39	4.28E-03	Inflammation
Nr0b2	nuclear receptor subfamily 0, group B, member 2 (SHP)	NM_011 850	3.23	4.28E-03	Stress
Ngfr	nerve growth factor receptor (TNFR superfamily, member 16)	NM_033 217	3.15	4.28E-03	Stress
Reg3a	regenerating islet-derived 3 alpha	NM_011 259	3.13	4.28E-03	Inflammation
Klk1b8	kallikrein 1-related peptidase b8	NM_008 457	3.12	1.54E-02	Inflammation
Atf3	activating transcription factor 3	NM_007 498	3.07	7.26E-03	Inflammation
Gfra3	glial cell line derived neurotrophic factor family receptor alpha 3	NM_010 280	3.01	4.28E-03	Inflammation
Zfp36	zinc finger protein 36	NM_011 756	2.96	4.28E-03	Inflammation
Cish	cytokine inducible SH2-containing protein	NM_009 895	2.90	4.28E-03	Inflammation
Csf2rb	colony stimulating factor 2 receptor, beta, low-affinity (granulocyte-macrophage)	NM_007 780	2.89	4.28E-03	Inflammation
Il1rn	interleukin 1 receptor antagonist	NM_001 039701	2.87	4.28E-03	Inflammation
Ifit3	interferon-induced protein with tetratricopeptide repeats 3	NM_010 501	2.77	4.28E-03	Inflammation
Lck	lymphocyte protein tyrosine kinase	NM_001 162433	2.74	3.85E-02	Inflammation
Gbp5	guanylate binding protein 5	NM_153 564	2.58	4.28E-03	Inflammation
Ifit1	interferon-induced protein with tetratricopeptide repeats 1	NM_008 331	2.58	4.28E-03	Inflammation
Nr5a2	nuclear receptor subfamily 5, group A, member 2	NM_030 676	2.45	4.28E-03	Inflammation
Il22ra1	interleukin 22 receptor, alpha 1	NM_178 257	2.40	4.28E-03	Inflammation
Crispld2	cysteine-rich secretory protein LCCL domain containing 2	NM_030 209	2.38	4.28E-03	Inflammation
Tnfrsf11 b	tumor necrosis factor receptor superfamily, member 11b (osteoprotegerin)	NM_008 764	2.37	4.28E-03	Inflammation
Klk1b11	kallikrein 1-related	NM_010	2.37	7.26E-03	Stress

	peptidase b11	640			
Iigp1	interferon inducible GTPase 1; interferon-inducible GTPase-like	NM_001 146275	2.36	4.28E-03	Inflammation
Rsad2	radical S-adenosyl methionine domain containing 2	NM_021 384	2.34	4.28E-03	Inflammation
Tnip3	TNFAIP3 interacting protein 3	NM_001 001495	2.32	2.90E-02	Inflammation
C4b	complement component 4B (Childo blood group)	NM_009 780	2.25	4.28E-03	Inflammation
C3	complement component 3; similar to complement component C3 prepropeptide, last	NM_009 778	2.18	4.28E-03	Inflammation
C2cd4a	family with sequence similarity 148, member A	NM_001 163143	2.17	4.28E-03	Inflammation
Xaf1	XIAP associated factor 1	NM_001 037713	2.16	4.38E-02	Inflammation
Anxa1	annexin A1	NM_010 730	2.14	2.90E-02	Inflammation
Sntb1	syntrophin, basic 1	NM_016 667	2.13	7.26E-03	Inflammation
Chac1	ChaC, cation transport regulator-like 1 (E. coli)	NM_026 929	2.13	1.54E-02	Stress
Oasl2	2'-5' oligoadenylate synthetase-like 2	NM_011 854	2.08	7.26E-03	Inflammation
Fgfr2	fibroblast growth factor receptor 2	NM_010 207	2.07	4.85E-02	Inflammation
Parp14	poly (ADP-ribose) polymerase family, member 14	NM_001 039530	2.05	4.28E-03	Inflammation
Tap1	transporter 1, ATP-binding cassette, sub-family B (MDR/TAP)	NM_001 161730	2.05	4.28E-03	Inflammation
Socs2	suppressor of cytokine signaling 2; predicted gene 8000	NM_007 706	2.03	4.28E-03	Inflammation
Sgk1	serum/glucocorticoid regulated kinase 1	NM_011 361	2.03	4.28E-03	Stress
F13a1	coagulation factor XIII, A1 subunit	NM_001 166391	0.16	4.28E-03	Inflammation
Dapl1	death associated protein-like 1	NM_029 723	0.32	4.28E-03	Stress
Mlf1	myeloid leukemia factor 1	NM_001 039543	0.34	4.28E-03	Inflammation
Lyve1	lymphatic vessel endothelial hyaluronan receptor 1	NM_053 247	0.36	4.28E-03	Inflammation

Ccdc8	coiled-coil domain containing 8	NM_001 101535	0.42	2.57E-02	Stress
Gimap6	GTPase, IMAP family member 6	NM_153 175	0.42	4.28E-03	Inflammation
Il10	interleukin 10	NM_010 548	0.43	4.85E-02	Inflammation
Capsl	calcyphosine-like	NM_029 341	0.45	4.28E-03	Inflammation
Prdm1	PR domain containing 1, with ZNF domain	NM_007 548	0.46	1.77E-02	Inflammation
Sele	selectin, endothelial cell	NM_011 345	0.46	3.85E-02	Inflammation
Il1b	interleukin 1 beta	NM_008 361	0.48	4.28E-03	Inflammation
Mum1l1	melanoma associated antigen (mutated) 1-like 1	NM_001 164631	0.50	4.28E-03	Inflammation
Defb1	defensin beta 1	NM_007 843	0.50	4.28E-03	Inflammation

Table 3. **Single-gene Analysis**. The table highlights 52 significant DEGs which involve inflammatory response and stress.

[*]Abbreviations: DEG, differentially expressed genes; FDR, false discovery rate.

Gene Symbol	Full Name	RefSeq ID	Fold Change	FDR-adjusted p-value	Annotation
Sntg2	syntrophin, gamma 2	NM_172951	9.10	4.28E-03	Ion Channel
Duox2	dual oxidase 2	NM_177610	8.29	4.28E-03	Metabolism
Hs3st1	heparan sulfate (glucosamine) 3-O-sulfotransferase 1	NM_010474	6.28	4.28E-03	Metabolism
Syt10	synaptotagmin X	NM_018803	6.13	4.28E-03	Exocytosis
Car2	carbonic anhydrase 2	NM_009801	5.92	4.28E-03	Glucose metabolism
Cftr	cystic fibrosis transmembrane conductance regulator homolog	NM_021050	5.42	4.28E-03	Ion Channel
Fmo1	flavin containing monooxygenase 1	NM_010231	5.41	4.28E-03	Metabolism
Rasgrp1	RAS guanyl releasing protein 1	NM_011246	5.28	4.28E-03	Ras-related protein/ GTPase
Gpr26	G protein-coupled receptor 26	NM_173410	4.87	1.54E-02	cAMP-PKA signaling
Kcnj5	potassium inwardly-rectifying channel, subfamily J, member 5	NM_010605	4.62	4.28E-03	Membrane polarization
Rph3a	rabphilin 3A	NM_011286	4.48	4.28E-03	Exocytosis
Hcn1	hyperpolarization-activated, cyclic nucleotide-gated K+ 1	NM_010408	4.12	4.28E-03	Ion Channel
Slc39a4	solute carrier family 39 (zinc transporter), member 4	NM_028064	4.12	3.08E-02	Metabolism
Rasl11b	RAS-like, family 11, member B	NM_026878	3.86	3.21E-02	Metabolism
Grem2	gremlin 2 homolog, cysteine knot superfamily (Xenopus laevis)	NM_011825	3.72	4.28E-03	Metabolism
Lrrc55	leucine rich repeat containing 55	NM_001033346	3.46	4.28E-03	Membrane polarization
Tph2	tryptophan hydroxylase 2	NM_173391	3.45	4.28E-03	Metabolism
Kcnk10	IFI16	NM_029911	3.27	4.28E-03	Membrane polarization
Hk2	hexokinase 2	NM_013820	3.21	4.28E-03	Glucose metabolism
Tdh	L-threonine dehydrogenase; predicted gene 13929	NM_021480	2.91	4.28E-03	Metabolism

Tph1	tryptophan hydroxylase 1	NM_009414	2.87	4.28E-03	Metabolism
Kctd14	potassium channel tetramerisation domain containing 14	NM_0010108 26	2.81	4.28E-03	cAMP-PKA signaling
Klf15	Kruppel-like factor 15	NM_023184	2.73	4.28E-03	Metabolism
Gpr126	G protein-coupled receptor 126	NM_0010022 68	2.67	4.28E-03	cAMP-PKA signaling
Enpp2	ectonucleotide pyrophosphatase/phosph odiesterase 2	NM_0011360 77	2.65	4.28E-03	cAMP-PKA signaling
Rerg	RAS-like, estrogen-regulated, growth-inhibitor	NM_181988	2.61	4.28E-03	Ras-related protein/ GTPase
Pde7b	phosphodiesterase 7B	NM_013875	2.60	4.28E-03	cAMP-PKA signaling
Fam13a	family with sequence similarity 13, member A	NM_153574	2.59	7.26E-03	Ras-related protein/ GTPase
Cckar	cholecystokinin A receptor	NM_009827	2.55	3.98E-02	cAMP-PKA signaling
Pfkfb3	6-phosphofructo-2-kinase/fructose-2,6-biphosphatase 3	NM_0011777 52.1	2.54	4.28E-03	Glucose metabolism
UGT1A1	UDP glucuronosyltransferase 1 family, polypeptide A1	NM_201645	2.48	4.28E-03	Metabolism
Chst2	carbohydrate sulfotransferase 2	NM_018763	2.36	1.54E-02	Metabolism
Tmc5	transmembrane channel-like gene family 5	NM_028930	2.29	4.28E-03	Ion Channel
Adm	adrenomedullin	NM_009627	2.27	3.98E-02	Secreted insulinotropic factor
Cachd1	cache domain containing 1; similar to Cache domain containing 1	NM_198037	2.20	7.26E-03	Ion Channel
Gnb1l	guanine nucleotide binding protein (G protein), beta polypeptide 1-like	NM_023120	2.18	2.22E-02	Ras-related protein/ GTPase
B3galt1	UDP-Gal:betaGlcNAc beta 1,3-galactosyltransferase, polypeptide 1	NM_020283	2.18	2.78E-02	Metabolism
Kcnq1	potassium voltage-gated channel, subfamily Q, member 1; similar to Potassium voltage-gated channel, subfamily Q,	NM_008434	2.17	4.28E-03	Membrane polarization

					member 1
Bmp7	bone morphogenetic protein 7	NM_007557	2.15	4.28E-03	Secreted insulinotropic factor
Hkdc1	hexokinase domain containing 1	NM_145419	2.11	2.90E-02	Glucose metabolism
Dhrs3	dehydrogenase/reductase (SDR family) member 3	NM_011303	2.07	7.26E-03	Metabolism
Ptger3	prostaglandin E receptor 3 (subtype EP3)	NM_011196	2.07	1.54E-02	cAMP-PKA signaling
Clic6	chloride intracellular channel 6	NM_172469	2.06	4.53E-02	Ion Channel
Rasd2	RASD family, member 2	NM_029182	2.21	4.28E-03	Ras-related protein/ GTPase
Ppargc1 a	peroxisome proliferative activated receptor, gamma, coactivator 1 alpha	NM_008904	0.28	4.28E-03	Glucose metabolism
Trpc4	transient receptor potential cation channel, subfamily C, member 4	NM_0012536 82	0.31	4.28E-03	Ion Channel
Phactr3	phosphatase and actin regulator 3 (Scapinin)	NM_0010071 54	0.38	1.77E-02	Glucose metabolism
Rasgrf2	RAS protein-specific guanine nucleotide- releasing factor 2	NM_009027	0.38	4.28E-03	Ras-related protein/ GTPase
Rgs7bp	regulator of G-protein signalling 7 binding protein	NM_029879	0.41	4.28E-03	Ras-related protein/ GTPase
Ppp1r3c	protein phosphatase 1, regulatory (inhibitor) subunit 3C	NM_016854	0.42	3.42E-02	Metabolism
Ust	uronyl-2-sulfotransferase	NM_177387	0.43	1.28E-02	Metabolism
Vsnl1	visinin-like 1	NM_012038	0.43	1.77E-02	Ion Channel
Dse	dermatan sulfate epimerase	NM_172508	0.45	7.26E-03	Metabolism
Gpr161	G protein-coupled receptor 161	NM_0010811 26	0.46	3.42E-02	cAMP-PKA signaling
Kctd12	potassium channel tetramerisation domain containing 12	NM_177715	0.47	4.28E-03	cAMP-PKA signaling
Hapln1	hyaluronan and proteoglycan link protein 1	NM_013500	0.49	1.28E-02	Metabolism

Table 4. **Single-gene Analysis.** The table highlights 36 significantly DEGs which involve ion channel, glucose metabolism, cAMP-PKA signaling, membrane polarization, and exocytosis.

Figure 11. **Single-gene analysis pie chart**. Dysregulated genes were involved in inflammation and stress, as well as insulin secretion.
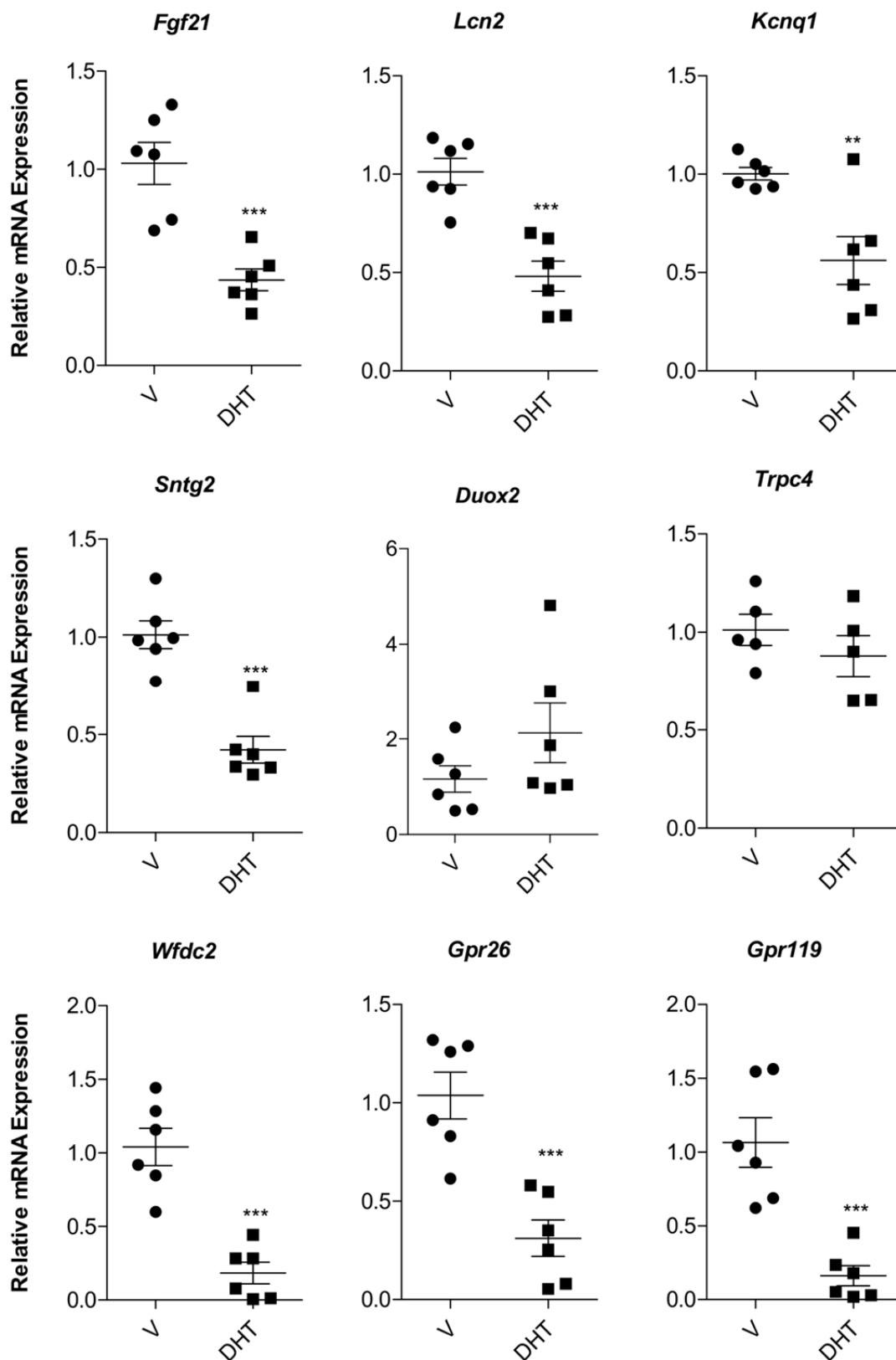
Figure 12. **qRT-PCR validation of RNA-seq analysis**. Min6 cells were treated with vehicle or DHT for 24 minutes/24 hours. mRNA expression of target gene was normalized to that of TBP.

signals [90]. Thus, grouping genes by biological pathways is often the most relevant approach, because it takes into account the cooperative nature of genes and considers that genes involved in the same process are dysregulated together. Such an approach yields more robust results and may reveal novel insights about molecular mechanisms of disease [91]. The 312 DEGs at FDR < 0.05 were interpreted in a biological pathway context. Based on GeneCodis3 analysis of Kyoto Encyclopedia of Genes and Genomes (KEGG) pathways, 23 significantly enriched pathways were revealed (**Table 5**). The representative pathways are cytokine-cytokine receptor interaction (Kegg: 04060), Jak-STAT signaling pathways (Kegg: 04630), MAPK signaling pathway (Kegg: 04010), insulin signaling pathway (Kegg: 04910), and pancreatic secretion (Kegg: 04972). Based on the KEGG pathway results and our analysis of the literature, we combined these pathways and summarized them into three biologically relevant pathways: insulin secretion (**Figure 13A**), stress/growth factor signaling (**Figure 13B**), and inflammatory pathways (**Figure 13C**).

Gene Ontology (GO) Analysis

Ontologies provide a formal representation of knowledge that is amenable to computational as well as human analysis, an obvious underpinning of systems biology [92]. The GO, like other formal ontologies, consists of a structured hierarchical controlled vocabulary for standardizing representations of gene and gene product attributes in relation to a large and growing context of biological knowledge [93]. Scientists have used GO terms to evaluate the characteristics of sets of genes [94]. The GO classifies gene functions into three categories: biological process (BP), cellular component (CC), and molecular function (MF) (**Table 6**). For the 312 significant DEGs, based on GeneCodis3 and GeneTrail analyses of GO categories, 43 BP, 17 CC, and 23 MF categories were identified (selection criteria: # genes in GO category ≥ 2 and FDR < 0.05 for both programs). For BP, representative categories included inflammatory response

Pathway	Pathway ID	P Value	# Genes
Cytokine-cytokine receptor interaction	Kegg:04060	5.78E-06	11
Jak-STAT signaling pathway	Kegg:04630	2.68E-04	7
Tryptophan metabolism	Kegg:00380	4.48E-04	4
Butirosin and neomycin biosynthesis	Kegg:00524	6.47E-04	2
Glycosphingolipid biosynthesis - lacto and neolacto series	Kegg:00601	1.07E-03	3
Cell adhesion molecules (CAMs)	Kegg:04514	1.15E-03	6
Leishmaniasis	Kegg:05140	1.85E-03	4
African trypanosomiasis	Kegg:05143	2.01E-03	3
Gastric acid secretion	Kegg:04971	2.57E-03	4
Osteoclast differentiation	Kegg:04380	2.63E-03	5
Bile secretion	Kegg:04976	2.70E-03	4
Complement and coagulation cascades	Kegg:04610	3.46E-03	4
Fructose and mannose metabolism	Kegg:00051	3.63E-03	3
Insulin signaling pathway	Kegg:04910	5.02E-03	5
Hepatitis C	Kegg:05160	5.18E-03	5
Malaria	Kegg:05144	5.49E-03	3
MAPK signaling pathway	Kegg:04010	5.96E-03	7
Starch and sucrose metabolism	Kegg:00500	6.22E-03	3
Glycosphingolipid biosynthesis - globo series	Kegg:00603	6.44E-03	2
Glycosaminoglycan biosynthesis - keratan sulfate	Kegg:00533	6.44E-03	2
Type II diabetes mellitus	Kegg:04930	7.84E-03	3
Staphylococcus aureus infection	Kegg:05150	7.84E-03	3
Pancreatic secretion	Kegg:04972	9.40E-03	4

Table 5. Significantly Enriched KEGG Pathways.[*]

[*]Abbreviations: KEGG, Kyoto Encyclopedia of Genes and Genomes
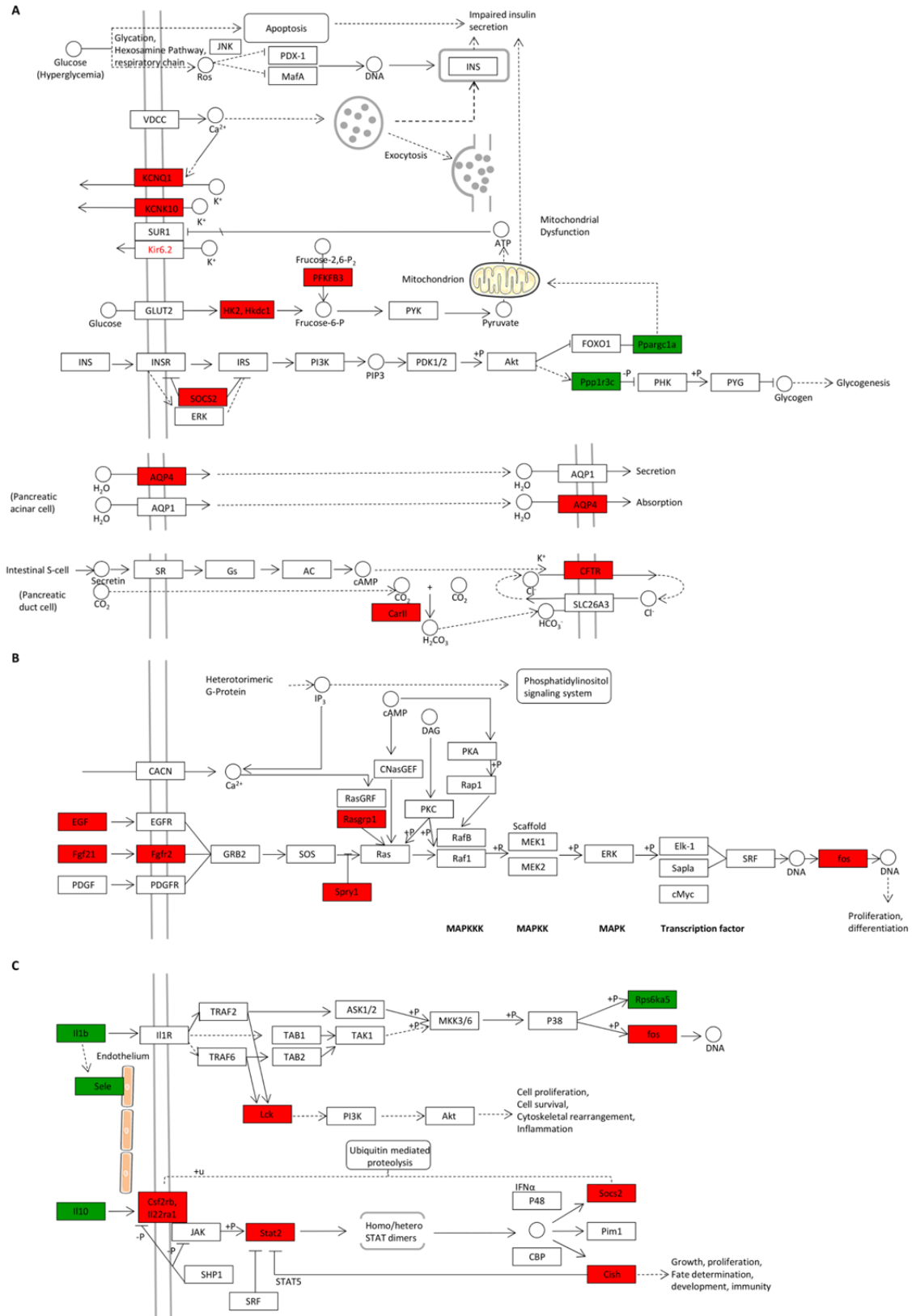
Figure 13. **KEGG pathways** were summarized in three biological pathways: (A) insulin secretion, (B) stress/growth factor signaling, and (C) inflammatory pathway. Within the context of AR deficiency in β cells, in (A), genes involved in membrane polarization (*Kcnq1, kcnk10*), ion channel (*Cftr*), glucose metabolism (*Hk2, Hkdc1, Pfkfb3, Ppargc1a*), and metabolism (*Ppp1r3c*) were differentially expressed leading to dysregulated insulin secretion pathway. In (B), increased *Fgf21* expression and subsequent alteration in the pathway suggested compensatory response of islets in response to stress. In (C), inflammatory pathway was highly enriched upon AR knockout, demonstrating the protective role AR in β cells. Red color, up-regulated genes; green color, down-regulated genes.

GO Category	GO ID	GO Name	GeneTrail # Genes	GeneTrail FDR	GeneCoDis3 # Genes	GeneCoDis3 FDR
BP	GO:0006950	response to stress	35	2.09E-05	5	3.92E-02
BP	GO:0005975	carbohydrate metabolic process	16	4.50E-04	6	0.0380599
BP	GO:0030073	insulin secretion	7	7.59E-04	4	1.04E-02
BP	GO:0006954	inflammatory response	12	8.04E-04	10	5.56E-04
BP	GO:0006811	ion transport	21	8.98E-04	15	4.80E-03
BP	GO:0040008	regulation of growth	11	4.32E-03	4	2.82E-02
BP	GO:0007155	cell adhesion	16	5.15E-03	11	2.65E-02
BP	GO:0009968	negative regulation of signal transduction	5	1.06E-02	4	1.88E-02
BP	GO:0006915	apoptosis	18	2.33E-02	12	2.28E-02
BP	GO:0032870	cellular response to hormone stimulus	4	0.0467718	2	0.0285125
CC	GO:0016021	integral to membrane	81	1.62E-03	79	2.19E-06
CC	GO:0008076	voltage-gated potassium channel complex	4	1.65E-02	4	1.72E-02
CC	GO:0005576	extracellular region	51	2.81E-10	44	1.75E-12
CC	GO:0005887	integral to plasma membrane	11	4.91E-02	13	1.53E-03
MF	GO:0003924	GTPase activity	8	1.10E-03	8	4.48E-03
MF	GO:0005249	voltage-gated potassium channel activity	5	1.13E-02	4	4.13E-02
MF	GO:0005215	transporter activity	24	1.15E-03	7	2.24E-02
MF	GO:0005216	ion channel activity	10	1.44E-02	9	2.26E-02
MF	GO:0005509	calcium ion binding	13	6.47E-03	17	2.04E-04
MF	GO:0004396	hexokinase activity	2	9.44E+01	2	2.14E-02

MF	GO:0005525	GTP binding	10	9.44E-03	10	1.69E-02
MF	GO:0005267	potassium channel activity	6	9.64E-03	4	4.44E-02

Table 6. **GO Analysis**.[*] A total of 43, 17, and 23 BP, CC and MF categories were detected significantly enriched (FDR<0.05) by GeneTrail and GeneCoDis3. Among them, representative GO categories include (i) BP: "inflammatory response", "ion transport" and "insluin secretion" (ii) CC: "extracellular region", "extracellular space" and "integral to membrane", and (iii) MF: "GTPase activity", "calcium ion binding", and "GTP binding", respectively.

[*]Abbreviations: BP, biological process; CC, cellular component; FDR, false discovery rate; GO, gene ontology; MF, molecular function. Selection criteria: # genes in GO category ≥2 and FDR < 0.05 for both programs. GO terms are first sorted by "GO Category" in ascending order, then by "GeneTrail FDR" in ascending order, and then by "GeneCoDis3 FDR" in ascending order.

(GO: 0006954), ion transport (GO: 0006811), insulin secretion (GO: 0030073), negative regulation of signal transduction (GO: 0009968), apoptosis (GO: 0006915), cell adhesion (GO: 0007155), regulation of growth (GO: 0040008), and response to stress (GO: 0006950), indicating alteration in the β-cell function and stress. For CC, significantly enriched categories included extracellular region (GO: 0005576), integral to membrane (GO: 0016021), voltage-gated potassium channel complex (GO: 0008076), and integral to plasma membrane (GO: 00058887), revealing structural alterations in membrane proteins involved in insulin secretion. For MF, enriched categories were GTPase activity (GO: 0003924), calcium ion binding (GO: 0005509), GTP binding (GO: 0005525), hexokinase activity (GO: 0004396), transporter activity (GO: 0005215), ion channel activity (GO: 0005216), voltage-gated potassium channel activity (GO: 0005249), and potassium channel activity (GO: 0005267), also indicating functional changes in β-cell secretory capacity.

Discussion

Using islets from adult male βARKO$^{-/y}$ mice, we identified 214 dysregulated genes involved in β-cell insulin secretion and stress, confirming that AR plays a vital role in male β-cell health. A third of these genes are coding for proteins mediating or responding to inflammation and cellular stress, demonstrating that islets with prolonged AR deficiency are injured and suffering. These include genes coding for *Fgf21* [95], *Lcn2* [96], the member of the tumor necrosis factor receptor superfamily osteoprotegerin (*tnfrsf11b*) [97, 98], chemokine ligands 5 and 10 (*Cxcl5* and *Cxcl10*) [99, 100], several interferon (IFN)-gamma-induced guanylate-binding proteins (*Gbp4, Gbp 5, Gbp 6, Gbp 8, Gbp 9, Gbp 10,* and *Gbp 11*) [101], intra islet pro-inflammatory cytokines and associated receptors like interleukin-1β (*Il1b*), the interleukin 22 receptor-α1 (*Il22ra1*) [102], the IL-1 receptor antagonist (*Il1rn*) [103] and interleukin-10 (*Il10*) [104]. The coagulation factor XIII, A1 subunit (*F13a1*) has also been implicated in chronic low-grade inflammatory islets in T2D subjects [105].

The second finding is that 20% of dysregulated genes are involved in β-cell function. These include genes coding for GPRs such as *Gpr161* [106], *Gpr126* [107], *Gpr26* [108], ion channels altering membrane polarization like the potassium inwardly-rectifying channel, subfamily J, member 5 (*kcnj5*), the potassium voltage-gated channel, subfamily Q, member 1 (*kcnq1*) (33), and *trpc4* [109], as well as proteins involved in β-cell exocytosis machinery such as the Ca(2+)-sensor synaptotagmin-10 (*Syt10*) [110], the GTP binding protein rabphilin 3a (*Rph3a*) [111], heparan sulfate (glucosamine) 3-O-sulfotransferase 1 (*Hs3st1*) [112] and enzymes involved in glucose metabolism, hexokinase 2 (*hk2*), hexokinase domain containing 1 (*hkdc1*) [113], glucokinase binding protein 6-phosphofructo-2-kinase/fructose-2,6-biphosphatase 3 (*Pfkfb3*) [114] and zinc transport in β-cells like the zinc transporter, member 4 (*Slc39a4*) [115].

Dysregulated genes seem to fall into two categories. Some are detrimental to β-cell health

and could be instrumental in impairing GSIS. For example, genome-wide association studies identified *Kcnq1* and *Rasgrp1* (RAS guanyl releasing protein 1) as susceptible genes for T2DM [116, 117] and βARKO$^{-/y}$ islets exhibit increased expression of both. *Kcnq1* impairs insulin secretion by enhancing the β-cell potassium currents [118]. Increased expression of *Nr0b2* in βARKO$^{-/y}$ islets, coding the orphan nuclear receptor small heterodimer partner (SHP), is also expected to impair insulin gene transcription and decrease GSIS [119] while increased *Car2* expression (carbonic anhydrase 2) [120] is a genetic marker of poor GSIS, and increased *Sostdc1* (sclerostin domain containing 1) expression inhibits Bmp and Wnt which impairs β-cell function [121]. Other adverse upregulated genes include *lcn2*, induced in β-cells by inflammatory cytokines [96], the chemokines (*Cxcl5* and *Cxcl10*) increased in islets from T2D humans and rodents and which are known to impair β-cell function and survival [99, 100], and multiple GBPs that activate the inflammasome and produce β-cell inflammation [101].

In contrast, another set of dysregulated genes seems to be part of a concerted compensatory mechanism attempting to preserve β-cell function from the deleterious effect of the AR knockout. For example, increased expression of *Fgf21* [95] *or Il1rn* (IL-1β receptor antagonist) [103] is expected to protect islet function and survival during inflammation, and the increased *Hs3st1* expression is expected to enhance GSIS [112]. Other adaptive mechanisms include increased expression of genes coding for proteins that could enhance GSIS by increasing β-cell glucose metabolism (*Hk2, Pfkfb3*) [113], cAMP production (*Gpr119, Gpr26, GPR126, Gpr161,* activating transcription factor 3, (*Atf3*)), insulin vesicle exocytosis (*Syt10, Rph3a*), and β-cell membrane depolarization (*Trpc4*) [109].

Our pathway analysis revealed 23 significantly enriched pathways that we combined into two biologically relevant pathways, inflammatory pathways and insulin secretion, confirming our observation from individually dysregulated genes. Ontologies used to evaluate the

characteristics of differentially expressed genes in βARKO$^{-/y}$ islets were also enriched for GO terms "response to stress," "inflammatory response," "apoptosis," "insulin secretion," "ion transport," and "cell adhesion." Taken together, these results of GO analysis confirmed the results of the pathway analysis and our individual gene evaluation that AR deficiency promotes β-cell dysfunction and inflammation. Consistent with our findings, testosterone protects early apoptotic damage induced by streptozotocin in male rat pancreas through AR suggesting that AR activation may protect male islets from inflammation [122, 123]. In addition, neuronal specific AR-deficient mice exhibit hypothalamic inflammation via activation of nuclear factor-κB [40] which promotes obesity, insulin resistance and glucose intolerance.

A limitation of the present study is that we did not validate all our individual gene expression results by qRT-PCR. However, previous studies have reported high consistencies between RNA-seq and qRT-PCR results [124]. RNA-seq shows both high reproducibility and low frequency of false positives [125] and has been used for transcriptional profiling of specific cell types or tissues at unprecedented precision [126].

In conclusion, a transcriptome analysis of islets from adult male βARKO$^{-/y}$ mice revealed alterations in genes involved in inflammation and insulin secretion, demonstrating the importance of androgen action in β-cell health in males, with implications for the development of T2D in androgen deficient men.

CHAPTER 4

Activation of the Androgen Receptor in Male Pancreatic β-cell Enhances Glucagon-like

Peptide-1 Insulinotropic Action to Enhance Insulin Secretion

Overview

We investigated in the current study the molecular mechanisms by which AR and GLP-1R collaboratively potentiate GSIS in male β-cells. DHT amplifies the islet-derived, not gut-derived, GLP-1 to induce GSIS in male mice. GLP-1R is essential for the AR signaling in the insulin secretion, but DHT-activated AR is not necessary for the action of the GLP-1. DHT does not amplify the insulinotropic effect of other ligands of G-protein coupled receptors (GPCRs) coupled to Gαs and activating AC, like GIP or glucagon, and shows the specificity towards GLP-1. Consistently, DHT increases GLP-1 induced cAMP production but not that of GIP and glucagon, and it signals via a cAMP/PKA/EPAC pathway and the activation of mTOR to amplify GSIS.

Materials and Methods

Generation of mutant mice

To generate βARKO^{MIP} mice we crossed mice carrying the AR gene with floxed exon 2 on their X chromosome (AR^{lox}) with the Ins1-Cre/ERT (MIP-Cre$^{+/-}$) transgenic mouse (Jackson Lab). Generation and characterization of ARlox$^{-/-}$ have been described [44]. We induced Tamoxifen (Tam; Sigma) inactivation of AR after puberty and following a 4 weeks of TAM treatment in silastic tubing and all of metabolic measures were taken after 4-week wait period. 10mm silastic laboratory tubing (Dow Corning) was filled with 15mg tam, capped with wooden applicator sticks, and sealed with silastic medical adhesive (Dow Corning). The βARKO^{RIP} mouse was generated by crossing AR^{lox} with transgenic mice overexpressing the Cre recombinase under control of the RIP promoter (RIP-Cre, Jackson Laboratory). The βGLP-1KO^{RIP} mouse was generated by crossing GLP-1R^{lox} (a kind gift from Dr. David A. D'Alessio of Duke University) with RIP-Cre.

All studies were performed with the approval of Tulane University Animal Care and Use Committees in accordance with the NIH Guidelines.

Western Diet

Mice were weaned onto a customized diet designed to be high in saturated fat and simple sugars (sucrose and fructose) to mimic a western diet (30% AMF; 14.9% Kcal protein, 33.2% Kcal carbohydrates, 51.9% Kcal fat; Harlan Teklad) for 9 weeks.

Metabolic studies

Blood glucose was measured from tail vein blood using True Metrix (Trividia Health). Insulin was measured in plasma by ELISA kit (Millipore). For IP-GTT (2 g/kg) and GSIS (3 g/kg), mice were fasted overnight before glucose injection.

Islet isolation and insulin secretion in static incubation

Islet isolation was performed following pancreatic duct injection with collagenase (Sigma) as described [45]. For measurement of insulin secretion, islets were hand-picked under a dissection microscope, and treated with DHT (10^{-8} M; Steraloids), or vehicle (95% ethanol) for 40 minutes. Insulin release from islets was measured as described [45].

Dynamic measurement of islet cAMP

Epac2 responses to cAMP were monitored online in islets infected with adenovirus harboring the FRET probe Epac2-camps (plasmid was a kind gift from Prof. Dermot Cooper, University of Cambridge), as previously described [127]. Live cell imaging was performed using a Crest X-Light spinning disk head, coupled to a Lumencor SPECTRA X light engine and Nikon 10 x/0.45 NA objective, controlled using custom scripts in MetaMorph software (Molecular Devices). Excitation was delivered at λ = 430-450 nm and emission collected at λ = 460-500 nm and 520-550 nm for cerulean and citrine, respectively, using a highly-sensitive Photometrics Delta Evolve EMCCD camera. FRET response were calculated as the fluorescence ratio of cerulean:citrine, and normalized as R/R_0 where R = fluorescence at any given time point and R_0 = fluorescence a time zero. Islets were maintained in HEPES-bicarbonate buffer, containing (in mM): 120 NaCl, 4.8 KCl, 24 $NaHCO_3$, 0.5 Na_2HPO_4, 5 HEPES, 2.5 $CaCl_2$, 1.2 $MgCl_2$, 3-17 *D*-glucose.

Ca^{2+}. Vehicle (0.01% EtOH), DHT (10 nM), Ex4 (1-39) (10 nM), GIP (100nM) and glucagon (20nM) were applied at the indicated timepoints.

Statistical analysis

Results are presented as mean ± SEM as specified in figures. All statistical analyses were performed using the unpaired Student's *t* test. A P value less than 0.05 was considered statistically significant. * P<0.05, ** P<0.01.

Results

Male βARKO^MIP mice exhibit impaired glucose-stimulated insulin secretion following IP, not oral glucose challenge

We assessed glucose homeostasis in male control and βARKO^MIP mice, fed a western diet since weaning. βARKO^MIP and control mice exhibited comparable body weight up to 28 weeks of age (**Figure 14.1A**). However, βARKO^MIP mice developed fed hyperglycemia compared to control which became significant at 12 weeks (4 weeks after tamoxifen-mediated recombination) (**Figure 14.1B & C**). They also displayed fed hypoinsulinemia as assessed by decreased insulin/glucose ratio, an index of β-cell function (**Figure 14.1D & E**). We showed that DHT amplifies the effect of islet-derived GLP-1 in cultured mouse islets [42]. To explore the physiological relevance of these findings *in vivo*, we asked whether gut GLP-1 requires a functional β-cell AR to stimulate GSIS in vivo by comparing IP-GTT (that explores glucose effect on β-cells without gut GLP-1) to an oral-GTT (that explores glucose and gut GLP-1 effects on β-cells) in βARKO^MIP mice. Following an IP glucose challenge βARKO^MIP developed impaired GSIS (**Figure 14.2A**), accompanied by glucose intolerance (**Figure 14.2B**) with decreased insulin secretion 30 minutes into the GTT (**Figure 14.2C).** Note that βARKO^MIP showed no alteration in arginine-stimulated insulin secretion (ASIS) (**Figure 14.2D**). In contrast, during an oral glucose challenge, βARKO^MIP exhibited similar glucose tolerance than littermate controls (**Figure 14.2E**), without alteration in β-cell function (I/G ratio at 30 min) (**Figure 14.2F**). This suggests that loss of β-cell AR impair the insulinotropic action of the islet GLP-1 but not the gut GLP-1.

Prolonging half-life of GLP-1 improves oral glucose homeostasis in absence of β-cell AR

To further explore whether prolonging GLP-1 half-life would enhance DHT effect on GSIS, we used linagliptin, a dipeptidyl peptidase-4 (DPP-4) inhibitor [128]**.** In cultured male mouse
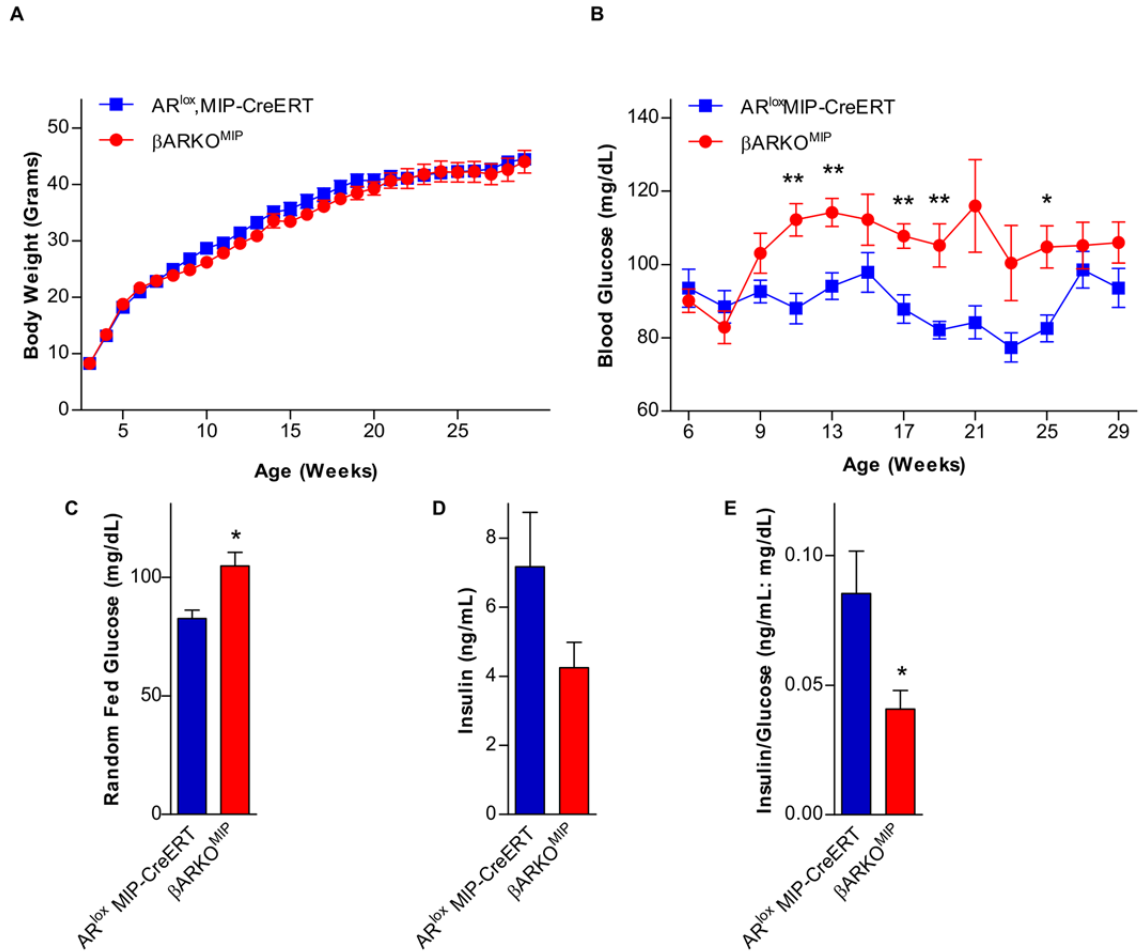
Figure 14.1. Data are from mice fed a western diet since weaning. **(A)** Body weight of male βARKO[MIP] and controls. Data from group 2 (i.p. TAM induction)**. (B-E)** Data from group 2 (i.p. TAM induction) **(B)** Random fed blood glucose of the same group (measurements taken around 10-11am). **(C) & (D)** Ram fed blood glucose and insulin at 25 weeks. **(E)** Insulin over glucose ratio of **(C and D).**
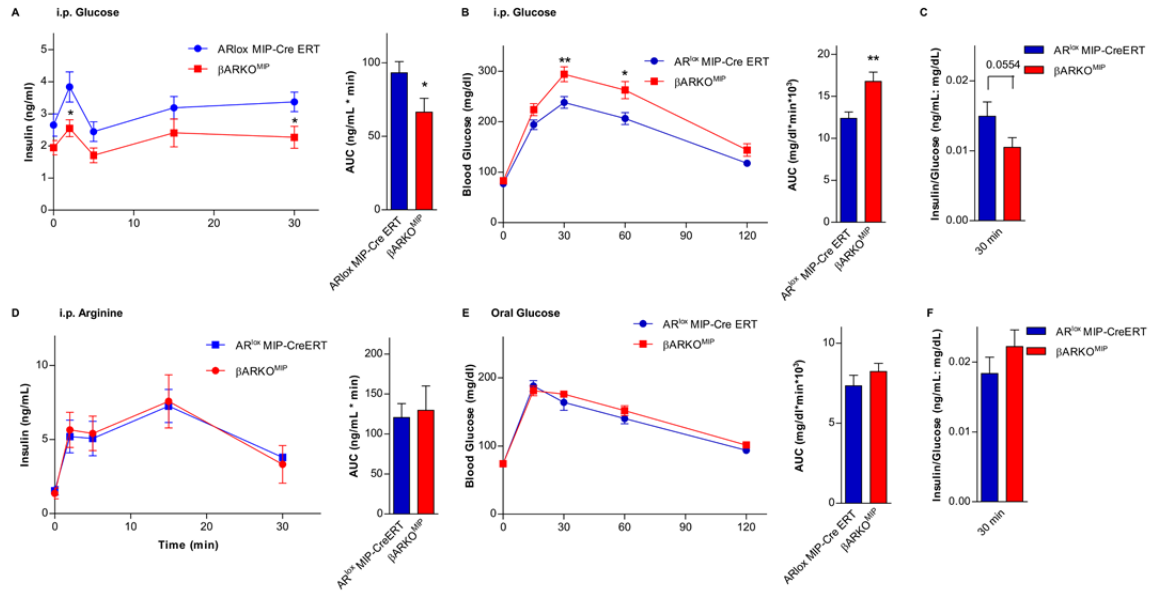
Figure 14.2. **(A)** IP-GSIS (3 g/kg) with insulin area under the curve (AUC). **(B)** IP-GTT (2 g/kg) with glucose AUC. **(C)** Insulin over glucose ratio at 30 minutes during IP-GTT. **(D)** IP-ASIS (1 g/kg) with insulin area AUC. **(E)** Oral-GTT (2 g/kg) with glucose AUC . **(F)** Insulin over glucose ratio at 30 minutes during Oral-GTT. Mice were studied at 23-35 weeks of age (n = 10-15). Values represent the mean ± SE. * P < 0.05, ** P < 0.01.

islets, linagliptin did not amplify the insulinotropic effect of DHT (**Figure 15A**) during GSIS. Accordingly, following a 4-week treatment, linagliptin did not significantly improve IP glucose tolerance in male control and βARKO^{MIP} mice (**Figure 15B**). In contrast, linagliptin treatment similarly improved oral glucose tolerance in both controls and βARKO^{MIP} mice (**Figure 15D**). There is a trend of increased insulin secretion at 30 minutes during IP and Oral GTT in linagliptin-treated control mice compared to controls without linagliptin treatment, but the same effect was not observed in βARKO^{MIP} mice (**Figure 15C & E**). Under oral glucose challenge, linagliptin also improved GSIS in both control and βARKO^{MIP} mice (**Figure 15F**). Thus linagliptin improved glucose homeostasis in absence of β-cell AR.

The insulinotropic effect of DHT requires the islet GLP-1R and AR

We showed that DHT enhances the insulinotropic action of islet-derived and exogenous GLP-1 in cultured mouse and human islets [42]. To explore to what extent DHT requires the GLP-1R to enhance GSIS, we examined GSIS in static incubation of islets from male control and β-cell specific GLP-1 knockout (βGLP1RKO^{RIP}) mice. Consistent with the previous results, in control islets, DHT increased GSIS and amplified the effect of exogenous GLP-1 compared to vehicle-treated islets. In βGLP1RKO^{RIP} islets, DHT was no longer capable of potentiating GSIS, and DHT-amplified GLP-1 effect was abolished (**Figure 16A**). Next, we explored how important AR signaling is in the GLP-1 action using male islets from control and β-cell specific AR knockout (βARKO^{RIP}) mice. Not surprisingly, with the deletion of AR, DHT failed to enhance GSIS alone or in presence of GLP-1 in βARKO^{RIP} islets. Notably, in βARKO^{RIP} islets, GLP-1 was still capable of inducing GSIS to the same level as control islets treated with GLP-1 (**Figure 16B**). Similar results were obtained with islets from βARKO^{MIP} mice fed a western diet (**Figure 16C**).
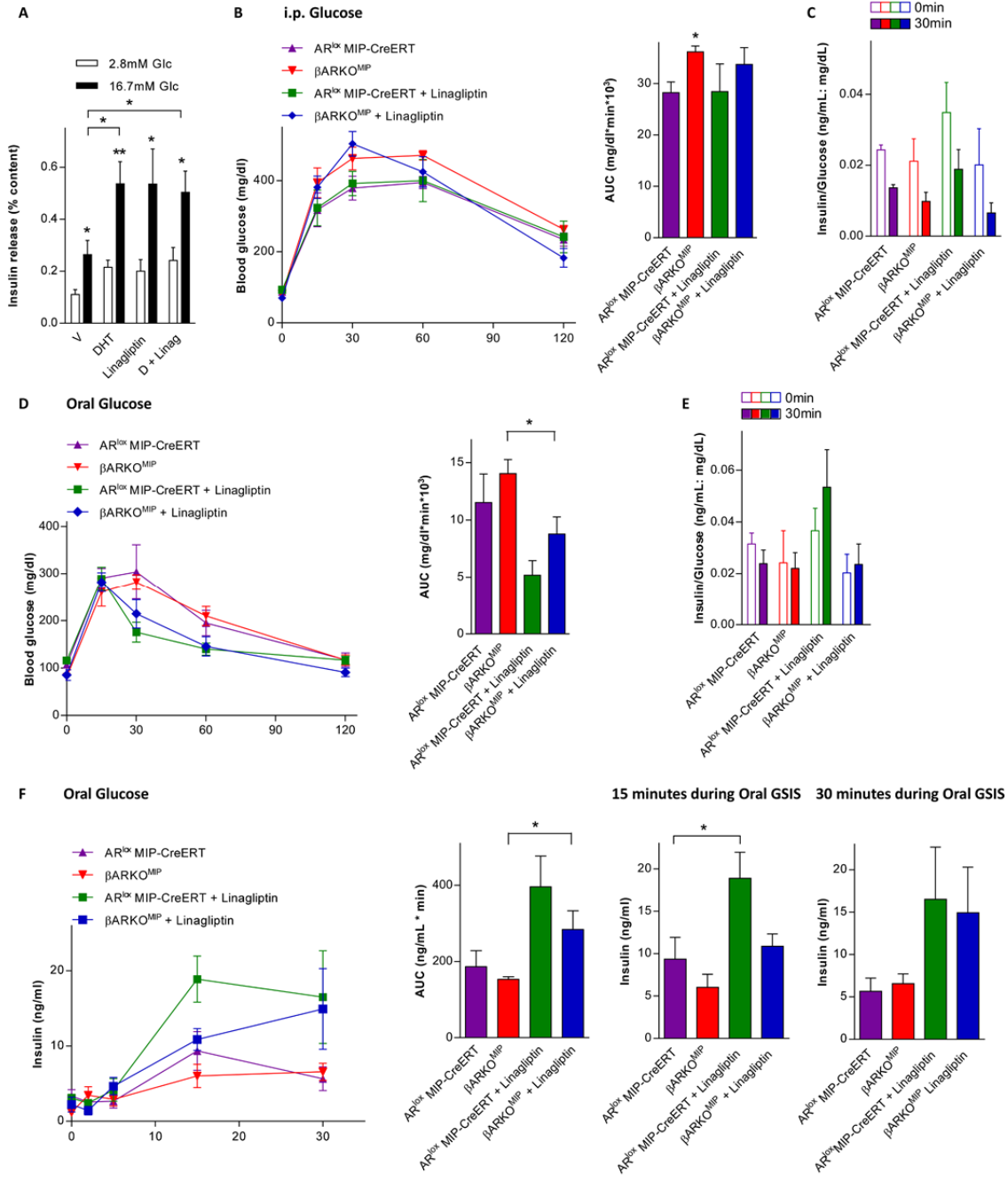
Figure 15. **(A)** GSIS measured in static incubation in male C57/BL6N islets and treated with vehicle, DHT (10nM), linagliptin (50nM), or DHT plus linagliptin *in vitro* for 40 minutes. Data **(B-F)** are from mice fed a western diet since weaning, and they were then fed with western diet mixed with linagliptin (83mg/kg of western diet) for 4 weeks before and during i.p. GTT and oral GTT. **(B**) IP-GTT (2 g/kg) with glucose AUC. **(C**) Insulin over glucose ratio at 0 and 30 minutes during IP-GTT. **(D)** Oral-GTT (2 g/kg) with glucose AUC . **(E)** Insulin over glucose ratio at 0 and 30 minutes during Oral-GTT. **(F)** IP-GSIS (3 g/kg) with insulin area under the curve (AUC) and insulin levels at 15 and 30 minutes during Oral-GSIS. Values represent the mean ± SE. *P < 0.05, **P < 0.01.
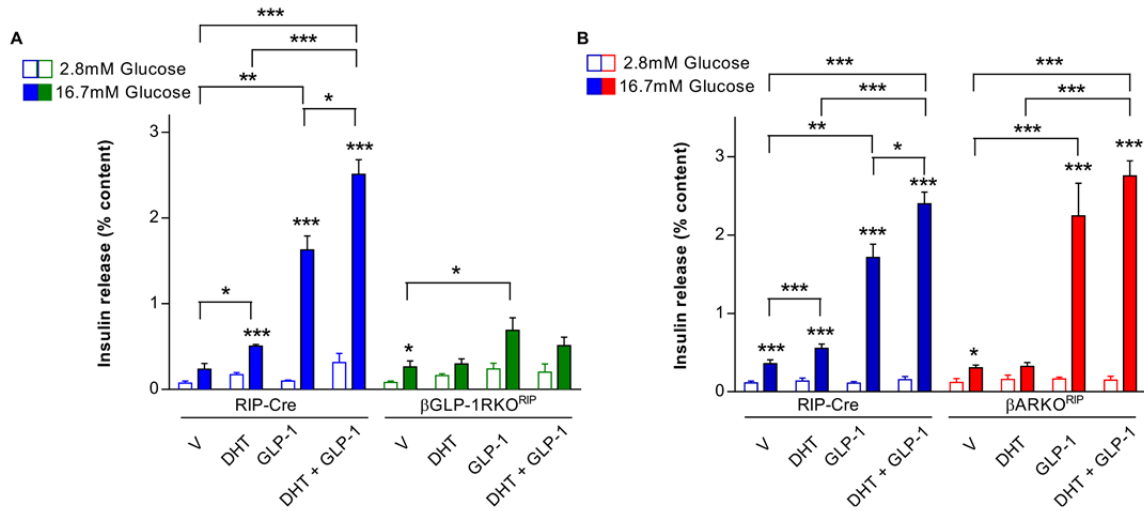
Figure 16. **(A)** GSIS measured in static incubation in normal chow fed control and βGLP-1RKO[RIP] islets treated with DHT (10nM) and GLP-1 (10nM) (n= 2 mice/group) **(B)** GSIS measured in static incubation in normal chow fed control and βARKO[RIP] islets treated with DHT (10nM) and GLP-1 (10nM) (n= 2 mice/group).

DHT amplifies the insulinotropic effect of GLP-1

Since DHT amplifies the insulinotropic effect of both endogenous and exogenous GLP-1 and requires a GLP-1R in male mouse and human islets [42], we sought to determine to what extent DHT could also amplifiy the insulintropic action of GIP and glucagon, acting via G-protein coupled receptor (GPCR) coupled to $G\alpha_S$ and adenylate cyclase (AC). We used 832/3 insulin-secreting cells, a sub-clone of INS-1 cell line with high incretin response, to eliminate confounding effect from intra-islet GLP-1 [129]. In these cells, DHT amplified the insulinotropic effect of exogenous, GLP-1; but failed to amplify the insulinotropic effect of neither GIP nor glucagon (**Figure 17A**). Similar results were obtained wild type male islets; DHT amplified the insulinotropic effect of GLP-1, but did not amplify the effects of GIP or glucagon (**Figure 17B**).

DHT enhances GLP-1 induced cAMP production

We previously reported that DHT insulinotropic action is associated with increased islet cAMP accumulation. To accurately quantify DHT-induced cAMP production, we used 832/3 cells infected with an adenovirus expressing an EPAC-based fluorescence resonance energy transfer (FRET) sensor [127]. DHT treatment enhances GLP-1 induced cAMP production, not that of Glucagon or GIP (**Figure 18A**), which is confirmed by measuring the cAMP amplitude (**Figure 18B**). Downstream of cAMP are two pathways involved in the insulin secretion by potentiating insulin granule exocytosis. cAMP either binds to PKA (PKA-dependent pathway), or associates with a PKA-independent pathway, which involves exchange protein activated by cAMP 2 (Epac2) [130]. To determine to what extent DHT-induced insulin secretion is dependent on PKA and or EPAC activation, we measured GSIS in wild type male mouse islets in static incubation in the presence of H89 (PKA inhibitor) and ESI-09 (EPAC inhibitor). DHT potentiation of GSIS was
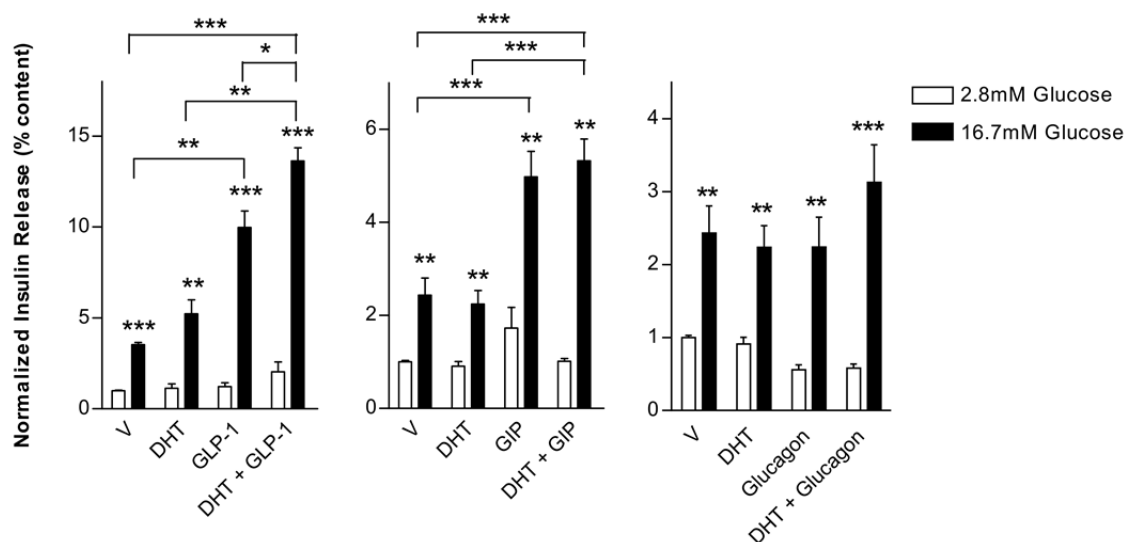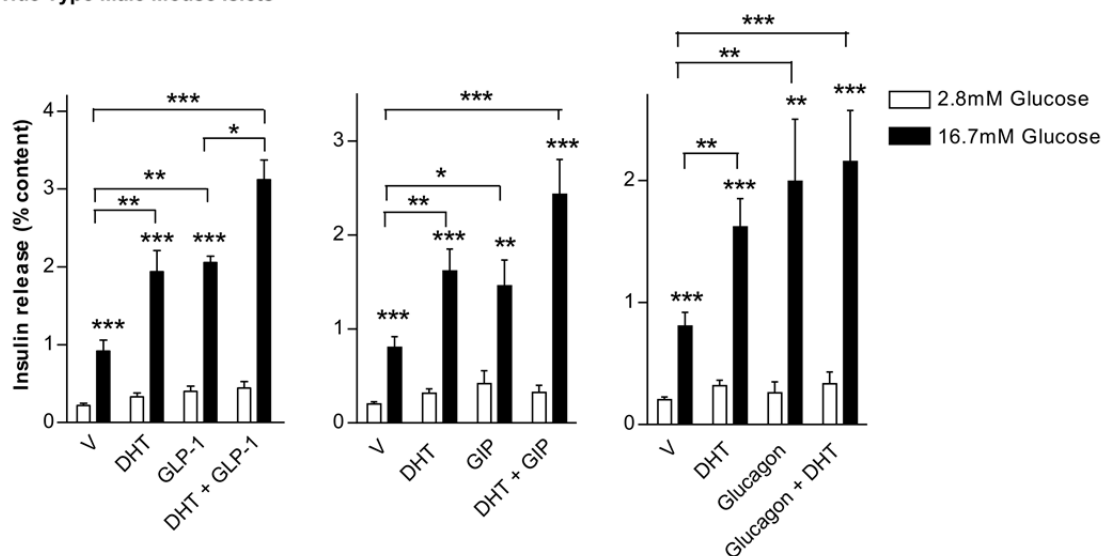
Figure 17. **(A)** 832/3 cells were treated with vehicle, DHT (10nM), GLP-1 (10nM), GIP (100nM), and glucagon (20nM) for 40 minutes (n = 3 independent wells, and 2-4 independent experiments) **(B)** Wild-type male mouse islets were treated with vehicle, DHT (10nM), GLP-1 (10nM), GIP (100nM), and glucagon (20nM) for 40 minutes. Values represent the mean ± SE. [*] P < 0.05, [**] P < 0.01.
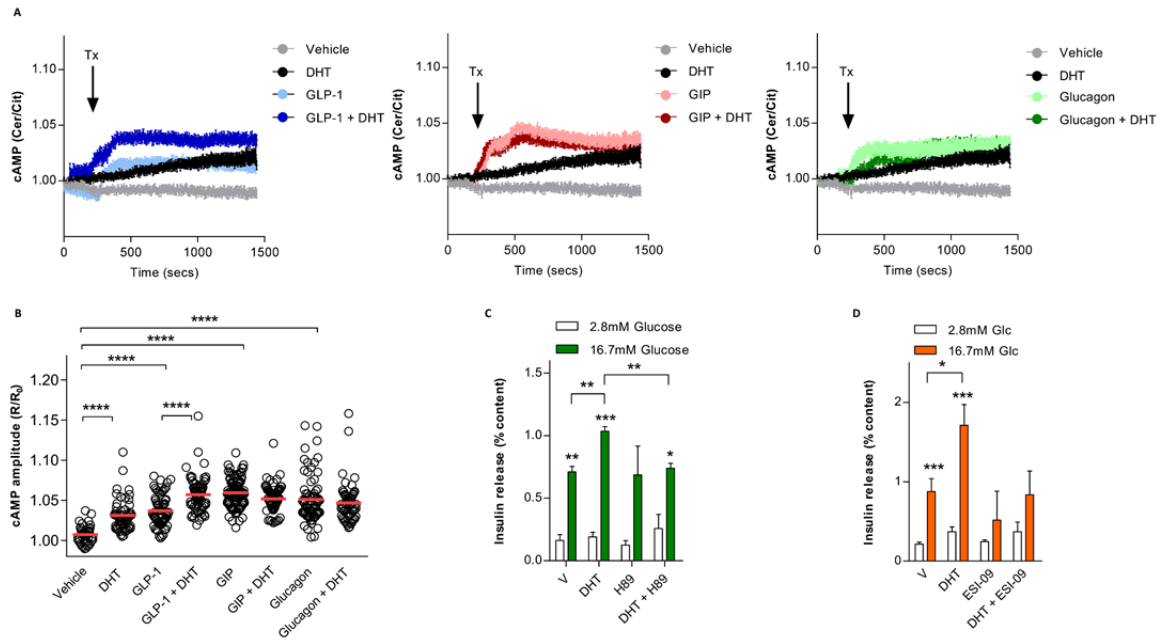
Figure 18. **(A)** 832/3 cell line is treated in static incubation with DHT (10nM), GLP-1 (10nM), GIP (100nM), and glucagon (20nM)for 30 minutes. **(B)** Summary graph of **(A-C)** showing amplitude of cAMP responses to DHT, GLP-1, glucagon. GSIS in static incubation in wild type male mouse islets treated with H89 (10uM) **(C)** and ESI-09 (10uM) **(D)**.

abolished by both H89 (**Figure 18C**) and ESI-09 (**Figure 18D**). Together, these data suggest that

AR signals via a cAMP-PKA and EPAC pathway to amplify GSIS.

DHT increased GSIS via mTORC1 signaling pathway

Since DHT activation of AR stimulates insulin secretion via production of cAMP and

without increasing β-cell mass, we reasoned that AR activation may enhance GSIS via the

protein kinase mechanistic target of rapamycin (mTOR). Indeed, in β-cells, activation of mTOR

stimulates insulin secretion downstream of cAMP and independently from an increase in β-cell

mass [131]. In addition, AR is known to activate mTOR in the prostate [132-134]. In wild type

male mouse islets, inhibition of the TORC1 complex using rapamycin blocked the effect of DHT

in enhancing GSIS (**Figure 19A**). Further, we also used islets from a mouse overexpressing one

copy of a kinase-dead mTOR mutant (KD-mTOR) transgene exclusively in β-cells [131]. Similarly,

in cultured islets from male KD-mTOR mice fed a normal chow, DHT failed to increase GSIS when

mTOR signaling is deficient (**Figure 19B**).

Figure 19. **(A)** GSIS in static incubation in wild type male mouse islets treated with (10uM). (**B**)

GSIS in static incubation in KD-mTOR male mouse islets treated with V and DHT (10uM).

Discussion

Though the intestinal L cells is the main source of circulating GLP-1, many studies have stressed the importance of intra-islet GLP-1 on glucose homeostasis in the pancreatic β-cells [135-137]. As a result, we asked whether DHT amplifies the islet-derived and/or gut-derived GLP-1 activity *in vivo*. We challenged male βARKO^{MIP} and control mice with IP and oral glucose. βARKO^{MIP} mic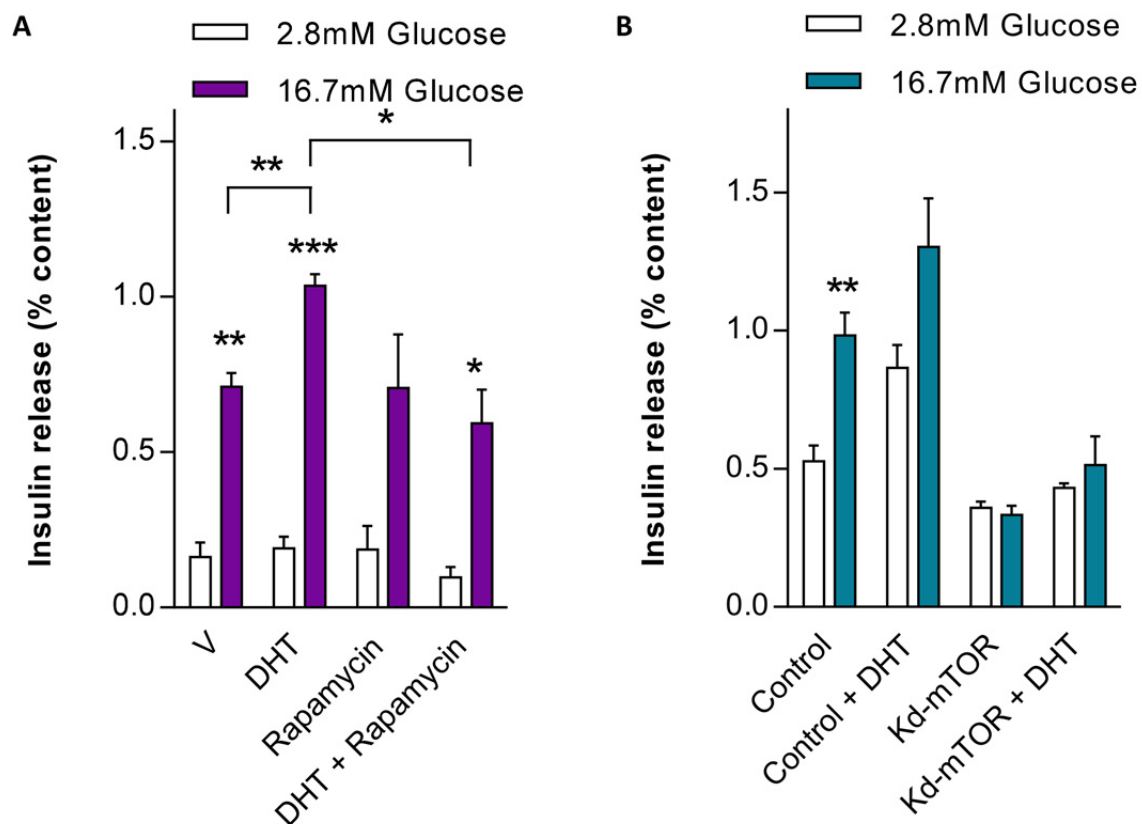e develop IP glucose intolerance without the change in oral glucose tolerance. Together with the results in the male islets that DHT amplifies the islet-derived GLP-1 activity by using GLP-1R antagonist, exendin (9-39) [42], we conclude that DHT amplifies the insulinotropic effect of islet-derived, not gut-derived, GLP-1 to regulate glucose homeostasis. We have also observed that βARKO^{MIP} mice display impaired IP GSIS without alteration in the IP ASIS, suggesting that AR involves in glucose- but not arginin-induced insulin secretion.

Since DHT and intra-islet GLP-1 collaboratively improve GSIS in male islets as well as in vivo, we wanted to explore whether AR is necessary in GLP-1R signaling and whether prolonging the half-life of GLP-1 improves glucose homeostasis in the absence of AR. Linagliptin, a DPP4 inhibitor, does not synergize with DHT to increase GSIS in male mouse islets, and accordingly, linagliptin does not improve IP glucose tolerance in both βARKO^{MIP} and control mice. Together, this suggests that prolonging the half-life of islet-derived GLP-1 does not improve GSIS and thus glucose homeostasis. Conversely, linagliptin similarly improves glucose tolerance and GSIS under oral glucose challenge, suggesting that prolonging the half-life of GLP-1 systemically ameliorates glucose homeostasis and is independent of AR signaling. Our findings are consistent with other study that DPP-4 inhibitors enhance glucose tolerance via non- β-cell GLP-1R [135].

To dissect the roles of GLP-1R and AR in insulin secretion in β-cells, we specifically knocked out the GLP-1R and AR in β-cells by breeding respective floxed mice and RIP-Cre mice. Since the MIP-CreERT induced partial knockout of AR in our hands compared to 100% by RIP-Cre

[42], the latter was chosen to generate βGLP1RKO[RIP] and βARKO[RIP]. Consistent with results obtained in male islets treated with exendin (9-39) [42], GLP-1R deficiency in β-cells impairs the ability of DHT to increase GSIS, and DHT fails to amplify the insulinotropic action of GLP-1. Note that GLP-1 is still capable of inducing GSIS in the βGLP1RKO[RIP] islets, possibly due to incomplete GLP-1R knockout or GLP-1 cross-reacting with other incretin receptors. On the other hand, while potentiation of GSIS is abolished with AR knockout, the effect of the GLP-1 is maintained. Altogether, it suggests that the action of GLP-1R is indispensable for AR signaling; DHT-activated AR amplifies the insulinotropic effect of GLP-1, but is not mandatory for the GLP-1 signaling in the β-cells.

The GLP-1R, GIP receptor (GIPR) and glucagon receptor (GCGR) belong to the secretin-receptor family (Class B GPRC), which are all involved in cAMP-mediated signaling pathways [138]. Since DHT amplifies the insulinotropic effect of GLP-1, we asked whether it can also amplify the action of GIP and glucagon, which also induce the activation of G protein and subsequent activation of AC. By treating the 832/3 cell and wild-type male islets with GLP-1, GIP and glucagon, we find that the effect of DHT to enhance GSIS is indeed specific to GLP-1.

We previously showed that DHT enhances GSIS by increasing cAMP accumulation in β-cells and this pathway is PKA-dependent [42]. Using the EPAC-based FRET sensor, and consistently with the GSIS, we show that DHT also elevates GLP-1-induced cAMP production, not that of GIP and glucagon. Using the PKA inhibitor, H89, and EPAC inhibitor, ESI-09, we show that DHT acts on both PKA and EPAC pathways to enhance GSIS in β-cells. Altogether, these data suggest that AR amplifies the insulinotropic effect both exogenous and endogenous GLP-1, enhances GLP-1 induced cAMP production, and functions in a cAMP/PKA/EPAC dependent pathway.

Since DHT specifically amplifies the insulinotropic action of GLP-1, not that of GIP and glucagon, we hypothesize that AR and GLP-1R are likely at a close proximity to each other. Our immunocytochemistry staining shows particular AR localizations resembling that of endosomal compartments [42]. Many studies revealed the persistent cAMP generation after GLP-1R internalization and its implications for prolonged insulin secretion [139-141], A recent study suggested that retaining the GLP-1R at the plasma membrane and preventing β-arrestin recruitment increases cAMP production and insulin release [142]. Further studies are needed to determine to explore whether AR is close to GLP-1R spatially and plays a role in the GLP-1R trafficking process by reducing GLP-1R internalization, promoting receptor recycling, or hindering β-arrest response.

In addition, DHT-activated AR and mTORC1 collaboratively potentiate GSIS in β-cells. mTOR pathway has long been known to involve in β-cell mass regulation [143-146], and recent studies also identified its role in insulin secretion in β-cell [131] through both mTORC1 [146] and mTORC2 [145, 147]. Since AR and mTOR pathways are both anabolic, this may explain their collaboration inducing insulin secretion from male β-cells. Moreover, studies have revealed cross-talk between cAMP and mTOR signaling [148-151]. Further studies using transgenetic model with knockout of mTORC1 or mTORC2 are warranted to dissect their respective role in AR signaling in β-cells, and studies exploring the relationship among AR/GLP-1R-cAMP/mTOR signaling pathways are also needed.

In conclusion, our study uncovers molecular pathways by which AR potentiates GSIS in male β-cell through activation of mTOR and amplification of the intra-islet GLP-1/cAMP signaling (**Figure 20**) with implications for the role of AR signaling in the GLP-1 based therapy in the T2D treatment for men with hypogonadism.
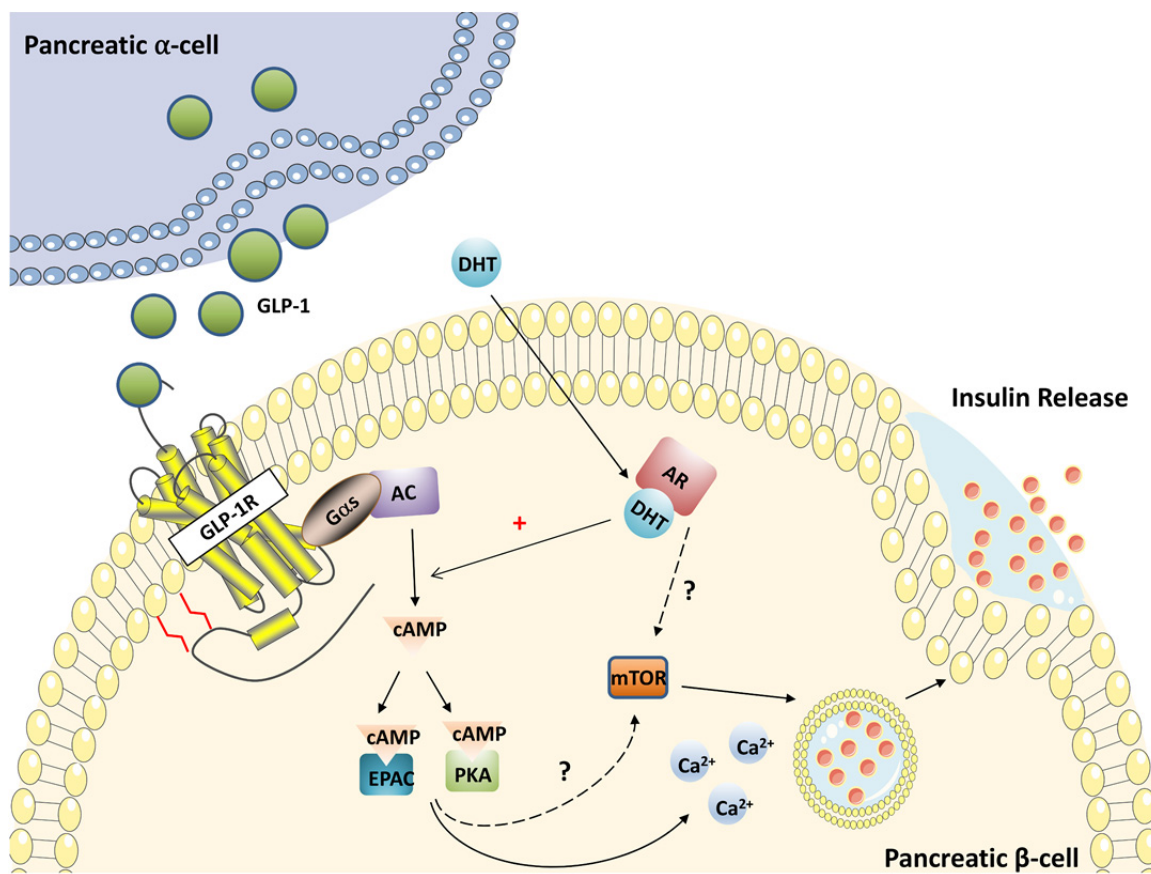
Figure 20. Proposed Molecular Mechanism

REFERENCES

1.   Araujo, A.B., et al., *Prevalence of symptomatic androgen deficiency in men.* J Clin Endocrinol Metab, 2007. **92**(11): p. 4241-7.
2.   Khaw, K.T. and E. Barrett-Connor, *Lower endogenous androgens predict central adiposity in men.* Ann Epidemiol, 1992. **2**(5): p. 675-82.
3.   Pitteloud, N., et al., *Relationship between testosterone levels, insulin sensitivity, and mitochondrial function in men.* Diabetes Care, 2005. **28**(7): p. 1636-42.
4.   Zitzmann, M., S. Faber, and E. Nieschlag, *Association of specific symptoms and metabolic risks with serum testosterone in older men.* J Clin Endocrinol Metab, 2006. **91**(11): p. 4335-43.
5.   Stellato, R.K., et al., *Testosterone, sex hormone-binding globulin, and the development of type 2 diabetes in middle-aged men: prospective results from the Massachusetts male aging study.* Diabetes Care, 2000. **23**(4): p. 490-4.
6.   Oh, J.Y., et al., *Endogenous sex hormones and the development of type 2 diabetes in older men and women: the Rancho Bernardo study.* Diabetes Care, 2002. **25**(1): p. 55-60.
7.   Ho, C.H., et al., *Prediabetes is associated with an increased risk of testosterone deficiency, independent of obesity and metabolic syndrome.* PLoS One, 2013. **8**(9): p. e74173.
8.   Basaria, S., et al., *Hyperglycemia and insulin resistance in men with prostate carcinoma who receive androgen-deprivation therapy.* Cancer, 2006. **106**(3): p. 581-8.
9.   Inaba, M., et al., *Marked hyperglycemia after androgen-deprivation therapy for prostate cancer and usefulness of pioglitazone for its treatment.* Metabolism, 2005. **54**(1): p. 55-9.
10.   Keating, N.L., A.J. O'Malley, and M.R. Smith, *Diabetes and cardiovascular disease during androgen deprivation therapy for prostate cancer.* J Clin Oncol, 2006. **24**(27): p. 4448-56.
11.   Keating, N.L., et al., *Diabetes and cardiovascular disease during androgen deprivation therapy: observational study of veterans with prostate cancer.* J Natl Cancer Inst, 2012. **104**(19): p. 1518-23.
12.   Hackett, G., et al., *Testosterone replacement therapy with long-acting testosterone undecanoate improves sexual function and quality-of-life parameters vs. placebo in a population of men with type 2 diabetes.* J Sex Med, 2013. **10**(6): p. 1612-27.
13.   Jones, T.H., et al., *Testosterone replacement in hypogonadal men with type 2 diabetes and/or metabolic syndrome (the TIMES2 study).* Diabetes Care, 2011. **34**(4): p. 828-37.
14.   Dimitriadis, G.K., et al., *Metabolic phenotype of male obesity-related secondary hypogonadism pre-replacement and post-replacement therapy with intra-muscular testosterone undecanoate therapy.* Endocrine, 2018. **60**(1): p. 175-184.
15.   Zitzmann, M., *Testosterone deficiency, insulin resistance and the metabolic syndrome.* Nat Rev Endocrinol, 2009. **5**(12): p. 673-81.
16.   Mauvais-Jarvis, F., *Estrogen and androgen receptors: regulators of fuel homeostasis and emerging targets for diabetes and obesity.* Trends Endocrinol Metab, 2011. **22**(1): p. 24-33.
17.   Bojesen, A., et al., *The metabolic syndrome is frequent in Klinefelter's syndrome and is associated with abdominal obesity and hypogonadism.* Diabetes Care, 2006. **29**(7): p. 1591-8.

18. Moverare-Skrtic, S., et al., *Dihydrotestosterone treatment results in obesity and altered lipid metabolism in orchidectomized mice.* Obesity (Silver Spring), 2006. **14**(4): p. 662-72.

19. Finkelstein, J.S., E.W. Yu, and S.A. Burnett-Bowie, *Gonadal steroids and body composition, strength, and sexual function in men.* N Engl J Med, 2013. **369**(25): p. 2457.

20. Mauvais-Jarvis, F., D.J. Clegg, and A.L. Hevener, *The role of estrogens in control of energy balance and glucose homeostasis.* Endocr Rev, 2013. **34**(3): p. 309-38.

21. Zitzmann, M., et al., *The CAG repeat polymorphism in the androgen receptor gene modulates body fat mass and serum concentrations of leptin and insulin in men.* Diabetologia, 2003. **46**(1): p. 31-9.

22. Fan, W., et al., *Androgen receptor null male mice develop late-onset obesity caused by decreased energy expenditure and lipolytic activity but show normal insulin sensitivity with high adiponectin secretion.* Diabetes, 2005. **54**(4): p. 1000-8.

23. Lin, H.Y., et al., *Insulin and leptin resistance with hyperleptinemia in mice lacking androgen receptor.* Diabetes, 2005. **54**(6): p. 1717-25.

24. Lanfranco, F., et al., *Serum adiponectin levels in hypogonadal males: influence of testosterone replacement therapy.* Clin Endocrinol (Oxf), 2004. **60**(4): p. 500-7.

25. Nishizawa, H., et al., *Androgens decrease plasma adiponectin, an insulin-sensitizing adipocyte-derived protein.* Diabetes, 2002. **51**(9): p. 2734-41.

26. Singh, R., et al., *Androgens stimulate myogenic differentiation and inhibit adipogenesis in C3H 10T1/2 pluripotent cells through an androgen receptor-mediated pathway.* Endocrinology, 2003. **144**(11): p. 5081-8.

27. Singh, R., et al., *Testosterone inhibits adipogenic differentiation in 3T3-L1 cells: nuclear translocation of androgen receptor complex with beta-catenin and T-cell factor 4 may bypass canonical Wnt signaling to down-regulate adipogenic transcription factors.* Endocrinology, 2006. **147**(1): p. 141-54.

28. Gentile, M.A., et al., *Androgen-mediated improvement of body composition and muscle function involves a novel early transcriptional program including IGF1, mechano growth factor, and induction of {beta}-catenin.* J Mol Endocrinol, 2010. **44**(1): p. 55-73.

29. Fernando, S.M., et al., *Myocyte androgen receptors increase metabolic rate and improve body composition by reducing fat mass.* Endocrinology, 2010. **151**(7): p. 3125-32.

30. Yu, I.C., et al., *Hyperleptinemia without obesity in male mice lacking androgen receptor in adipose tissue.* Endocrinology, 2008. **149**(5): p. 2361-8.

31. Ophoff, J., et al., *Androgen signaling in myocytes contributes to the maintenance of muscle mass and fiber type regulation but not to muscle strength or fatigue.* Endocrinology, 2009. **150**(8): p. 3558-66.

32. Holmang, A. and P. Bjorntorp, *The effects of testosterone on insulin sensitivity in male rats.* Acta Physiol Scand, 1992. **146**(4): p. 505-10.

33. Haren, M.T., et al., *Testosterone modulates gene expression pathways regulating nutrient accumulation, glucose metabolism and protein turnover in mouse skeletal muscle.* Int J Androl, 2011. **34**(1): p. 55-68.

34. Mootha, V.K., et al., *PGC-1alpha-responsive genes involved in oxidative phosphorylation are coordinately downregulated in human diabetes.* Nat Genet, 2003. **34**(3): p. 267-73.

35. Lin, H.Y., et al., *Increased hepatic steatosis and insulin resistance in mice lacking hepatic androgen receptor.* Hepatology, 2008. **47**(6): p. 1924-35.

36. Dowman, J.K., et al., *Loss of 5alpha-reductase type 1 accelerates the development of hepatic steatosis but protects against hepatocellular carcinoma in male mice.* Endocrinology, 2013. **154**(12): p. 4536-47.

37.   Livingstone, D.E., et al., *5alpha-Reductase type 1 deficiency or inhibition predisposes to insulin resistance, hepatic steatosis, and liver fibrosis in rodents.* Diabetes, 2015. **64**(2): p. 447-58.

38.   Volzke, H., et al., *Hepatic steatosis is associated with low serum testosterone and high serum DHEAS levels in men.* Int J Androl, 2010. **33**(1): p. 45-53.

39.   Fan, W., et al., *Functional potentiation of leptin-signal transducer and activator of transcription 3 signaling by the androgen receptor.* Endocrinology, 2008. **149**(12): p. 6028-36.

40.   Yu, I.C., et al., *Neuronal androgen receptor regulates insulin sensitivity via suppression of hypothalamic NF-kappaB-mediated PTP1B expression.* Diabetes, 2013. **62**(2): p. 411-23.

41.   Dubois, V., et al., *Androgen Deficiency Exacerbates High-Fat Diet-Induced Metabolic Alterations in Male Mice.* Endocrinology, 2016. **157**(2): p. 648-65.

42.   Navarro, G., et al., *Extranuclear Actions of the Androgen Receptor Enhance Glucose-Stimulated Insulin Secretion in the Male.* Cell Metab, 2016. **23**(5): p. 837-51.

43.   Xu, W., et al., *Androgen receptor-deficient islet beta-cells exhibit alteration in genetic markers of insulin secretion and inflammation. A transcriptome analysis in the male mouse.* J Diabetes Complications, 2017. **31**(5): p. 787-795.

44.   De Gendt, K., et al., *A Sertoli cell-selective knockout of the androgen receptor causes spermatogenic arrest in meiosis.* Proc Natl Acad Sci U S A, 2004. **101**(5): p. 1327-32.

45.   Tiano, J.P., et al., *Estrogen receptor activation reduces lipid synthesis in pancreatic islets and prevents beta cell failure in rodent models of type 2 diabetes.* J Clin Invest, 2011. **121**(8): p. 3331-42.

46.   Snoek, R., et al., *Induction of cell-free, in vitro transcription by recombinant androgen receptor peptides.* J Steroid Biochem Mol Biol, 1996. **59**(3-4): p. 243-50.

47.   Jacobson, D.A., et al., *Modulation of the pancreatic islet beta-cell-delayed rectifier potassium channel Kv2.1 by the polyunsaturated fatty acid arachidonate.* J Biol Chem, 2007. **282**(10): p. 7442-9.

48.   Gao, M., et al., *Facile radiosynthesis of new carbon-11-labeled propanamide derivatives as selective androgen receptor modulator (SARM) radioligands for prostate cancer imaging.* Steroids, 2011. **76**(13): p. 1505-12.

49.   Marhefka, C.A., et al., *Design, synthesis, and biological characterization of metabolically stable selective androgen receptor modulators.* J Med Chem, 2004. **47**(4): p. 993-8.

50.   Kim, S.H. and J.A. Katzenellenbogen, *Hormone-PAMAM dendrimer conjugates: polymer dynamics and tether structure affect ligand access to receptors.* Angew Chem Int Ed Engl, 2006. **45**(43): p. 7243-8.

51.   Lee JY, R.M., Lin X, White MF, Magnuson MA, Hennighausen L, *RIP-Cre revisited, evidence for impairments of pancreatic β-cell function.* J Biol Chem, 2006.

52.   Ahren, B., *Autonomic regulation of islet hormone secretion--implications for health and disease.* Diabetologia, 2000. **43**(4): p. 393-410.

53.   Schoch, S., G. Cibelli, and G. Thiel, *Neuron-specific gene expression of synapsin I. Major role of a negative regulatory mechanism.* J Biol Chem, 1996. **271**(6): p. 3317-23.

54.   Wicksteed, B., et al., *Conditional gene targeting in mouse pancreatic ss-Cells: analysis of ectopic Cre transgene expression in the brain.* Diabetes, 2010. **59**(12): p. 3090-8.

55.   Oropeza, D., et al., *Phenotypic Characterization of MIP-CreERT1Lphi Mice With Transgene-Driven Islet Expression of Human Growth Hormone.* Diabetes, 2015. **64**(11): p. 3798-807.

56.   Lacy, P.E., M.M. Walker, and C.J. Fink, *Perifusion of isolated rat islets in vitro. Participation of the microtubular system in the biphasic release of insulin.* Diabetes, 1972. **21**(10): p. 987-98.

57.   Chang, C.S., J. Kokontis, and S.T. Liao, *Molecular cloning of human and rat complementary DNA encoding androgen receptors.* Science, 1988. **240**(4850): p. 324-6.

58.   Lubahn, D.B., et al., *Cloning of human androgen receptor complementary DNA and localization to the X chromosome.* Science, 1988. **240**(4850): p. 327-30.

59.   Tilley, W.D., et al., *Characterization and expression of a cDNA encoding the human androgen receptor.* Proc Natl Acad Sci U S A, 1989. **86**(1): p. 327-31.

60.   Matsumoto, T., et al., *The androgen receptor in health and disease.* Annu Rev Physiol, 2013. **75**: p. 201-24.

61.   Wong, W.P., et al., *Extranuclear estrogen receptor-{alpha} stimulates NeuroD1 binding to the insulin promoter and favors insulin synthesis.* Proc Natl Acad Sci U S A, 2010. **107**(29): p. 13057-62.

62.   Tiano, J. and F. Mauvais-Jarvis, *Selective estrogen receptor modulation in pancreatic beta-cells and the prevention of type 2 diabetes.* Islets, 2012. **4**(2): p. 173-6.

63.   Tiano, J.P. and F. Mauvais-Jarvis, *Molecular mechanisms of estrogen receptors' suppression of lipogenesis in pancreatic beta-cells.* Endocrinology, 2012. **153**(7): p. 2997-3005.

64.   Tiano, J.P. and F. Mauvais-Jarvis, *Importance of oestrogen receptors to preserve functional beta-cell mass in diabetes.* Nat Rev Endocrinol, 2012. **8**(6): p. 342-51.

65.   Zhu, Y.S., et al., *Androgen-induced prostate-specific antigen gene expression is mediated via dihydrotestosterone in LNCaP cells.* J Androl, 2003. **24**(5): p. 681-7.

66.   Jones, P.M., J. Stutchfield, and S.L. Howell, *Effects of Ca2+ and a phorbol ester on insulin secretion from islets of Langerhans permeabilised by high-voltage discharge.* FEBS Lett, 1985. **191**(1): p. 102-6.

67.   Lin, B.J. and R.E. Haist, *Effects of some modifiers of insulin secretion on insulin biosynthesis.* Endocrinology, 1973. **92**(3): p. 735-42.

68.   Nesher, R., et al., *Beta-cell protein kinases and the dynamics of the insulin response to glucose.* Diabetes, 2002. **51 Suppl 1**: p. S68-73.

69.   Liu, Z., et al., *Stromal cell-derived factor-1 (SDF-1)/chemokine (C-X-C motif) receptor 4 (CXCR4) axis activation induces intra-islet glucagon-like peptide-1 (GLP-1) production and enhances beta cell survival.* Diabetologia, 2011. **54**(8): p. 2067-76.

70.   Marchetti, P., et al., *A local glucagon-like peptide 1 (GLP-1) system in human pancreatic islets.* Diabetologia, 2012. **55**(12): p. 3262-72.

71.   Goke, R., et al., *Exendin-4 is a high potency agonist and truncated exendin-(9-39)-amide an antagonist at the glucagon-like peptide 1-(7-36)-amide receptor of insulin-secreting beta-cells.* J Biol Chem, 1993. **268**(26): p. 19650-5.

72.   Bruchovsky, N. and J.D. Wilson, *The intranuclear binding of testosterone and 5-alpha-androstan-17-beta-ol-3-one by rat prostate.* J Biol Chem, 1968. **243**(22): p. 5953-60.

73.   Prescott, J. and G.A. Coetzee, *Molecular chaperones throughout the life cycle of the androgen receptor.* Cancer Lett, 2006. **231**(1): p. 12-9.

74.   Ashcroft, S.J., *Glucoreceptor mechanisms and the control of insulin release and biosynthesis.* Diabetologia, 1980. **18**(1): p. 5-15.

75.   Kaihara, K.A., et al., *beta-Cell-specific protein kinase A activation enhances the efficiency of glucose control by increasing acute-phase insulin secretion.* Diabetes, 2013. **62**(5): p. 1527-36.

76.   Song, W.J., et al., *Snapin mediates incretin action and augments glucose-dependent insulin secretion.* Cell Metab, 2011. **13**(3): p. 308-19.

77.   Morimoto, S., et al., *Insulin gene expression pattern in rat pancreas during the estrous cycle.* Life Sci, 2001. **68**(26): p. 2979-85.

78.   Egan, J.M., et al., *Glucagon-like peptide-1 augments insulin-mediated glucose uptake in the obese state.* J Clin Endocrinol Metab, 2002. **87**(8): p. 3768-73.

79.   Fehse, F., et al., *Exenatide augments first- and second-phase insulin secretion in response to intravenous glucose in subjects with type 2 diabetes.* J Clin Endocrinol Metab, 2005. **90**(11): p. 5991-7.

80.   Drucker, D.J. and M.A. Nauck, *The incretin system: glucagon-like peptide-1 receptor agonists and dipeptidyl peptidase-4 inhibitors in type 2 diabetes.* Lancet, 2006. **368**(9548): p. 1696-705.

81.   Visakorpi, T., et al., *In vivo amplification of the androgen receptor gene and progression of human prostate cancer.* Nat Genet, 1995. **9**(4): p. 401-6.

82.   Mohler, M.L., et al., *Nonsteroidal selective androgen receptor modulators (SARMs): dissociating the anabolic and androgenic activities of the androgen receptor for therapeutic benefit.* J Med Chem, 2009. **52**(12): p. 3597-617.

83.   Mauvais-Jarvis, F., *Role of Sex Steroids in beta Cell Function, Growth, and Survival.* Trends Endocrinol Metab, 2016.

84.   Navarro, G., et al., *The role of androgens in metabolism, obesity, and diabetes in males and females.* Obesity (Silver Spring), 2015. **23**(4): p. 713-9.

85.   Trapnell, C., et al., *Differential gene and transcript expression analysis of RNA-seq experiments with TopHat and Cufflinks.* Nat Protoc, 2012. **7**(3): p. 562-78.

86.   Li, P., et al., *Comparing the normalization methods for the differential analysis of Illumina high-throughput RNA-Seq data.* BMC Bioinformatics, 2015. **16**: p. 347.

87.   Reiner, A., D. Yekutieli, and Y. Benjamini, *Identifying differentially expressed genes using false discovery rate controlling procedures.* Bioinformatics, 2003. **19**(3): p. 368-75.

88.   Tabas-Madrid, D., R. Nogales-Cadenas, and A. Pascual-Montano, *GeneCodis3: a non-redundant and modular enrichment analysis tool for functional genomics.* Nucleic Acids Res, 2012. **40**(Web Server issue): p. W478-83.

89.   Backes, C., et al., *GeneTrail--advanced gene set enrichment analysis.* Nucleic Acids Res, 2007. **35**(Web Server issue): p. W186-92.

90.   Haynes, W.A., et al., *Differential expression analysis for pathways.* PLoS Comput Biol, 2013. **9**(3): p. e1002967.

91.   Lee, E., et al., *Inferring pathway activity toward precise disease classification.* PLoS Comput Biol, 2008. **4**(11): p. e1000217.

92.   Thomas, P.D., H. Mi, and S. Lewis, *Ontology annotation: mapping genomic regions to biological function.* Curr Opin Chem Biol, 2007. **11**(1): p. 4-11.

93.   Boyle, E.I., et al., *GO::TermFinder--open source software for accessing Gene Ontology information and finding significantly enriched Gene Ontology terms associated with a list of genes.* Bioinformatics, 2004. **20**(18): p. 3710-5.

94.   Consortium, T.G.O., *Expansion of the Gene Ontology knowledgebase and resources.* Nucleic Acids Res, 2017. **45**(D1): p. D331-d338.

95.   Wente, W., et al., *Fibroblast growth factor-21 improves pancreatic beta-cell function and survival by activation of extracellular signal-regulated kinase 1/2 and Akt signaling pathways.* Diabetes, 2006. **55**(9): p. 2470-8.

96.   Chang, S.Y., et al., *Induction mechanism of lipocalin-2 expression by co-stimulation with interleukin-1beta and interferon-gamma in RINm5F beta-cells.* Biochem Biophys Res Commun, 2013. **434**(3): p. 577-83.

97.   Reid, P. and I. Holen, *Pathophysiological roles of osteoprotegerin (OPG).* Eur J Cell Biol, 2009. **88**(1): p. 1-17.

98.   Maruyama, K., et al., *Receptor activator of NF-kappa B ligand and osteoprotegerin regulate proinflammatory cytokine production in mice.* J Immunol, 2006. **177**(6): p. 3799-805.

99.   Schulthess, F.T., et al., *CXCL10 impairs beta cell function and viability in diabetes through TLR4 signaling.* Cell Metab, 2009. **9**(2): p. 125-39.

100.   Nunemaker, C.S., et al., *Increased serum CXCL1 and CXCL5 are linked to obesity, hyperglycemia, and impaired islet function.* J Endocrinol, 2014. **222**(2): p. 267-76.

101.   Kim, B.H., et al., *Interferon-induced guanylate-binding proteins in inflammasome activation and host defense.* Nat Immunol, 2016. **17**(5): p. 481-9.

102.   Shioya, M., et al., *Interleukin 22 receptor 1 expression in pancreas islets.* Pancreas, 2008. **36**(2): p. 197-9.

103.   Dayer-Metroz, M.D., et al., *A natural interleukin 1 (IL-1) inhibitor counteracts the inhibitory effect of IL-1 on insulin production in cultured rat pancreatic islets.* J Autoimmun, 1989. **2**(2): p. 163-71.

104.   Russell, M.A. and N.G. Morgan, *The impact of anti-inflammatory cytokines on the pancreatic beta-cell.* Islets, 2014. **6**(3): p. e950547.

105.   Sharma, P.R., et al., *An Islet-Targeted Genome-Wide Association Scan Identifies Novel Genes Implicated in Cytokine-Mediated Islet Stress in Type 2 Diabetes.* Endocrinology, 2015. **156**(9): p. 3147-56.

106.   Bachmann, V.A., et al., *Gpr161 anchoring of PKA consolidates GPCR and cAMP signaling.* Proc Natl Acad Sci U S A, 2016. **113**(28): p. 7786-91.

107.   Mogha, A., et al., *Gpr126 functions in Schwann cells to control differentiation and myelination via G-protein activation.* J Neurosci, 2013. **33**(46): p. 17976-85.

108.   Zhang, L.L., et al., *GPR26-deficient mice display increased anxiety- and depression-like behaviors accompanied by reduced phosphorylated cyclic AMP responsive element-binding protein level in central amygdala.* Neuroscience, 2011. **196**: p. 203-14.

109.   Islam, M.S., *TRP channels of islets.* Adv Exp Med Biol, 2011. **704**: p. 811-30.

110.   Cao, P., A. Maximov, and T.C. Sudhof, *Activity-dependent IGF-1 exocytosis is controlled by the Ca(2+)-sensor synaptotagmin-10.* Cell, 2011. **145**(2): p. 300-11.

111.   Arribas, M., et al., *The stimulatory effect of rabphilin 3a on regulated exocytosis from insulin-secreting cells does not require an association-dissociation cycle with membranes mediated by Rab 3.* Eur J Cell Biol, 1997. **74**(3): p. 209-16.

112.   Takahashi, I., K. Ohashi, and K. Nata, *Involvement of heparan sulfate 3-O-sulfotransferase isoform-1 in the insulin secretion pathway.* J Diabetes Investig, 2012. **3**(4): p. 362-70.

113.   Ludvik, A.E., et al., *HKDC1 Is a Novel Hexokinase Involved in Whole-Body Glucose Use.* Endocrinology, 2016. **157**(9): p. 3452-61.

114.   Arden, C., et al., *A role for PFK-2/FBPase-2, as distinct from fructose 2,6-bisphosphate, in regulation of insulin secretion in pancreatic beta-cells.* Biochem J, 2008. **411**(1): p. 41-51.

115.   Hardy, A.B., et al., *Zip4 mediated zinc influx stimulates insulin secretion in pancreatic beta cells.* PLoS One, 2015. **10**(3): p. e0119136.

116.   Yasuda, K., et al., *Variants in KCNQ1 are associated with susceptibility to type 2 diabetes mellitus.* Nat Genet, 2008. **40**(9): p. 1092-7.

117.   Zeng, H., et al., *An Isogenic Human ESC Platform for Functional Evaluation of Genome-wide-Association-Study-Identified Diabetes Genes and Drug Discovery.* Cell Stem Cell, 2016. **19**(3): p. 326-40.

118.   Yamagata, K., et al., *Voltage-gated K+ channel KCNQ1 regulates insulin secretion in MIN6 beta-cell line.* Biochem Biophys Res Commun, 2011. **407**(3): p. 620-5.

119.   Park, K.G., et al., *Glucotoxicity in the INS-1 rat insulinoma cell line is mediated by the orphan nuclear receptor small heterodimer partner.* Diabetes, 2007. **56**(2): p. 431-7.

120.   Yamato, E., F. Tashiro, and J. Miyazaki, *Microarray analysis of novel candidate genes responsible for glucose-stimulated insulin secretion in mouse pancreatic beta cell line MIN6.* PLoS One, 2013. **8**(4): p. e61211.

121.   Henley, K.D., et al., *Inactivation of the dual Bmp/Wnt inhibitor Sostdc1 enhances pancreatic islet function.* Am J Physiol Endocrinol Metab, 2012. **303**(6): p. E752-61.

122.   Morimoto, S., et al., *Protective effect of testosterone on early apoptotic damage induced by streptozotocin in rat pancreas.* J Endocrinol, 2005. **187**(2): p. 217-24.

123.   Palomar-Morales, M., et al., *The protective effect of testosterone on streptozotocin-induced apoptosis in beta cells is sex specific.* Pancreas, 2010. **39**(2): p. 193-200.

124.   Trost, B., et al., *Concordance between RNA-sequencing data and DNA microarray data in transcriptome analysis of proliferative and quiescent fibroblasts.* R Soc Open Sci, 2015. **2**(9): p. 150402.

125.   Richard, H., et al., *Prediction of alternative isoforms from exon expression levels in RNA-Seq experiments.* Nucleic Acids Res, 2010. **38**(10): p. e112.

126.   Schmid, M.W., et al., *A powerful method for transcriptional profiling of specific cell types in eukaryotes: laser-assisted microdissection and RNA sequencing.* PLoS One, 2012. **7**(1): p. e29685.

127.   Hodson, D.J., et al., *ADCY5 couples glucose to insulin secretion in human islets.* Diabetes, 2014. **63**(9): p. 3009-21.

128.   Eckhardt, M., et al., *8-(3-(R)-aminopiperidin-1-yl)-7-but-2-ynyl-3-methyl-1-(4-methyl-quinazolin-2-ylme thyl)-3,7-dihydropurine-2,6-dione (BI 1356), a highly potent, selective, long-acting, and orally bioavailable DPP-4 inhibitor for the treatment of type 2 diabetes.* J Med Chem, 2007. **50**(26): p. 6450-3.

129.   Hohmeier, H.E., et al., *Isolation of INS-1-derived cell lines with robust ATP-sensitive K+ channel-dependent and -independent glucose-stimulated insulin secretion.* Diabetes, 2000. **49**(3): p. 424-30.

130.   Seino, S., et al., *Roles of cAMP signalling in insulin granule exocytosis.* Diabetes Obes Metab, 2009. **11 Suppl 4**: p. 180-8.

131.   Alejandro, E.U., et al., *Overexpression of Kinase-Dead mTOR Impairs Glucose Homeostasis by Regulating Insulin Secretion and Not beta-Cell Mass.* Diabetes, 2017. **66**(8): p. 2150-2162.

132.   Xiang, X., et al., *AMP-activated protein kinase activators can inhibit the growth of prostate cancer cells by multiple mechanisms.* Biochem Biophys Res Commun, 2004. **321**(1): p. 161-7.

133.   Xu, Y., et al., *Androgens induce prostate cancer cell proliferation through mammalian target of rapamycin activation and post-transcriptional increases in cyclin D proteins.* Cancer Res, 2006. **66**(15): p. 7783-92.

134.   Recchia, A.G., et al., *A cross-talk between the androgen receptor and the epidermal growth factor receptor leads to p38MAPK-dependent activation of mTOR and cyclinD1 expression in prostate and lung cancer cells.* Int J Biochem Cell Biol, 2009. **41**(3): p. 603-14.

135. Smith, E.P., et al., *The role of beta cell glucagon-like peptide-1 signaling in glucose regulation and response to diabetes drugs.* Cell Metab, 2014. **19**(6): p. 1050-7.
136. Chambers, A.P., et al., *The Role of Pancreatic Preproglucagon in Glucose Homeostasis in Mice.* Cell Metab, 2017. **25**(4): p. 927-934.e3.
137. Traub, S., et al., *Pancreatic alpha Cell-Derived Glucagon-Related Peptides Are Required for beta Cell Adaptation and Glucose Homeostasis.* Cell Rep, 2017. **18**(13): p. 3192-3203.
138. Harmar, A.J., *Family-B G-protein-coupled receptors.* Genome Biol, 2001. **2**(12): p. Reviews3013.
139. Kuna, R.S., et al., *Glucagon-like peptide-1 receptor-mediated endosomal cAMP generation promotes glucose-stimulated insulin secretion in pancreatic beta-cells.* Am J Physiol Endocrinol Metab, 2013. **305**(2): p. E161-70.
140. Girada, S.B., et al., *Galphas regulates Glucagon-Like Peptide 1 Receptor-mediated cyclic AMP generation at Rab5 endosomal compartment.* Mol Metab, 2017. **6**(10): p. 1173-1185.
141. Jones, B., et al., *Control of insulin secretion by GLP-1.* Peptides, 2018. **100**: p. 75-84.
142. Jones, B., et al., *Targeting GLP-1 receptor trafficking to improve agonist efficacy.* Nat Commun, 2018. **9**(1): p. 1602.
143. Blandino-Rosano, M., et al., *mTORC1 signaling and regulation of pancreatic beta-cell mass.* Cell Cycle, 2012. **11**(10): p. 1892-902.
144. Rachdi, L., et al., *Disruption of Tsc2 in pancreatic beta cells induces beta cell mass expansion and improved glucose tolerance in a TORC1-dependent manner.* Proc Natl Acad Sci U S A, 2008. **105**(27): p. 9250-5.
145. Gu, Y., et al., *Rictor/mTORC2 is essential for maintaining a balance between beta-cell proliferation and cell size.* Diabetes, 2011. **60**(3): p. 827-37.
146. Hamada, S., et al., *Upregulation of the mammalian target of rapamycin complex 1 pathway by Ras homolog enriched in brain in pancreatic beta-cells leads to increased beta-cell mass and prevention of hyperglycemia.* Diabetes, 2009. **58**(6): p. 1321-32.
147. Xie, Y., et al., *The mTORC2/PKC pathway sustains compensatory insulin secretion of pancreatic beta cells in response to metabolic stress.* Biochim Biophys Acta, 2017. **1861**(8): p. 2039-2047.
148. Scott, P.H. and J.C. Lawrence, Jr., *Attenuation of mammalian target of rapamycin activity by increased cAMP in 3T3-L1 adipocytes.* J Biol Chem, 1998. **273**(51): p. 34496-501.
149. Blancquaert, S., et al., *cAMP-dependent activation of mammalian target of rapamycin (mTOR) in thyroid cells. Implication in mitogenesis and activation of CDK4.* Mol Endocrinol, 2010. **24**(7): p. 1453-68.
150. Kim, H.W., et al., *Cyclic AMP controls mTOR through regulation of the dynamic interaction between Rheb and phosphodiesterase 4D.* Mol Cell Biol, 2010. **30**(22): p. 5406-20.
151. de Joussineau, C., et al., *mTOR pathway is activated by PKA in adrenocortical cells and participates in vivo to apoptosis resistance in primary pigmented nodular adrenocortical disease (PPNAD).* Hum Mol Genet, 2014. **23**(20): p. 5418-28.